



Texas Journal of Microscopy



500 um

Volume 38, Number 2, 2007 • ISSN 1554-0820

Visit our web site at: www.texasmicroscopy.org

gatan gets it

Can your
3D microscopy system
automatically produce
perfectly aligned
images showing
10,000 synapses?

To learn how our
3View™ microscopy
system accomplishes
this, visit us at
www.gatan.com/answers

3D image set
generated by 3View™
of a neuron (blue) with
its synapses (red) in
the barrel cortex of a
mouse. Reconstruction
from 800 perfectly
aligned image slices.

3View™
DigitalMicrograph™
3D Visualization
tool

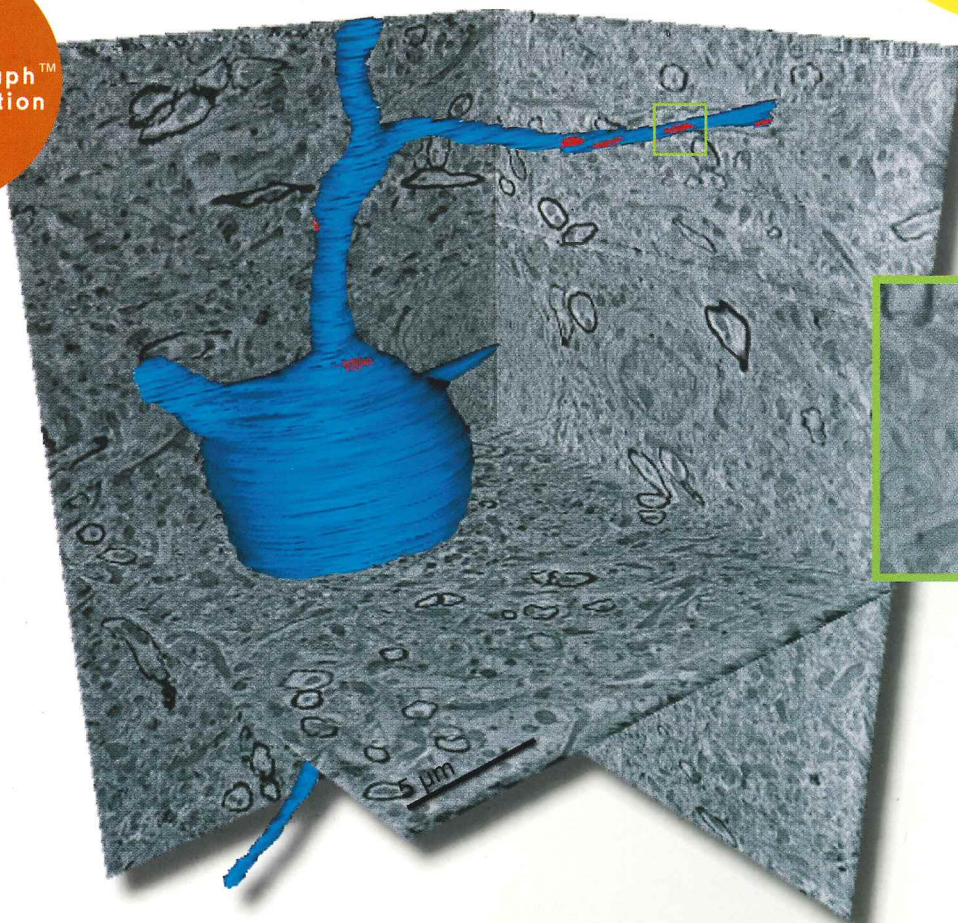


Image showing a neuropil area through a mouse barrel cortex (neuron shown in blue and synapses shown in red) processed for EM and generated using Gatan's 3View™ SBFSEM microscopy system. Eight hundred perfectly aligned image slices of 50 nm were acquired. Gatan's DigitalMicrograph™ 3D Visualization tool was used to show the Z projection of the 800 slices. Manual segmentation using Reconstruct (GNU General Public License version 2) software generated a 3D reconstruction of the neuronal cell including the dendrites and axon. The inset image shows an identified synapse between a dendrite of the reconstructed neuron and the axon labeled for parvalbumine (pre-embedding immunocytochemistry with biotinylated antibody). Sample courtesy of Dr. Graham Knott, DBCM, University of Lausanne.



TSM OFFICERS 2007-2008

President:

ERNEST F. COUCH
Department of Biology
Texas Christian University
Fort Worth, Texas 76129
(817) 257-7165 FAX (817) 257-6177
E-mail: e.couch@tcu.edu

President-elect:

NABARUN GHOSH
Dept. of Life, Earth, and Environmental Sciences
West Texas A&M University, P.O. Box 60808
Canyon, Texas 79016-0001
(806) 651-2571 FAX (806) 651-2928
E-mail: nghosh@mail.wtamu.edu

Past President:

JOANNE T. ELLZEY
Department of Biological Sciences
University of Texas at El Paso
El Paso, Texas 79968-0519
(915) 747-6880
E-mail: jellzey@utep.edu

Secretary:

TINA HALUPNIK
5917 Inks Lake Drive
Arlington, Texas 76018
(817) 468-0325
E-mail: fishstix@tx.rr.com

Secretary-elect:

MICHAEL W. PENDLETON
Microscopy and Imaging Center
Texas A&M University
College Station, Texas 77843-2257
(979) 845-1182
E-mail: mpendleton@mic.tamu.edu

Treasurer:

E. ANN ELLIS
Microscopy and Imaging Center
Texas A&M University
College Station, Texas 77843-2257
(979) 845-1129
E-mail: elisa@mic.tamu.edu

Program Chairman:

PHOEBE J. DOSS
Alcon Research, Ltd.
6201 S. Freeway
Fort Worth, Texas 76134-2099
(817) 568-6090
E-mail: phoebe.doss@alconlabs.com

APPOINTED OFFICERS

Corporate Member Representative:

GERMAN NEAL
Carl Zeiss SMT, Inc.
2800 Primwood Path
Cedar Park, Texas 78613
(512) 249-6296 FAX (512) 249-6406
E-mail: neal@smt.zeiss.com

Student Representative:

ANDREW J. WALTKE
Department of Biology
Texas Christian University
Winton Scott Room 401
2800 South University Drive
Fort Worth, TX 76129
(817) 257-7165 FAX (817) 257-6177
E-mail: ajwaltke@hotmail.com

TSM Journal Editor:

CAMELIA G.-A. MAIER
Department of Biology
Texas Woman's University, Denton, Texas 76204-5799
(940) 898-2358 FAX (940) 898-2382
E-mail: cmaier@twu.edu

TSM Web Page Master:

BECKY HOLDFORD
Texas Instruments, Inc.
13536 N. Central Texas Expressway
MS 940, Dallas, Texas 75243
(972) 995-2360
E-mail: r-holdford@ti.com

Contents



TEXAS JOURNAL OF MICROSCOPY VOLUME 38, NUMBER 2, 2007 ISSN 1554-0820

Camelia G.-A. Maier, Editor

Department of Biology, Texas Woman's University, Denton, TX 76204

Official Journal of the Texas Society for Microscopy

"TSM - Embracing all forms of microscopy"

www.texasmicroscopy.org

President's Message	97
Corporate Members	98
TSM Member Honored	99
Research Article:	
<i>Epicardial Formation In Situ And In Culture</i>	
Jessica Green, Randy Crossland and J. Kevin Langford	100
Answer to "What Is It" from Tex. J. Micros. 38:1	106
Research Article:	
<i>Avian Proepicardial Cells Retain Vasculogenic Potential in Culture</i>	
Randy Crossland, Jessica and J. Kevin Langford	108
Research Article:	
<i>Arsenic-Induced Steatosis in C57BL/6J Male Mice</i>	
<i>Chronically Exposed Through Drinking Water</i>	
Jaime B. Vigo, Joanne T. Ellzey, Thomas P. Baker,	
Julia O. Bader and Thomas G. Oliver	117
Advertiser's Index	124
Fall 2007 Meeting Abstracts	126
Short Communication	
<i>Structure and Significance of Termite Reaction</i>	
<i>Wood in the Life History of the Joshua Tree (Yucca brevifolia)</i>	
Howard J. Arnott	129
"What Is It?"	134
Editorial Policy	134
Application for Membership	136

ON THE COVER

Feather mites on Kentucky Warbler - colorized version of a Hitachi TM-1000 SEM micrograph. The original micrograph was taken by Curtis Hoagland (National Park Service) as part of a bird-banding study in the Big Thicket National Preserve, Texas. The color art was performed by C. Bryan Alberts (Eastfield College recent alumnus). Both Curtis Hoagland and C. Bryan Alberts were associated with the Eastfield College NSF STEP Summer Institute (National Science Foundation Science Talent Expansion Program). Micrograph sent by Jill DeVito, Research Coordinator, NSF STEP, Eastfield College, Dallas Community College District, 3737 Motley Drive, Mesquite, Texas 75150.

DiATOME

diamond knives

Development, Manufacturing,
and Customer Service since 1970

What have we achieved in this period?

ultra 45° the first diamond knife with an absolutely score-free, hydrophilic cutting edge.

semi the first diamond knife for alternating sectioning ultrathin/semithin.

cryo the diamond knife for sectioning at low temperature.

histo the first diamond knife for semithin sections for light microscopy.

ultra 35° the diamond knife for optimized sectioning results in almost all applications.

STATIC LINE II the ionizer for eliminating electrostatic charging in ultramicrotomy.

cryo-P a cryo knife with a patented platform for section pick up.

cryo immuno the optimized cryo diamond knife for the Tokuyasu technique.

ultra sonic the oscillating diamond knife for room temperature sectioning.

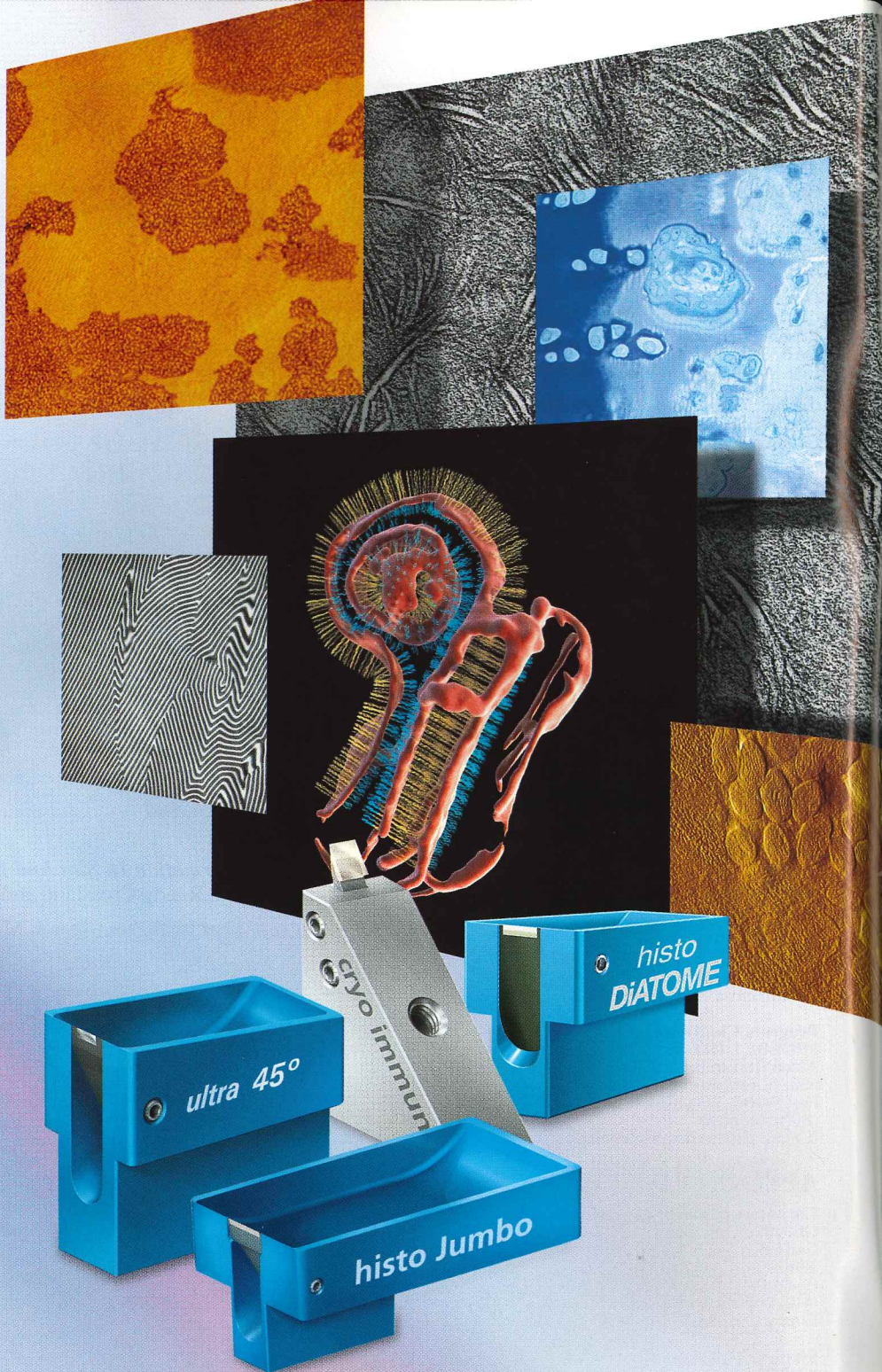
cryotrim 45 and 25 optimizing trimming with diamond blades.

ultra AFM & cryo AFM the first diamond knives for AFM at room and low temperatures.

cryo 25° for sectioning frozen hydrated specimens.

What services can we offer you?

- Technical assistance in all fields of ultramicrotomy.
- Free sectioning tests for all types of samples.
- Make use of our many years of experience in perfecting our knives.
- Custom knives, tools, and boats.
- Special purchase programs.
- Workshops and training.



**For more information,
please call or write us today,
or visit us online at:**

www.emsdiasum.com

DiATOME

for all your sectioning requirements

P.O. Box 410 • 1560 Industry Rd.
Hatfield, Pa 19440
(215) 412-8390 • Toll Free: 1-(800) 523-5874
Fax: (215) 412-8450 or 8452
email: sgkcck@aol.com • stacie@ems-secure.com
www.emsdiasum.com

President's Message

I would like to thank Brian Gorman and the Department of Materials Science and Engineering at the University of North Texas for hosting our fall meeting 2007. We are especially grateful to Brian for accepting our request to be the Keynote Speaker. I would also like to extend my thanks to the TSM officers for their support and help with the spring meeting 2007 on the Texas Christian University campus in Fort Worth. I am especially indebted to Pam Neill as Program Chair for her superb work and preparations for the meeting. Thanks also go out to our present Program Chair, Phoebe Doss. Thanks are also due to our Past President, Judi Ellzey for her leadership and counsel. Also I would like to recognize the hard work put in by our secretary, Tina Halupnik, our past treasurer, Bob Droleskey, and Webmaster Becky Holford. And finally, all of us in the Society must give thanks to Camelia Maier for accepting the arduous task of Journal Editor. This is a vital organ that gives publicity and legitimacy to TSM.

Now we are anticipating an excellent spring meeting 2008 in Austin. We are indeed fortunate to already have local contacts in place. Paulo Ferreira, with the help of Miguel Yacaman, will be smoothing the way for us. Keynote speakers are already being lined up for this meeting. I cannot stress enough the importance of such local contacts. It is of vital importance that the Program Chair has clear and frequent access to these contacts during the planning period.

I have heard from several members concerned with the health of our Society about the need to undertake long-range planning for future meetings. I completely concur with this sentiment. This planning would include not only future locations, but would include the

invitation of distinguished speakers. This summer Ann Ellis and I attended the breakfast held for the officers of local affiliates while at the Microscopy Society of America in Fort Lauderdale, Florida. We were encouraged to invite speakers on the MSA speakers list for our meetings. I invited three speakers from this list, but all had prior commitments on the date of our fall meeting and expressed willingness to speak either next spring or some other time in the future. This clearly demonstrates the need to plan ahead.

Another issue that has arisen is the number of meetings per year. I have heard from some corporate members that coming to two meetings per year stretches their budget. The issue of one meeting vs. two meetings per year is something to explore and I would like members to give it a thought.

Finally, I would like to express how pleased I am to see that the Texas Society for Microscopy is alive and well. We serve as an excellent platform for students and young investigators to present their work. But beyond this, I think it is vital that faculty and staff also present papers and serve as role models for younger investigators. I think it would be excellent if we could recruit new members and encourage larger participation of students, faculty, and staff in biology departments and medical schools across the state. We are extremely pleased to see the strong representation in the material sciences, but the Texas Society for Microscopy encompasses all forms of microscopy. Membership and participation are vital to the health of our Society.

Ernest F. Couch
2007-2008 President,
Texas Society for Microscopy

Call For Papers

Manuscripts for publication in the Texas Journal of Microscopy are accepted any time. Please, send your work as research articles, review articles, or short communications in biological sciences, materials science and other disciplines employing microscopy techniques to:

Camelia G.-A. Maier, TSM Journal Editor
Department of Biology, TWU, Denton, Texas 76204-5799
(940) 898-2358, cmaier@twu.edu

CORPORATE MEMBERS



4pi Analysis, Inc.

Wendi Schierlinger
3500 Westgate Drive, Suite 403
Durham, NC 27707
(281) 282-9897
wendis@4pi.com

Applied Precision LLC

Monica Robinson
1040 12th Ave. NW
Issaquah, WA 98027
(425) 829-1193

Atomic Spectroscopy Instruments, Inc.

Graham R. Bird
1021 Yellow Rose Dr., PO Box 1035
Salado, TX 76571-1035
Phone/FAX (254) 947-8929
grbird@thegateway.net

Boeckeler/RMC Instruments, Inc.

Dave Roberts
4650 Butterfield Drive
Tucson, AZ 85714
(520) 745-0001 FAX (520) 745-0004
dave@boeckeler.com

Brook-Anco Co.

Richard Blair
7462 Dogwood Park
Fort Worth, TX 76118
(800) 388-7566
rick@brookanco.com

Bruker AXS (PGT)

Alan Hollaar
5465 E. Cheryl Parkway
Madison, WI 53711-5373
(805) 523-1882 FAX (805) 523-1896
Alan_Hollaar@bruker-axs.com

CARL ZEISS SMT

German Neil
1 Zeiss Dr.
Thornwood, NY 10594
(914) 747-7700 FAX (914) 681-7443
neal@smt.zeiss.com

EDAX, Inc.

Tina Wolodkowich
Sales & Marketing Coordinator
(201) 529-6277 FAX (201) 529-3156
Tina.Wolodkowich@ametec.com

Electron Microscopy Sciences/Diatome

Richard Rebert/Stacie Kirsch
1560 Industry Road, PO Box 550
Hatfield, PA 19440
(800) 523-5874
sgkck@aol.com
www.emsdiasum.com

EMITECH

Linda Dailey
PO Box 680221
Houston, TX 77268
(281) 580-0568 FAX (281) 580-0593
emitech@earthlink.net

Evex, Inc.

Caudio Tarquinio
852 State Road
Princeton, NJ 08540
(609) 252-9192

FEI Company

Dennis Richards
8522 Old Quarry Drive
Sugar Land, TX 77479-1970
(281) 545-1353 FAX (281) 545-1393
drichards@feico.com
www.feicompany.com

Gatan, Inc.

Chad Tabatt
5933 Coronado Lane
Pleasanton, CA 94588
925-224-7318
ctabatt@gatan.com

Hamamatsu Photonic Systems

Butch Moomaw
360 Foothill Road
Bridgewater, NJ 08807-0910
(830) 885-2636 FAX (830) 885-7339
BMoomaw@hamamatsu.com

Hitachi High Technologies America

Kevin Cronyn
1375 N 28th Ave., PO Box 612208
Irving, TX 75261
(972) 615-9086 FAX (972) 615-9300
Kevin.Cronyn@Hitachi-hita.com

IXRF Systems

Travis W. Witherspoon
15715 Brookford Drive
Houston, TX 77059
(281) 286-6485
travisw@ixrfsystems.com
www.ixrfsystems.com

JEOL USA, Inc.

Zane Marek
District Sales Manager
13810 Paisano Circle
Austin, TX 78737
(978) 495-2176

Leeds Instruments, Inc.

Alex Butzer / Jeff Lovett
8150 Springwood Drive, Ste. 125
Irving, TX 75063
(972) 444-8333 FAX (972) 444-8435
abutzer@leedsmicro.com
jlovett@leedsmicro.com
www.leedsmicro.com

Leica Microsystems, Inc.

Robert Seilor
2345 Waukegan Road
Bannockburn, IL 60015
(847) 922-8902 FAX (847) 362-8873
robert.seiler@leica-microsystems.com
www.leica-microsystems.com

M.E. Taylor Engineering, Inc.

SEMicro Division
21604 Gentry Lane
Brookeville, MD 20833
(301) 774-6246
www.semsupplies.com

Meyer Instruments

Rob Meyer
1304 Langham Creek, Ste. 235
Houston, TX 77084
(281) 579-0342 FAX (281) 579-1551
ces@meyerinst.com
www.meyerinst.com

Micro Star Technologies, Inc.

Cathy Ryan
511 FM 3179
Huntsville, TX 77340
(936) 291-6891 FAX (936) 294-9861
mistar@msn.com

Nanotech America

Kim Kanggasniemi
313 S Jupiter Road, Suite 105
Allen, TX 75002
(972) 954-8014
Kim@nt-america.com

Oxford Instruments, Inc.

John Haritos
6535 E. Superstition Springs Blvd., # 126
Mesa, AZ 85206
(512) 246-7551
haritos@ma.oxinst.com

Smart Imaging Technologies

Ira Bleiweiss
1770 St. James Place, Suite 414
Houston, TX 77056
info@smartimtech.com

Structure Probe Inc.

Charles A. Garber, Ph.D.
Div. of Structure Probe, Inc.
569 East Gay St.
West Chester, PA 19381-0656
http://www.2spi.com/

Ted Pella, Inc.

James Long
1807 Slaughter Lane #200-487
Austin, TX 78748
(512) 657-0898 FAX (530) 243-3761
James_Long@TedPella.com

Thermo Electron Co.

David Leland
2551 W. Beltline Hwy
Middleton, WI 53562-2609
(970) 266-1164 FAX (408) 516-9882
david.leland@thermo.com
www.thermo.com

Tousimis Research Corporation

Melissa Dubitsky
2211 Lewis Ave.
Rockville, MD 20851
(301) 881-2450 FAX (301) 881-5374
www.tousimis.com

TSM Member Honored with Cornelia Marschall Smith Professor of the Year Award

Ann E. Rushing, TSM past president, professor and associate chair of biology, was honored with the Cornelia Marschall Smith Professor of the Year Award by Baylor University at the annual Honors Convocation in spring 2007. This annual award, based on teaching, research, and service criteria, is presented to a Baylor faculty member who makes a superlative contribution to the learning environment at Baylor.

Dr. James Bennighof, vice provost for academic affairs and policy at Baylor University characterized Ann as follows: "Her contributions to learning at Baylor include not only teaching and mentoring students at all levels and pursuing her own independent research agenda, but also devising innovative ways of combining teaching and research that open exciting new opportunities to students" (Baylor University News).

Ann earned her bachelor's degree in botany magna cum laude from Duke University, an MS in biology from the University of Cincinnati, and Ph.D. in botany from Texas A&M University. Before joining Baylor, Rushing conducted post-doctoral research at the University of Illinois and was a research associate at the Muséum Na-

tional d'Histoire Naturelle in Paris and at Auburn University, where she studied electron microscopy and taught for a year in the general biology program.



Ann has been part of the faculty at Baylor in the Department of Biology and Institute of Biomedical Studies since 1989. Currently, she teaches several undergraduate courses, including general biology for majors and non-majors, an undergraduate biology seminar, electron microscopy and plant anatomy, helped develop and teach the Natural World sequence of integrated, interdisciplinary science courses for the Baylor Interdisciplinary Core (BIC), and directs the department of biology summer undergraduate research program. She also serves

as director of the departmental electron microscope facility and supervises undergraduate and graduate research projects that use electron microscopy. Her research interests include the ultrastructure and development of plants, particularly bryophytes; comparative sporogenesis, spermatogenesis, and sperm morphology in bryophytes; and systematics of plants. Her research has been published in numerous scholarly publications and journals, and she has presented her findings at conferences and meetings around the country.

EPICARDIAL FORMATION *IN SITU* AND IN CULTURE

JESSICA GREEN, RANDY CROSSLAND, AND J. KEVIN LANGFORD*

Department of Biology, Stephen F. Austin State University, Box 13061 SFA Station, Nacogdoches, Texas 75962

ABSTRACT

The epicardial layer of the heart was once thought to be derived from the primitive myocardium. Recent evidence demonstrates that it derives from the proepicardium (PE). During the early 1980s, several scanning electron microscopic studies described the migration of the mesothelial cells from villous projections of the PE onto the myocardial surface of the heart, thus creating the epicardial layer and a matrix-filled subepicardial space. Mesenchymal cells, present within the core of the PE, populate this space and give rise to the coronary vasculature of the developing heart. To better understand the growth and migration of these cells during developmental processes, cells derived from the PE have been observed in tissue culture on and within type I collagen lattices. While this is a well accepted model for tissue culture, the current study compares the morphology of epicardial cells *in situ* with that observed in culture using scanning electron microscopy. Cells present at the leading edge of the enlarging sheet of epicardium *in situ* displayed numerous filopodia as well as thin ruffling of the plasmalemma. On the surface of the most established area of the epicardium, the classic cobblestone morphology of mesothelial cells was evident. Small surface projections were common at the cellular junctions of these surface cells. In culture, the same cobblestone morphology and short projections were present throughout the epicardial cells. However, few filopodia were present at the edge of the mesothelial sheet in culture. This morphological difference may be due to the different substrates these cells were being challenged to spread upon, (*i.e.*, myocardial cells *in situ* and type I collagen in culture). Epicardial cells within the confluent sheet likely are spreading on epicardially-derived matrix, similar to that present in the subepicardial space. This study illustrates that, while collagen type I serves as an adhesive and migratory substratum for studying morphological processes, the interpretations must be tempered with the understanding that cells are continually modifying their substratum in culture, as they do *in situ*.

INTRODUCTION

Cardiac morphogenesis proceeds through defined developmental stages to transform mesodermal precursor cells into a functional organ, comprised of three distinct tissue types: the inner endocardial layer; the middle myocardium; and the outer epicardial covering of the heart. While the origins of the endocardium and myocardium have been well established (1), only since the late 1970's has the origin and the mechanisms leading to the formation of the epicardium been investigated in depth. Once thought to arise from precursor cells within the primitive myocardial layer (2), the epicardium has been definitively demonstrated to be derived from the extracardiac mesoderm of the proepicardium (3).

Although distinct origins for the epicardium and myocardium were suggested as early as 1909 (4), PE as the source of epicardial precursors was investigated first with TEM by Manasek in 1969 (5). Using SEM, Ho and Shimada (6) and Viragh and Challice (7) further demonstrated that PE was the source of epicardial precursors. These early and thorough investigations demonstrated that PE first forms as a mesothelial outgrowth adjacent to the developing liver and to the right of the sinus venosus (8).

Resembling a "cluster of grapes", PE enlarges and exhibits villous projections, covered with mesothelial epicardial precursor cells, which extend toward the atrioventricular sulcus of the early heart. In recent years, the mechanisms by which these mesothelial cells are transferred onto the myocardial surface of the heart have been debated. Proepicardium cells in avian species appear to utilize an extracellular matrix bridge to span the remaining distance between the villous projections of the PE and the heart surface (9). While this may also be the mechanism used in fish and mammals (10), some investigations have suggested that free-floating vesicles transport mesothelial cells to the myocardial surface in these species (3). Regardless of the mode of transport, once the PE mesothelial cells make contact with the AV sulcus of the heart, the cells migrate onto the surface, and expand in all directions to completely invest the developing heart with its outer layer, the epicardium.

Initially, epicardial cells utilize myocardial cells as a migratory substrate; however, as the epicardial sheet expands, a subepicardial space is created and filled with extracellular matrix molecules to which the overlying epicardial cells adhere (11). As more matrix is generated, the epicardium becomes increasingly separated from the myocardium. The expanding subepicardial space is then populated with mesenchymal cells, produced by an epithelial-mesenchymal transition of the proepicardially-derived cells (12), that give rise to many cells critical to cardiac morphogenesis and coronary function including coronary endothelium, smooth muscle cells, interstitial fibroblasts and atrioventricular cushion mesenchymal cells (11). In fact, the majority of the coronary arterial system is generated from cells of the PE (13).

The pluripotency of the PE-derived cells has garnered much attention of developmental biologists in recent years and generated numerous in-culture and chimeric model systems to try to decipher the cellular mechanisms required for such divergent cellular differentiation pathways. Since the subepicardial space is rich in extracellular adhesive proteins (14), including collagens, collagen lattices have been a commonly used substrate within which to assess the development of these precursor cells, as well as vehicles in which to manipulate growth conditions. Relative to cardiac morphogenesis, hydrated collagen gels have long been used to investigate the mechanisms active during the epithelial-mesenchymal-transition of the atrioventricular cushions (15) and the subsequent migration of the resultant cardiac mesenchyme (16, 17). Recently, a 3-dimensional collagen tube has been used in an attempt to more closely duplicate the physical environment and physical forces acting upon the migrating and differentiating PE-derived cells (10). However, little attention has been given

* Corresponding author

Phone (936) 468-2258

Fax (936) 468-6256

Email: Klangford@sfasu.edu

to the affect of these artificial substrates on the epicardial cells themselves.

In the present study, avian early PE cells were microsurgically explanted onto the surface of hydrated collagen gels and the resulting spread of surface epicardial cells observed. The morphology of these cells was directly compared to that of their *in situ* counterparts using SEM. Surface proepicardially-derived cells within the confluent portion of the cellular sheet possessed the flattened morphology and surface plasma membrane projections similar to those observed *in situ*. However, cells along the leading edge of the investing cellular sheet showed remarkable differences in culture. This morphological difference was overcome by cells forming a confluent cell layer in culture, most probably due to the adhesion molecules being produced and deposited beneath the epicardial cells. It seems that the adhesive substrate for the confluent cells is likely similar in culture to that found *in situ* and results in a similar morphology and possible similar level of cellular activity. Together, these data demonstrate that while the morphology of early epicardial precursors may be dissimilar from that occurring *in situ*, established layers of epicardially-derived cells on collagen lattices may represent a suitable model system for investigating the role of the subepicardial extracellular molecules, and the impact alterations of these proteins may play on epicardial formation and ultimately coronary morphogenesis.

MATERIALS AND METHODS

Preparation of hydrated collagen lattices – Collagen gels were prepared as previously described (15). Rat tail collagen type I (BD Biosciences, San Jose, CA) was diluted to a final working concentration of 1mg/ml as follows. Keeping all solutions chilled on ice, an appropriate volume of stock collagen was added to 50% volume of sterile water (e.g., a total working volume of 15 mls would require the volume of water added be 7.5 mls). After gently mixing by inversion, a 1/10 volume of 10x Media 199 (Gibco, Grand Island, NY) was added and mixed. To neutralize the acid present in the stock collagen solution and initiate polymerization, a 1/10 volume of 0.14 M NaOH was added and mixed by inversion. Additional sterile water was added at this point to adjust the volume to the desired final working volume. This diluted and neutralized collagen solution was then transferred using aseptic techniques to the appropriate tissue culture vessels. In this study, we used 1.3 mls of diluted collagen solution per 35 mm culture dishes. To finalize the polymerization of the collagen gels, the solutions were transferred to a tissue culture incubator at 37°C, 95% air and 5% CO₂ for 1 hour. Upon completion of polymerization, the gels were carefully equilibrated with “incomplete medium” (1x Medium 199 with 5000 µg/ml of penicillin, 5000 mg/ml of streptomycin (BD Biosciences, San Jose, CA) and 250 mg/ml of Fungizone (Invitrogen, Carlsbad, CA) for 1 hour at 37°C. The solution was replaced with fresh incomplete medium until 24 hours prior to explanation of embryonic tissue at which time the solution was decanted and replaced with “complete medium” (incomplete medium with 1% chicken serum (Biomeda, Burlingame, CA), 5mg/ml of insulin, 5mg/ml of transferrin, and 5ng/ml of selenium; BD Biosciences, San Jose, CA).

Proepicardium microdissection and tissue culture – Fertilized white leghorn chicken eggs (*Gallus gallus*) were incubated in a humidified chamber at 37.5°C until the appropriate stage [Hamburger-Hamilton (HH) stage 15-16] for the isolation of PE (18). Embryos were transferred into a sterile phosphate buffered saline solution (PBS, pH 7.4) and the PE microsurgically removed and explanted onto the surface of the collagen gels, which had been decanted of the complete medium. The PE explants were allowed to attach to the collagen gels for 24 hrs at 37°C before fresh complete medium was added to the cultures. PE cultures were allowed

to incubate and were processed for SEM at 24 hour intervals. For those cultures that incubated longer than 48 hours, the culture medium was decanted and replaced with complete medium every 48 hours.

Tissue fixation and SEM – PE explants, along with surrounding collagen, which contained epicardial and mesenchymal cells, were excised from the collagen culture and fixed in a solution of 2.5% (v/v) glutaraldehyde in PBS (pH 7.4). Likewise, embryonic chick hearts were excised and chemically fixed in the same manner. The samples were incubated in fixative overnight, at 4°C. Following three 15-minute washes in PBS, the samples were further fixed in a solution of 1% (v/v) osmium tetroxide in PBS (pH 7.4) for 2 hours at 4°C. Samples were then processed through two 10-minute rinses in distilled water. Dehydration of the samples was accomplished through 15-minute graded ethanol washes, until the tissues were equilibrated in 100% ethanol. All liquid was removed from the samples through critical-point-drying and the samples were coated with gold-palladium in a Denton Desk-II sputter coater. A Hitachi S2300 SEM was used to view the samples and micrographs documented on Kodak TMAX-100 Pro film. Micrographs presented are representative of cultures or hearts from a minimum of three independent samples for each *in situ* stage or each time point in culture.

RESULTS

Epicardial formation *in situ* – Although long believed to be derived from precursor cells which give rise to both the epicardium and myocardium, PE has clearly been established as the epicardial anlagen (3). Beginning at HH stage 16, the avian PE originates as a dorsal outgrowth of the intraembryonic coelom adjacent to the liver (19). The “grape-like” PE consists of villous projections comprised of a mesothelial sheet covering a mesenchymal cell core (20). Initially, these mesothelial cells displayed a distinct rounded and somewhat flattened appearance, characteristic of most epithelial (or mesothelial) cells (Fig. 1A, C). As the PE enlarges, the villous projections extended toward the bare myocardium of the atrioventricular sulcus. Upon contact with the surface myocardial cells, mesothelial cells elongated and migrated away from the villous projections of the PE and formed colonies of epicardial-precursors on the surface of the early heart (21) (Fig. 1B, D).

From these foci, cells spread over the myocardium to completely invest the heart with the outermost layer, the epicardium. This expansion of the epicardium relies on cellular proliferation as well as active cellular migration, thus creating two morphologically distinct regions of the epicardial layer: the leading edge (migratory border), and the more established cells within the confluent area of the epicardium. Cells of the latter displayed the distinctive cobblestone appearance of epithelial cells with numerous apical processes present on the surface of the cells (Fig. 1E). The majority of these cell surface specializations were concentrated on the periphery of the cell surface and intercellular spaces. In contrast, cells along the leading edge, the first to make contact with myocardial cells, displayed features characteristic of actively migrating cells (*i.e.*, filopodia and extensive ruffling of the plasma membrane; Fig. 1F).

Epicardial growth in culture – Culture systems have long been used to dissect the mechanisms of cellular adhesion and migration. The following are data illustrating the spreading and morphology of epicardial precursor cells on a hydrated collagen substrate. When isolated PE (from HH stage 16, prior to myocardial contact) was placed in culture, the primary explant retained a mesothelial/epithelial morphology (Fig. 2A-C), although the cells were less rounded than those present *in situ* (Fig. 1A-C).

The PE cells retained the above morphology even after several

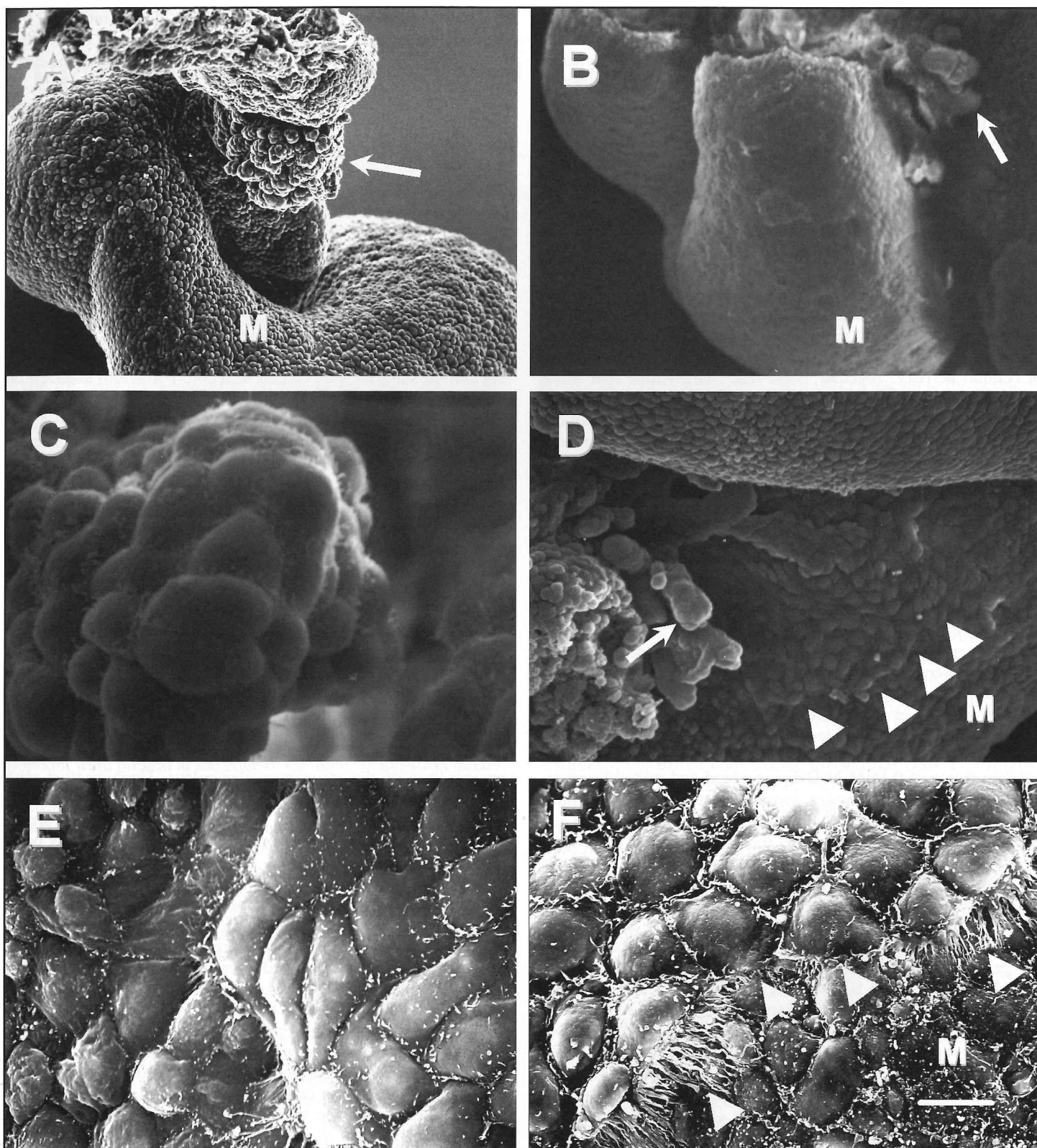


Figure 1. Representative SEMs of the *in situ* chicken proepicardia and proepicardially-derived cells. (A) HH stage 15 heart displaying PE beneath the sinus venosus. (B) Villous projections (arrow) of a HH stage 18 PE, which has made contact with the myocardial surface. (C) High magnification view of the mesothelial cells which cover a proepicardial villous projection. Note the small membrane projections at the lateral borders of each cell. (D) Epicardial cells spread onto the surface of the myocardium of a HH stage 18 heart. Arrowhead – leading edge of epicardial layer. (E) Epicardial cells exhibiting a characteristic epithelial morphology and continuing to display membrane processes. (F) Epicardial cells at the leading edge extend elongated filopodia and display ruffling of the free membrane surface, typical of migratory cells. Arrowhead – leading edge of epicardial layer. Scale Bar = 118 μ m (A, B); 7 μ m (C); 42 μ m (D); 13 μ m (E, F).

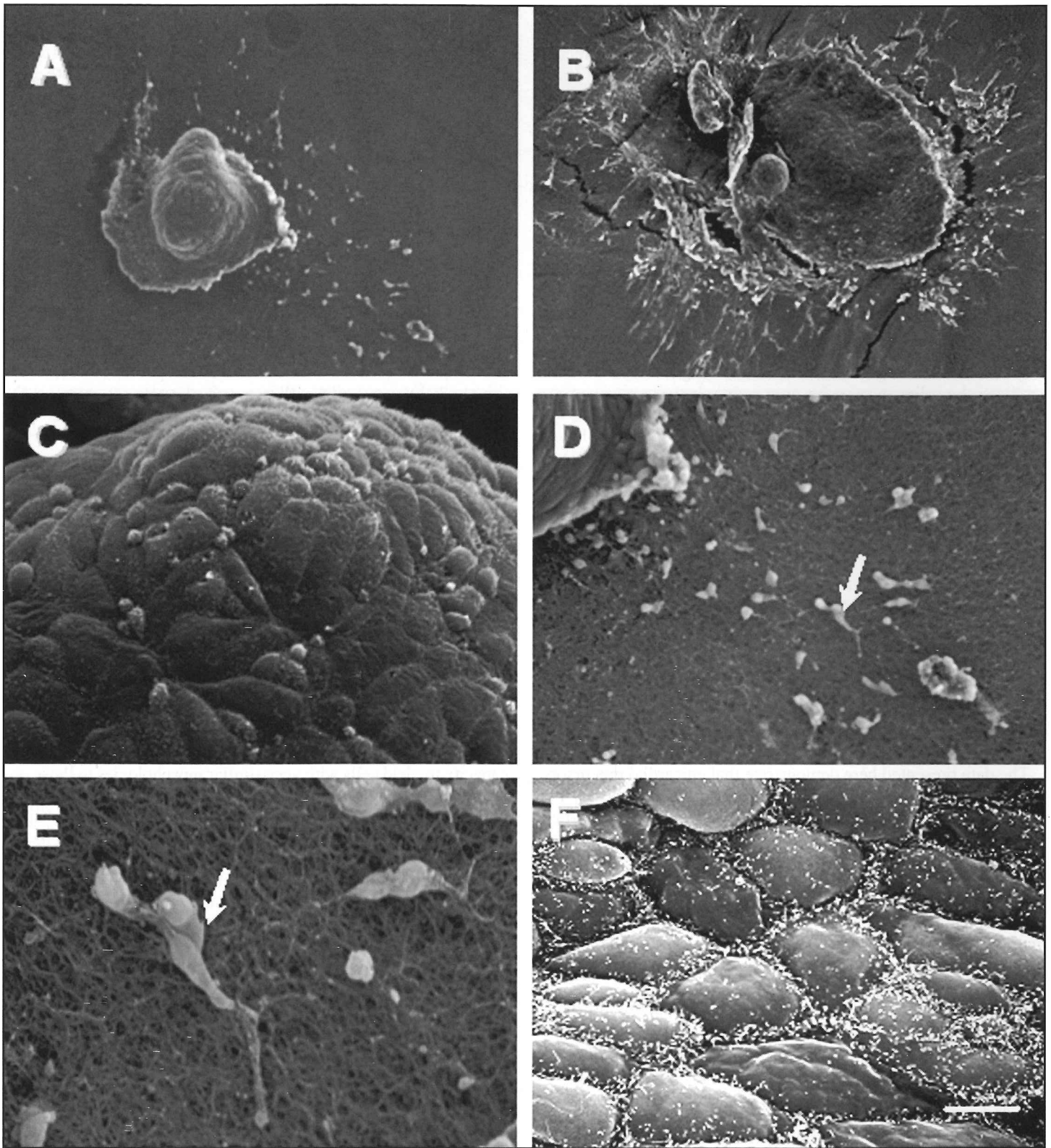


Figure 2. Representative SEMs of explanted proepicardia and proepicardially-derived cells in culture. (A) Proepicardium grown in culture for 24 hours demonstrating the spread of individual proepicardially-derived cells migrating on the collagen gel surface. (B) After 72 hours in culture, the extent of epicardial spreading, and the number of migrating mesenchymal cells has greatly increased. (C) High magnification view of the original proepicardial explant which continues to display the mesothelial morphology after 24 hours in culture. (D) Individual proepicardially-derived cells are visible migrating away from the original explanted tissue. (E) Many of these migratory cells display a mesenchymal-like morphology. (F) Cells within the epicardial layer display the characteristic "cobblestone" appearance and membrane projections that were observed *in situ*. Arrow – proepicardially-derived mesenchymal cells migrating along the collagen gel surface. Scale bar = 143 mm (A); 286 mm (B); 13 mm (C, F); 67 mm (D); 18 mm (E).

days in culture (Fig. 2B, D) and resembled established epicardial cells *in situ* (Fig. 1E). Unlike the *in situ* spreading of epicardial cells as a confluent sheet of cells, in culture, individual precursor cells initially migrated away from the primary explant (Fig. 2A). These pioneering cells lost their epithelial characteristics in favor of a more mesenchymal appearance (Fig. 2E). With continued growth in culture, a confluent sheet of epithelial cells became more distinct, comprised of cells with the same characteristics of established epicardial cells *in situ* (Fig. 2F). These data suggest that, while initial epicardial precursor cells display distinctly different morphologies in culture when compared to their *in situ* counterparts, these cells within the confluent sheet of epicardial cells do have the capacity to establish an *in situ* appearance after several days in culture.

The cells at the leading edge of PE cultures grown for several days displayed a smooth plasma membrane on the free surface devoid of any cell surface specializations rather than elongated filopodia and ruffling as observed *in situ* (Fig. 3A). Other cells visible in the collagen gel cultures appear to be migrating mesenchymal cells. *In situ*, these cells initially populate the subepicardial space where they contribute cells to the coronary vasculature as well as form cells that migrate within the myocardial layer. These areas are not visible from the external surface of the heart, but appear to be mimicked in the PE cultures on collagen gels. Mesenchymal cells could clearly be seen migrating within the collagen lattices, especially near the leading edge of the epicardial sheet (Fig. 3B). Groups or chains of mesenchymal cells are also evident in these cultures and are possibly the earliest indication of angioblastic groups of vascular precursors (Fig. 3C). In culture, the subepicardial space is not visible from the surface, however, at the leading edge, cells with only a few broad processes appear to invade the collagen gel from beneath the layer of epicardial precursors and likely are synonymous with subepicardial mesenchymal cells (Fig. 3D).

DISCUSSION

The data presented here demonstrate that epicardial precursors can produce confluent layers of cells in culture that closely resemble epicardial cells *in situ*. This similarity is in sharp contrast with the differences observed when leading edge cells were compared. The elongated filopodia and membrane ruffling present on cells *in situ* were absent from the free surface of cells on collagen gels. Although collagens have been shown to be a component of the subepicardial space, additional adhesive molecules, deposited by the epicardial cells themselves, likely are responsible for the maintenance of (*in situ*) and the eventual establishment of (*in culture*) this morphology.

The pioneering PE cells which must attach to and migrate upon the myocardial surface likely utilize similar adhesive cell surface molecules, or membrane bound adhesive ligands (14), that the epicardial cells at the leading edge adhere to *in situ*. Although the exact molecules and epicardial receptors used for the migration and spreading of epicardial cells remains unknown, several likely candidates have been implicated. The myocardial vascular cell adhesion molecule (VCAM-1) and the epicardial $\alpha 4$ subunit bearing integrins ($\alpha 4\beta 1$ and $\alpha 4\beta 7$) likely play an essential role in the formation and maintenance of the epicardium (22). Mice deficient in either VCAM (23) or $\alpha 4$ (24) fail to form an intact and sustainable epicardium and thus are lethal mutations.

Clearly, a collagen lattice is a distinctly different substrate encountered by leading cells in culture when compared to the *in situ* adhesive substrate of the myocardium. This distinction likely accounts for the altered morphology exhibited by these cells in culture. Interestingly, precursor cells appear to have the capacity to regain their *in situ* morphology within the confluent areas

of the epicardial sheet while in culture. Because the epicardium plays a role in the production of subepicardial matrix molecules (22), the reiteration of the *in situ* morphology, after a short time in culture, is likely due to the modifications in the substrate upon which the cells adhere.

Extracellular matrix components have long been known to have a tremendous regulatory impact on cellular morphology and activity. Epithelial cells growing on a thin film of collagen will appear morphologically dissimilar to the same cell type grown on different adhesive substrates (25). Furthermore, similar cells will exhibit distinct activities when grown on attached collagen gels versus free floating collagen rafts (26). Since epicardial cells have been shown to be a source of subepicardial extracellular matrix proteins, it is likely that these activities continue in culture and once an appropriate adhesive substrate has been generated, the *in situ* morphology of these cells can be accomplished in collagen gel cultures. PE-derived adhesive molecules offer but one possible explanation for the differences in morphology observed in this study. Future studies will be required to demonstrate that the molecules deposited *in situ* are also produced in culture.

An additional factor that may contribute to the delay in the expression of an *in situ* morphology may simply be a recovery period of the tissue resulting from the microsurgical manipulation of the primary explant. While this stress placed on the tissue is unavoidable, it will be a variable considered in future functional investigations using this model system to dissect what molecules are produced by the epicardial cells and which are required for the formation of an *in situ* morphology. Similarly, the mechanical tension placed on the collagen substrate by the cells and the tissue culture vessel could play a role in the eventual shape of the cells. To begin to investigate this variable, future studies using the current adhered collagen gel system will be compared to the morphologies of cells grown on or within floating collagen rafts, thus eliminating much of the tension within the cultures. However, even when considering the possible effectors acting to shape the epicardial cells in culture, this model system clearly has the capacity to yield cells with very similar morphologies to those observed and provides an excellent means for future investigations in the role adhesive molecules play in the formation of cell shapes.

Additionally, with the absence of myocardial cells, this model system is well suited to further define the components required for epicardial adhesion and spreading and to determine which molecules of the subepicardial matrix are produced by PE derived cells. The lack of a myocardial layer is also advantageous for observing the migration and differentiation of PE derived mesenchymal cells. While these cells initially populate the subepicardial space, they migrate and contribute cells of a fibroblastic, angioblastic, hemangioblastic and smooth muscle lineage to the subepicardial space, myocardial layer and even into the endocardial cushion tissue (11). Our understanding of the cellular fate of these PE derived mesenchymal cells largely comes from studies of retrovirally-labeled PE cells reintroduced into avian embryos (27) or chimeric studies using quail and chick tissues (28). These studies have demonstrated that PE-derived cells do contribute a wide diversity of cell types to the developing heart, including much of the coronary vasculature. However, working with avian shell-less cultures, and performing embryonic surgery are often problematic. Additionally, experimental manipulation within the embryo is challenging at best and may lead to the death of the embryo prior to the end point of the experiment.

The collagen gel culture used in this study shows the clear advantage of this model over shell-less culture when the experimental questions are focused on the PE-derived cells. Mesenchymal cells migrating away from the leading edge of the epicardial sheet are clearly visible in the collagen gel cultures, many of which

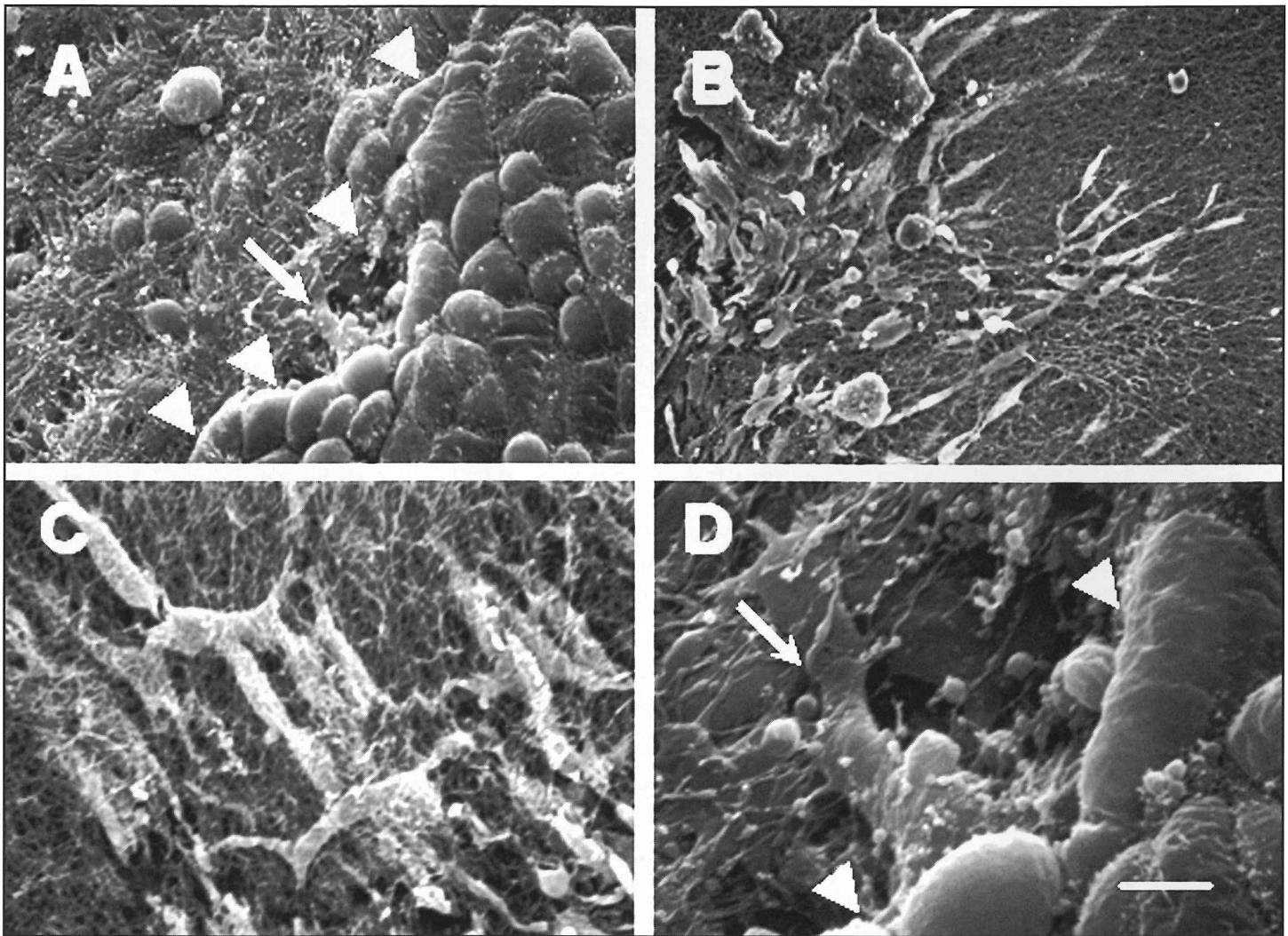


Figure 3. Representative SEMs of proepicardially-derived cells after 72 hours in culture. (A) Leading edge of epicardial sheet spreading on the collagen gel surface. (B) Numerous mesenchymal-like cells, spreading away from the leading edge of the epicardial sheet, on the surface of and within the collagen gel. (C) Higher magnification of the mesenchymal-like cells forming "chains" of cells within the collagen gel. (D) Higher magnification of a mesenchyme-like cell extending away from the leading edge of the epicardial sheet. Arrow – mesenchyme-like cell; arrowhead – leading edge of epicardial sheet. Scale bar = 14 mm (A); 48 mm (B); 16 mm (C); 5 mm (D).

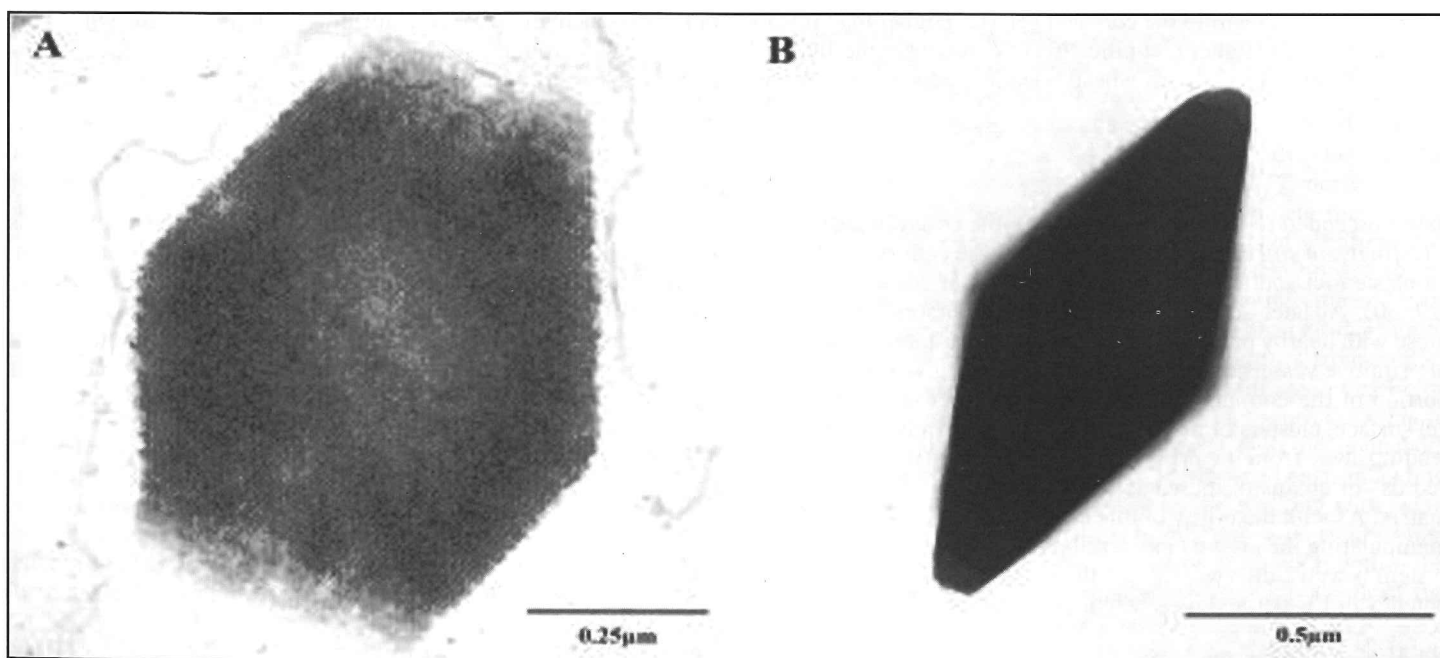
have descended to varying depths within the collagen lattice. Interestingly, *in situ* evidence suggests that these cells will form angioblastic foci and thus initiate the formation of coronary vessels (29, 30). At later stages, these vascular precursors will anastomose with nearby precursors and, in doing so, establish a network of primitive vessels that will be remodeled and give rise to a large portion of the coronary arterial system (30). From the collagen gel surface, clusters of mesenchymal cells are easily observed extending away from the primary explant and appear to be forming "cords" or chains of mesenchymal cells throughout the collagen matrix. As with the utility of this model system for observing and manipulating the growth and development of epicardial cells, this system is well suited to examine the differentiation and the pluripotency of PE-derived mesenchymal cells.

Much effort is being placed into understanding the mechanisms active within the PE-derived cells in the hopes of activating stem cells within human adult cardiac tissue to potentially reiterate these developmental processes and in doing so, naturally and non-invasively repair a damaged area. *In vitro* model systems will be invaluable tools with which to reveal many of the molecular partners essential for these processes, both during cardiac morphogenesis and coronary wound repair.

LITERATURE CITED

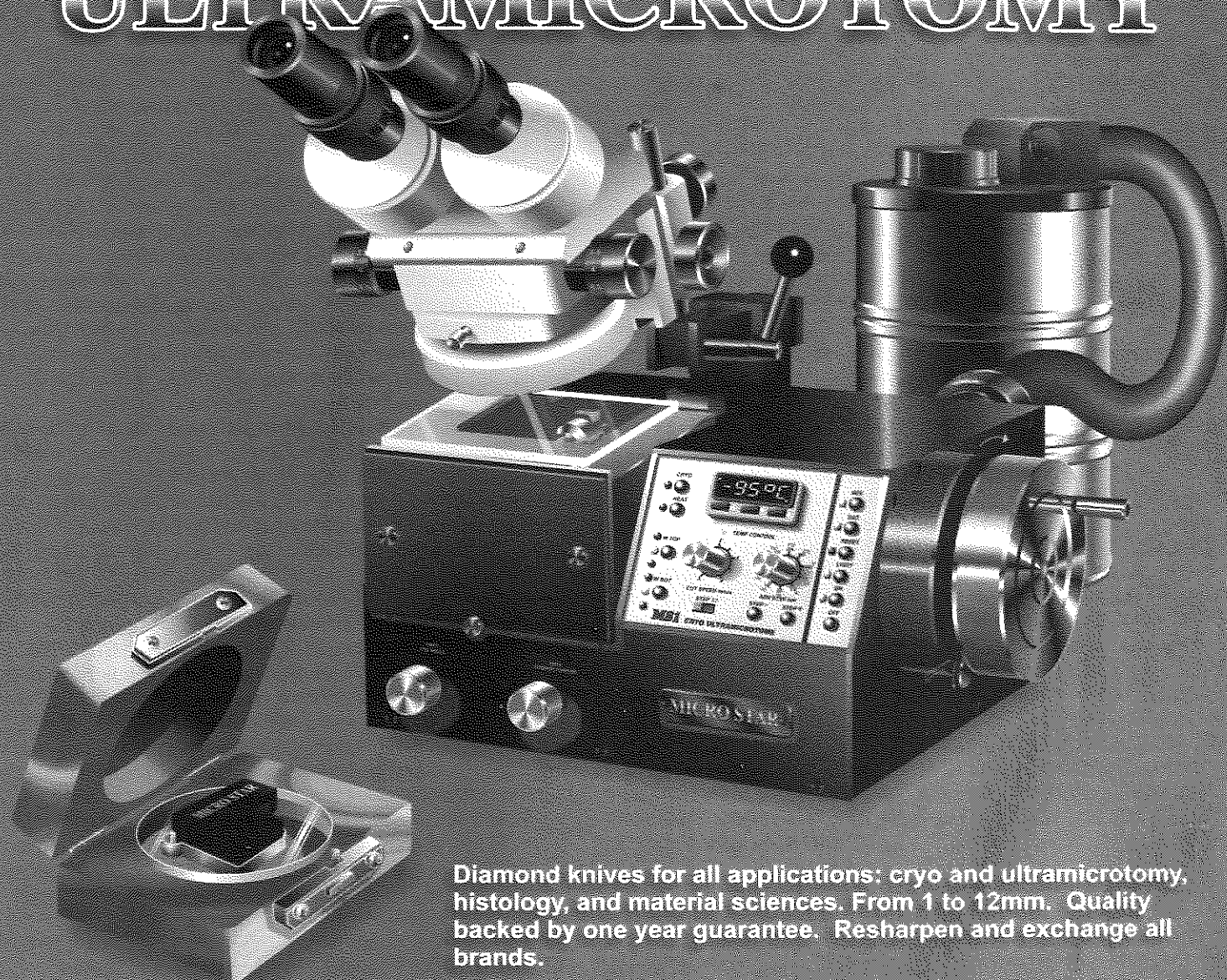
1. Manasek, F. J. (1968) *J Morphol* **125**(3), 329-365
2. Mollier, S. (1906) *Die erste Anlage des Herzens bei den Wirbeltieren*
3. Manner, J., Perez-Pomares, J. M., Macias, D., and Munoz-Chapuli, R. (2001) *Cells Tissues Organs* **169**(2), 89-103
4. Kurkiewicz, T. (1909) *Bull Acad Sci Cracovie* **1909**, 148-191
5. Manasek, F. J. (1969) *J Embryol Exp Morphol* **22**(3), 333-348
6. Ho, E. and Shimada, Y. (1978) *Dev Biol* **66**(2), 579-585
7. Viragh, S. and Challice, C. E. (1981) *Anat Rec* **201**(1), 157-168
8. Shimada, Y., Ho, E., and Toyota, N. (1981) *Scan Electron Microsc (Pt 2)*, 275-280
9. Nahirney, P. C., Mikawa, T. and Fischman, D. A. (2003) *Dev Dyn* **227**(4), 511-523
10. Nesbitt, T., Lemley, A., Davis, J., Yost, M. J., Goodwin, R. L., and Potts, J. D. (2006) *Microsc Microanal* **12**(5), 390-398
11. Wessels, A. and Perez-Pomares, J. M. (2004) *Anat Rec A Discov Mol Cell Evol Biol* **276**(1), 43-57
12. Perez-Pomares, J. M., Macias, D., Garcia-Garrido, L., and Munoz-Chapuli, R. (1997) *Dev Dyn* **210**(2), 96-105
13. Wilting, J., Buttler, K., Schulte, I., Papoutsis, M., Schweigerer, L., and Manner, J. (2007) *Dev Biol* **305**(2), 451-459
14. Munoz-Chapuli, R., Macias, D., Gonzalez-Iriarte, M., Carmona, R., Atencia, G., and Perez-Pomares, J. M. (2002) *Rev Esp Cardiol* **55**(10), 1070-1082
15. Bernanke, D. H. and Markwald, R. R. (1982) *Dev Biol* **91**(2), 235-245
16. Runyan, R. B. and Markwald, R. R. (1983) *Dev Biol* **95**(1), 108-114
17. Mjaatvedt, C. H. and Markwald, R. R. (1989) *Dev Biol* **136**(1), 118-128
18. Hamburger, V. and Hamilton, H. L. (1992) *Dev Dyn* **195**(4), 231-272
19. Bernanke, D. H. and Velkey, J. M. (2002) *Anat Rec* **269**(4), 198-208
20. Wada, A. M., Smith, T. K., Osler, M. E., Reese, D. E., and Bader, D. M. (2003) *Circ Res* **92**(5), 525-531
21. Mu, H., Ohashi, R., Lin, P., Yao, Q., and Chen, C. (2005) *Vasc Med* **10**(1), 37-44
22. Pinco, K. A., Liu, S. and Yang, J. T. (2001) *Mech Dev* **100**(1), 99-103
23. Kwee, L., Baldwin, H. S., Shen, H. M., Stewart, C. L., Buck, C., Buck, C. A., and Labow, M. A. (1995) *Development* **121**(2), 489-503
24. Yang, J. T., Rayburn, H., and Hynes, R. O. (1995) *Development* **121**(2), 549-560
25. Wicha, M. S., Lowrie, G., Kohn, E., Bagavandoss, P., and Mahn, T. (1982) *Proc Natl Acad Sci U S A* **79**(10), 3213-3217
26. Lee, E. Y., Parry, G., and Bissell, M. J. (1984) *J Cell Biol* **98**(1), 146-155
27. Mikawa, T., Borisov, A., Brown, A. M., and Fischman, D. A. (1992) *Dev Dyn* **193**(1), 11-23
28. Perez-Pomares, J. M., Macias, D., Garcia-Garrido, L., and Munoz-Chapuli, R. (1998) *Dev Biol* **200**(1), 57-68
29. Perez-Pomares, J. M., Carmona, R., Gonzalez-Iriarte, M., Atencia, G., Wessels, A., and Munoz-Chapuli, R. (2002) *Int J Dev Biol* **46**, 1005-1013
30. Kattan, J., Dettman, R. W., and Bristow, J. (2004) *Dev Dyn* **230**(1), 34-43

"Answer To What Is It?"



Transmission electron micrograph of a thin section through *Bacillus thuringiensis* (Bt) parasporal body (A) and a negatively stained body (B). The body contains a protein toxin, the alignment of which can be seen along a 115° by 65° axis in A, which is solubilized in the intestines of certain insects producing an activated protein that results in the death of the insect. **ROBERT DROLESKEY, USDA/ARS/SPARC, College Station, Texas, 77845.**

MICRO STAR ULTRAMICROTOMY



Diamond knives for all applications: cryo and ultramicrotomy, histology, and material sciences. From 1 to 12mm. Quality backed by one year guarantee. Resharpen and exchange all brands.

Cryo Ultramicrotome integrated in a single portable instrument. Designed for TEM and SPM sample preparation. Microprocessor controlled cryogenic system. Includes Dewar and complete set of attachments. Sections 25nm to 5 μ , cryo temperatures to -130°C. Fully automatic or manual operation. High precision and stability at a fraction of the cost of other systems.

Request information, manuals and complete price list, or see them at the web.

800 533 2509
FAX 936 294 9861
MICROSTARTECH.COM

MICRO STAR
TECHNOLOGIES

AVIAN PROEPICARDIAL CELLS RETAIN VASCULOGENIC POTENTIAL IN CULTURE

RANDY CROSSLAND, JESSICA GREEN, & J. KEVIN LANGFORD*

Department of Biology,
Stephen F. Austin State University
Box 13061 SFA Station
Nacogdoches, TX 75962

ABSTRACT

Cardiac morphogenesis culminates in the formation of a fully functioning heart comprised of three primary tissues, endocardium, muscular myocardium, and outer epicardium. For continued development and effective function, the heart eventually requires a coronary vascular system to supply its own tissues with essential raw material. While the origin of the epicardium and coronary vasculature remained undetermined until the early 1990's, evidence demonstrates that both have a common tissue of origin within the extracardiac tissue of the proepicardium (PE). Precursor cells within this structure have been shown to produce a number of cell types critical to the development of the heart. Using PE primary explants from avian hearts grown on collagen lattices, we confirm reports that PE-derived cells may differentiate into endothelial cells, smooth muscle cells, myocardial cells (*in vitro*) and blood cells (*via* hematopoiesis). More importantly, our data demonstrate that PE-derived cells in culture retain the capacity to form complex, multicellular vascular structures. Within the collagen matrix, lumenized structures were lined with cells expressing the endothelial marker QH-1. Additionally, these cells formed junctional complexes between adjacent cells, characteristic of endothelial cells. Cells peripheral to the endothelial cells represent pericytes or smooth muscle precursors. Cells resembling polymorphonuclear leukocytes were observed within the patent lumen of some of these structures in culture. Taken together, these data demonstrate that the PE-collagen gel model system is well suited for studying the mechanisms involved in coronary vasculogenesis.

INTRODUCTION

Cardiac morphogenesis is the sum of all the cellular and biochemical processes that must occur in a precise spatial and temporal pattern, leading to the formation of a fully functioning heart. The heart is unique in that it must perform its adult function while being constructed. The heart functions to supply the tissues of the growing embryo with the wealth of raw materials required for continued growth, beyond which simple diffusion is no longer an adequately supply. This leads to a paradox for the developing heart; it must enlarge to meet increasing demands of the body thus requiring a vascular supply of its own for the thickening cardiac muscle, which forms in response to the increasing workload of the heart.

The coronary vasculature, particularly the arterial supply, was

long believed to form *via* angiogenesis (formation of vascular branches from existing vessels) from the area of the aortic sinuses (1). As developmental biologists searched for evidence to support this hypothesis, none was found. In fact, data began to accumulate to the opposite: no angiogenic branches could be found originating from the aorta (2). Since coronary arterial flow does in fact stem from the aorta, an alternative explanation was that the vessels first formed within the cardiac tissue and were later connected to the aorta. As more observations were made, it was discovered that the formation of the coronary vascular supply always followed shortly after the formation of the epicardium. This correlation was further supported by data demonstrating that in VCAM-1/4-integrin null mice the epicardium and the coronary vasculature failed to form (3-5). Based on these studies, research efforts began to focus on the precursor tissue of the epicardium, the PE as a likely source of coronary vascular precursors.

Around stage HH15 of heart development, PE begins to develop as an outgrowth from the septum transversum on the dorsal wall of the intraembryonic coelom adjacent to the liver (6-9). The proepicardium has been described as a villous outgrowth or as a vesicular structure resembling a cluster of grapes, with each villous/vesicle containing an outer mesothelial layer surrounding an inner compartment containing extracellular matrix and mesenchymal cells (10, 11). In avian hearts, the villi will extend toward the heart, eventually making contact with the myocardium at the atrio-ventricular sulcus (AV). From this point, mesothelial cells migrate from the villi and spread over the myocardial surface forming the contiguous layer of the epicardium (9, 12-14). During the progressive spread of the epicardium along the myocardial surface, an extracellular matrix-filled space, the subepicardial space, is produced between the epicardium and the myocardium. The source of the subepicardial matrix is unclear; however, both the epicardium and myocardium appear to contribute to its formation (6). Mesenchymal cells soon populate this newly created space and appear to be produced by an epithelial-mesenchymal transition (EMT) of either or both the PE mesothelial cells or/and epicardial cells (9, 15-16).

The number of mesenchymal cells in the subepicardial space increases as the epicardium completes the investment of the heart. In certain regions of the heart, such as the AV, mesenchymal cells coalesce to form angioblasts, which are vascular precursors. Histological examination of these areas has demonstrated the formation of capillary-like structures that often contain blood-filled islands (6), suggesting that initial primitive capillaries form by vasculogenesis (*de novo* formation of blood vessels from an aggregate of endothelial precursors) (17, 18). The cells forming the lumen of the angioblasts are believed to differentiate into endothelial cells of the coronary vessels and once formed, they elongate by angiogenesis (19). As described by Bernanke and Velkey

* Corresponding author

Phone (936) 468-2258

Fax (936) 468-6256

Email - KLangford@sfasu.edu

(2002), continuation of both vasculogenesis and angiogenesis results in the formation of a complex array of capillary-sized vessels in the subepicardial space and within the myocardial layer (6). Initially starting near the AV sulcus, the capillary plexus will spread to the ventral interventricular sulcus, around the bulbus cordis region and eventually reach the truncus arteriosus forming a peritruncal ring of capillaries. Upon joining on the ventral aspect of the heart, angiogenic branches extend toward and form multiple attachments with the left and right aortic sinuses. Apoptosis then allows the developing vessel to penetrate through the aortic wall and establish a coronary arterial blood flow.

With evidence mounting in favor of the coronary vasculature originating from PE-derived cells, investigators developed creative approaches to test this hypothesis. Retroviral markers were first used to demonstrate that coronary endothelial cells (20) and smooth muscle (21) are in fact PE-derived. Manner (1999) utilized a quail-chick chimera model, in which a chicken PE was physically separated from the myocardium and explants of quail PE added. Their results showed that endothelial and smooth muscle cells of the coronary vessels were quail derived (22). Ratajska *et al.* (1995) examined the growth of coronary endothelial cells in collagen gel cultures and observed the formation of endothelial cord-like structures within the collagen matrix (23). Quail PE were cultured on a Matrigel substrate and yielded cells that expressed endothelial markers (24), including the quail endothelial specific marker, QH1 (18). More recently, a novel 3-dimensional collagen "tube" model system was used to examine the fate of rat PE-derived cells (25).

In the current study, the hydrated collagen gel model was used to examine not only the cellular fate of PE-derived cells, but also the organization and ultrastructure of the resulting vascular-like structures produced in culture. Rather than using endothelial cells from embryonic hearts, as previously examined (23), isolated avian PE were explanted onto the surface of hydrated collagen lattices and the resulting cellular structures examined by immunohistochemical and electron microscopic methods. Results demonstrate that PE-derived cells possess the capacity to produce not only endothelial chords, but also vascular structures with patent lumens. Taken together, this classical hydrated collagen gel model combined with isolated PE explants represents an excellent means by which to produce coronary vascular structures, with a greater organizational complexity than simple endothelial chords and an effective system to examine the influence of many different types of growth factors and substances on both coronary vasculogenesis and angiogenesis.

MATERIALS AND METHODS

Preparation of hydrated collagen lattices – Collagen gels were prepared as previously described (26, 27).

Proepicardium microdissection and tissue culture – Fertilized white leghorn chicken eggs (*Gallus gallus*) or Pharaoh quail eggs (B&T Quail Farm, Houston, TX) were used for the isolation of PE at HH stage 15-16 as previously described (28). The tissue cultures were performed as previously described. The explants for the tissue cultures were isolated from hearts before the PE had made myocardial contact. Once the villous projections of the PE attached to the heart, the ability to microscurgically remove the structure became increasingly challenging and resulted in portions of the PE remaining on the myocardial surface.

Tissue fixation and scanning electron microscopy – Avian PE explants, along with surrounding collagen were prepared for SEM as previously described (27).

Immunohistochemistry – Quail PE explants were chemically fixed for SEM as described in for the avian PE explants. Following fixation, the samples were routinely processed through a series of graded ethanol solutions (25% - 100%), infiltrated with the transition solvent Safeclear (Fisher Scientific, Pittsburgh, PA), embedded in paraffin and sectioned at a thickness of 5 μ m. After rou-

tine removal of the paraffin and rehydration of the tissue sections, the tissue was incubated in a blocking solution of 3% Carnation Instant Milk in PBS (pH 7.2) at room temperature for one hour. For some sections, prior to blocking, the sections were stained with hematoxylin and eosin (Fisher Scientific, Pittsburgh, PA) following routine histological procedures. Primary and secondary antibodies were each diluted in PBS containing 3% Carnation Instant Milk (pH 7.2). The primary antibody QH-1 (Developmental Studies Hybridoma Bank) was used at a dilution of 1:1000. Sections were then incubated with a fluorochrome isothiocyanate (FITC) conjugated donkey anti-mouse IgG (Jackson Immunologicals, West Grove, PA) at a dilution of 1:100. Sections were examined using an Olympus BX50F compound light microscope equipped with ultraviolet epi-illumination. Photographs were taken with a Nikon Coolpix 5000 digital camera. The micrographs presented are representative of tissue, cells and immunohistochemical patterns observed in a minimum of three independent cultures.

Transmission Electron Microscopy – Cultures of chicken PE were chemically fixed in 2.5% glutaraldehyde in PBS, pH 7.4. Although chicken PE was used in this study, no observable differences were identified between quail and chicken PE-derived cells. Following fixation in osmium tetroxide, the samples were rinsed three times with PBS, pH 7.4, for 5 minutes. Explants were further processed *en bloc* with 4% uranyl acetate (v/v) in 10% ethanol for one hour at room temperature. Dehydration of the samples was accomplished through 15-minute graded ethanol washes until the tissues were equilibrated in 100% ethanol, followed by infiltration and embedding of the samples in Spurr's resin (29). Ultrathin sections were stained with Reynold's lead citrate (30) and viewed using a Hitachi HS-9 TEM. The micrographs presented are representative of tissue, cells and vascular structures observed in a minimum of three independent cultures.

RESULTS

Individual PE-derived mesenchymal cells invade the collagen gels – In avian embryos between HH15-17, the PE can be seen as a "cluster of grapes" extending toward the myocardial surface of the heart (Fig. 1A). This structure, often erroneously referred to as the proepicardial organ (31), is transient and will expand rapidly, making contact with the surface of the heart (HH stage 17+/18) and distributing the mesothelial cells across the myocardial surface as the epicardium (Fig. 1B). In culture, explanted PE rapidly attached to the surface of the collagen gels and cells were observed migrating away from the primary tissue as early as 24 hours (earliest period observed; Fig. 1C, D). While these early observations demonstrate the migration of cells, likely PE-derived mesenchymal cells, on the surface of the gel, observations from cultures grown for 72 hours demonstrate that these migratory cells are capable of moving into the three-dimensional collagen lattice (Fig. 1E, F). Interestingly, this population of cells appears to be organizing into chords or tube-like structures within the gel. The darker collagen matrix is clearly distinguished from the light-colored lumen of the many hollow/cellular-bordered structures (Fig. 1F).

PE-derived mesenchymal cells express the endothelial marker QH-1 – To determine if the cells within the collagen gel and those lining the hollow structures were endothelial cells, quail PE were grown in culture and the resulting cells/structures were examined by immunohistochemical methods for the quail endothelial cell marker QH-1. This monoclonal antibody has been widely used as an excellent means of identifying avian endothelial cells *in situ* and in chimeric studies (22, 32). The QH-1 epitope is easily detectable as demonstrated by the *in situ* labeling of the endothelial lining of a quail heart (Fig. 2E). In the endocardial cushions, the mesenchymal cells that have formed through an epithelial-mesenchymal transition (EMT) were also slightly positive for the QH-1 epitope. In cultures of PE, intensely positive areas of the primary explant were visible (Fig. 2A-C). This may represent pre-existing

vascular structures or, as it has been suggested, vascular precursors from the liver primordium (33). Regardless of the source, PE in culture does possess cells expressing endothelial markers. More importantly, many of the migratory mesenchymal cells within the collagen lattice also expressed the QH-1 markers (Fig. 2A-D). As the population of mesenchyme within the gels was carefully examined, many instances were observed in which the cells had organized themselves into vascular-like structures, with clear, patent lumen. In most cases, the cells lining these structures expressed the QH-1 epitope, suggesting that they are in fact endothelial cells (Fig 2 A-D).

Vascular structures in collagen gels exhibit ultrastructural characteristics of blood vessels – To gain further evidence that vascular structures were being created from the PE-derived mesenchymal cells, the PE-cultures were examined by TEM. Vascular-like structures were observed in light microscopy sections (Fig. 3A, C) then examined by TEM (Fig. 3B, D). In each sample, the structures possessed a defined cell boundary that formed a contiguous lining and often exhibited tight-junctional complexes between adjacent lining cells or cellular processes, characteristic of endothelial cells (Fig. 3E, F). As has been reported from *in situ* data, perivascular cells are also generated from PE-derived cells (31). Many instances of cells peripheral to the vascular-like structures were observed in culture and may represent pericytes or smooth muscle precursors, suggesting that these structures are more complex than capillaries and may be an early stage in the formation of arterioles or venules (Fig 3B, D, 4B). Although *in situ* evidence indicated that cardiac muscle is not a PE-derived tissue (22), *in vitro* data demonstrates that under certain conditions cardiac muscle may contain PE-derived cells (34). In our cultures, approximately 50% of the primary PE explants exhibit spontaneous pulsating activity after 48 hours in culture and continues contractile activity through the duration of the culture period. In ultrastructural observation, we identified myofibrils present within the cultures, thus, likely representing cardiac muscle formation from PE-derived cells (Fig. 4B, C). While this appears to be an *in vitro* artifact, this consistent artifact may represent a useful model within which to study cardiac myogenesis. Yet another morphogenetic process can be observed in these collagen gel/PE cultures. Hematopoiesis has also been a described process that PE cells may undergo to yield blood cells (31). Within the patent lumen of a few of the vascular structures cells resembling polymorphonuclear leukocytes were observed, demonstrating that the capacity to undergo hematopoiesis is retained in PE cultures.

DISCUSSION

Until the past few decades, the origin of the epicardium and the coronary vasculature remained unsolved. However, through creative experimental designs and diligent research efforts, data clearly denoted the PE and PE-derived cells as the source of coronary endothelium and vascular peripheral cells. In the current study, we show that PE-derived cells do in fact have the capacity to differentiate into many different cell types. Moreover, these data demonstrate that the PE-derived cells are fully capable of organizing into complex, multicellular vascular structures in culture, exhibiting patent lumen lined with cells expressing the QH-1 marker (thus demonstrating that they are of endothelial lineage). Furthermore, endothelial cells create junctional complexes that define the lining of these hollow structures and resemble those observed in vascular endothelial cells *in situ*. Interestingly, PE-derived cells also may form perivascular structures in culture. Many examples of vascular structures grown in culture possessed cells peripheral to the endothelial cells and likely represent pericytes or early stages in the formation of vascular smooth muscle. However, data suggests that the driving force behind much of the

cellular determination and differentiation occurs *via* soluble factors in the cellular environment.

A myriad of growth factors reside within the developing cardiac tissue and many become sequestered within the subepicardial space, an ideal location upon which to direct the EMT and influence the cellular fate of PE-derived mesenchyme. Vascular endothelial growth factor (VEGF) (24), bone morphogenetic protein (BMP) (34, 35), transforming growth factor beta (TGF β) (36), platelet derived growth factor (PDGF) (37), and fibroblast growth factor (FGF) (38) are active constituents in cardiac tissue and play major roles throughout cardiac morphogenesis (34). As reviewed by Wessels and Perez-Pomares (2004), these distinct factors have, at times during cardiac morphogenesis, overlapping or antagonistic impacts on cellular differentiation of PE-derived cells (31). Thus, FGF, TGF β , and BMP2, -4 appear to promote the EMT of epicardial cells into subepicardial mesenchyme to begin the process of forming the anlagen of the coronary vasculature and connective tissue elements of the heart. However, VEGF also is involved in the differentiation pathway leading to endothelial cells and blood elements. PDGF and TGF β appear to be essential in determining PE-derived mesenchyme to follow a smooth muscle or fibroblastic cell fate. Interestingly, while these many factors cooperate *in vivo* to complete cardiac morphogenesis, many of these same processes that govern coronary vascular development proceed in cultures of PE explants. These studies suggest that while the myocardial layer may play an important role in directing the formation of structures *in vivo*, many of these cellular pathways are determined prior to excision and *in vitro* examination.

Many *in vitro* studies have shown the capacity of PE-derived mesenchyme to form endothelial cells when removed from the context of the developing cardiac tissue (31, 34, 38). However, the production of endothelial cells alone remains far removed from the processes required to form more complex vascular structures, such as arterioles. *In vivo*, the processes leading to coronary vascular development begin in regions of the heart where the subepicardial space is most heavily populated with mesenchymal cells. In these areas, mesenchymal cells begin to aggregate together into structures known as hemangioblasts that give rise to endothelial cells and blood elements through the process of vasculogenesis, the *de novo* formation of blood vessels (6). In the present study, we have observed evidence for this process. The presences of small, endothelially-lined compartments, as well as the observation of blood elements within the lumen of some of these structures suggest that vasculogenesis and hematopoiesis have produced these cells and structures in culture.

In vivo, the newly developed endothelial cells recruit adjacent mesenchymal cells and induce their differentiation into smooth muscle or other cell types by the release of factors such as PDGF, FGF-2, or epidermal growth factor (EGF). Evidence thus far suggests that PDGF is involved in the proliferation and migration of mesenchymal cells towards developing vessels (37). Again, data from the current study demonstrates that PE-derived cells possess the capacity to form endothelial cells and that these cells recruit other mesenchyme to a perivascular zone in culture, mimicking the mechanisms observed *in situ*. The continued expansion of the capillary nexus within the subepicardial space and throughout the myocardium appears to be produced through the process of angiogenesis, the elongation of, and vascular branching from existing vessels. Initially starting near the AV sulcus, the capillary network will spread to the ventral interventricular sulcus and then around the bulbus cordis region eventually reaching the truncus arteriosus forming a peritruncal ring of capillaries (6). These vessels will then join on the ventral aspect, producing sprouts extending towards the aorta where they will invade the aorta and

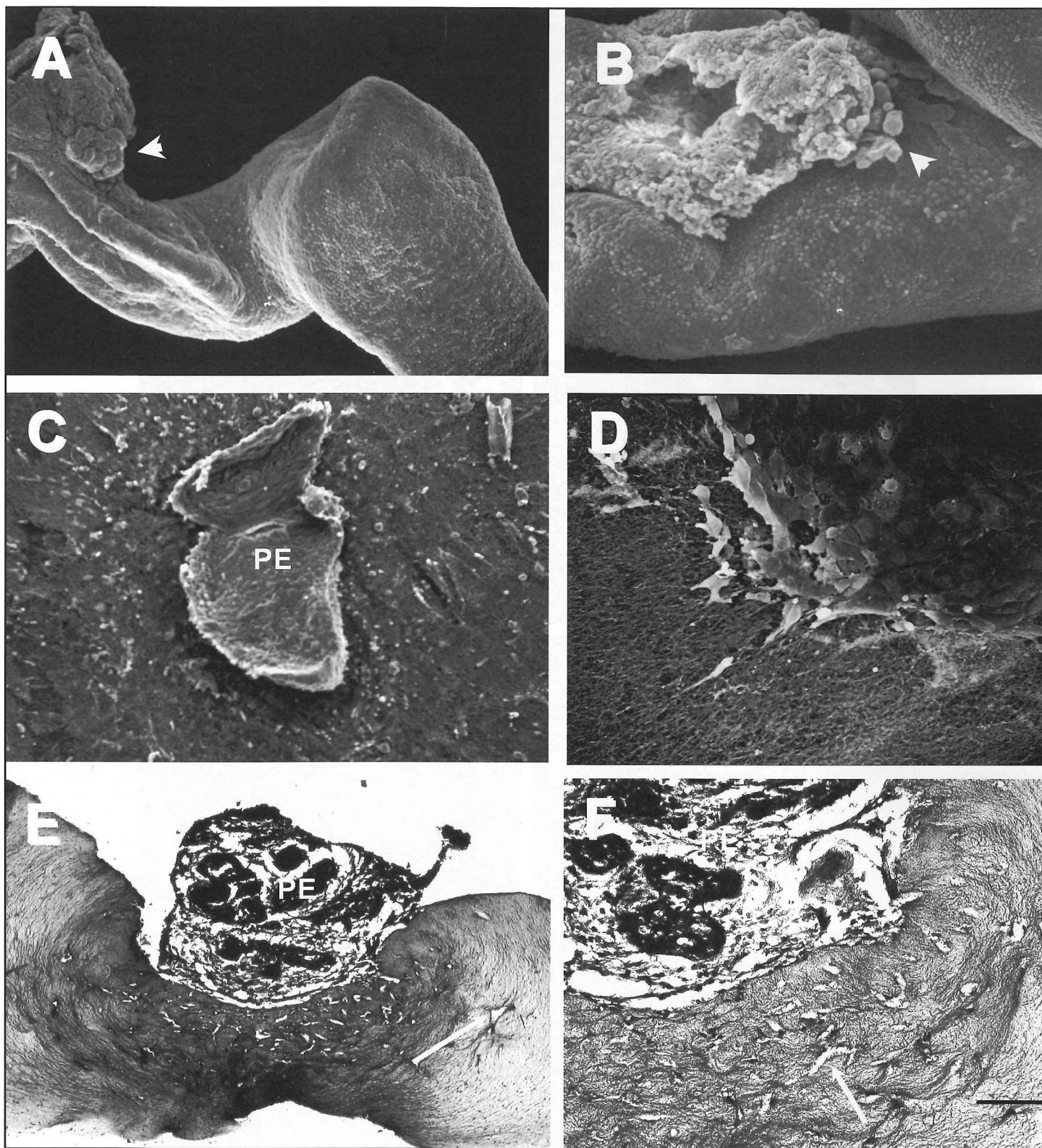


Figure 1. Representative micrographs of PE and PE-derived cells *in situ* and in collagen gel cultures. (A) Chicken HH stage 15 heart displaying the PE (arrowhead) beneath the sinus venosus. (B) Villous projections of a chicken HH stage 18 PE which has made contact with the myocardial surface (arrowhead). (C) Chicken PE grown in culture for 72 hours demonstrating the spread of proepicardially-derived cells on the collagen gel surface. (D) Individual migratory cells in advance of the leading edge of the epicardial sheet. (E) Individual quail PE-derived cells, not visible from the surface since they invaded the collagen gel, are visible within the collagen gel in cross-sections (arrow). (F) Quail mesenchymal cells organized into either spherical units or hollow chords within the collagen gel, resembling structures undergoing either vasculogenesis or angiogenesis respectively (arrow). PE – primary explant of the PE in culture. Scale Bar = 130 mm (A); 85 mm (B); 160 mm (C); 50 mm (D); 180 mm (E); 90 mm (F).

establish coronary blood flow. Given longer times in culture, the initial vascular structures formed *via* vasculogenesis, likely will expand by angiogenesis and thus this model system would be beneficial for studying either or both of these processes.

While the picture of the PE as a source for vascular precursors as well as smooth muscle and fibroblasts progenitors is becoming more clearly focused, the role of PE-derived cells in cardiac myogenesis is becoming more complex. Studies have effectively demonstrated that no PE-derived myocytes can be detected within the myocardial layer of the heart *in situ* (22). However, *in vitro* studies have shown that at least a population of PE-derived cells has the capacity to undergo cardiac myogenesis (34). In the present study, approximately 50% of the PE primary explants begin to spontaneously and rhythmically contract after 3 days in culture. Kruithof *et al.* (2006) demonstrated that the addition of BMP2 or BMP4 lead to myogenesis, yet FGFs inhibited the formation

of myocytes *in vitro* (34). Taken together, their data suggest that a negative regulation of the myogenic pathway is active *in situ*; while, in culture, the subpopulation of myogenically-capable cells is freed to differentiate into cardiac muscle (34).

Our data fully support their hypothesis as cardiac myocytes are also present in our model system. Regardless of its physiological relevance to development, this model may yield valuable information about precursor cell determination in PE-derived cells that could possibly be extrapolated to adult cardiac stem cells. This type of research is being fervently pursued in an attempt to find a natural and non-invasive means of repairing damaged cardiac muscle. Future experimentation using this model system will likely shed invaluable information on the processes of PE-derived hematopoiesis and myogenesis that may someday result in non-invasive means of stimulating repair of damaged cardiac tissue *in vivo*.

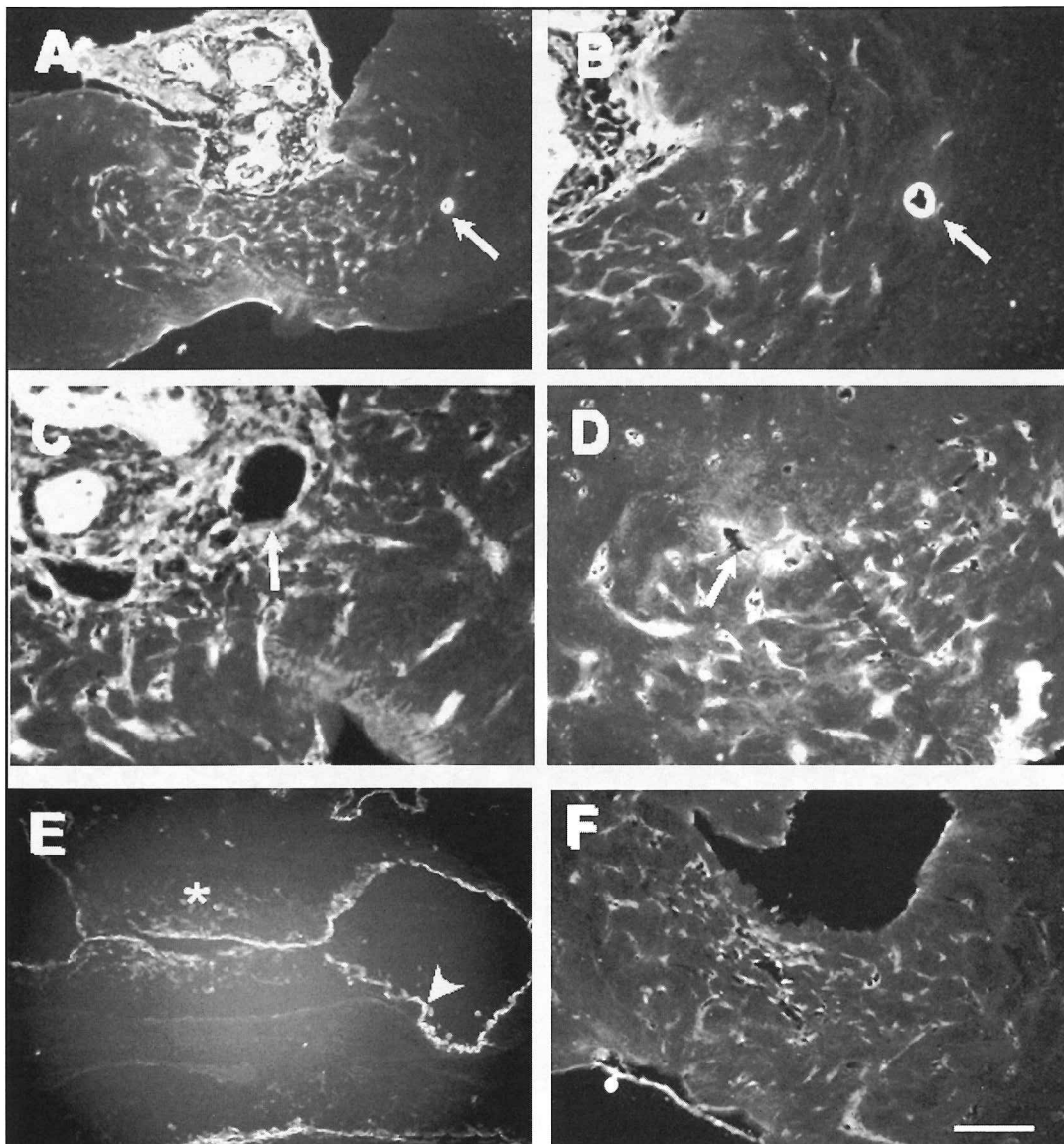


Figure 2. Immunohistochemical analysis of quail PE-derived cells in culture for the endothelial specific marker QH (A-D) PE-derived cells expressed the endothelial specific marker QH-1 (7 days in culture). Most of the mesenchyme cells within the collagen gel exhibit a moderate level of QH-1, while areas of the original explant are intensely positive for QH-1 and may represent angioblasts present in the PE prior to explantation in culture. An intensely stained vascular-like structure was observed within the collagen matrix at a distance from the original explant (arrows in A and B). High magnification of the cells within the collagen lattice reveal that many have organized themselves into structures with defined lumen bounded by a cellular layer (arrows in C and D). (E) QH-1 clearly identifies the endocardium of the heart as well as endocardially-derived mesenchymal cells migrating into the endocardial cushion tissue. (F) Negative controls lack the QH-1 primary antibody. Asterisk – endocardially-derived mesenchyme within the cushion tissue; PE – primary explant of the PE. Scale Bar = 180 mm (A); 90 mm (B-F).

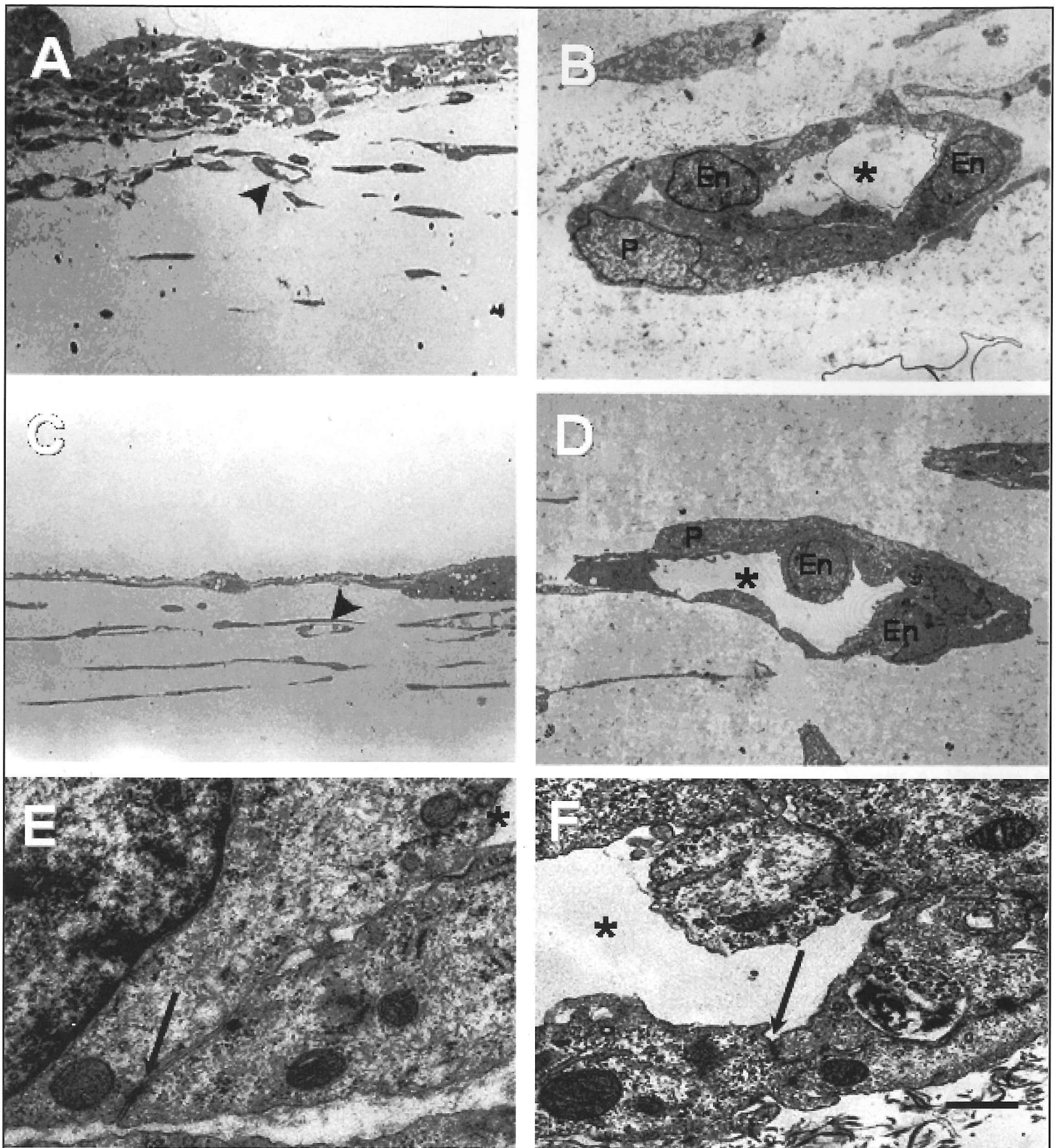


Figure 3. Representative transmission electron micrographs of chicken PE-derived cells in culture. (A, C) Thick sections PE cultures examined under light microscopy to identify possible vascular-like structures. (B, D) Corresponding TEM demonstrate that the putative vascular structures are cellularly lined and possess a patent lumen. In many instances, peripheral cells were found adjacent to the endothelial lining and likely represent pericyte-like cells or smooth muscle precursors. (E, F) Closer examination of the lining cells reveals that junctional complexes are present between adjoining cells, a characteristic of the endothelial cells. Arrow – junctional complexes between adjacent endothelial cells; arrowhead – vascular-like structures; asterisk – lumen of vessel; En – endothelial cell; P – pericyte or smooth muscle precursor. Scale bar = 60 μ m (A,C); 5 μ m (B,D); .05 μ m (E,F).

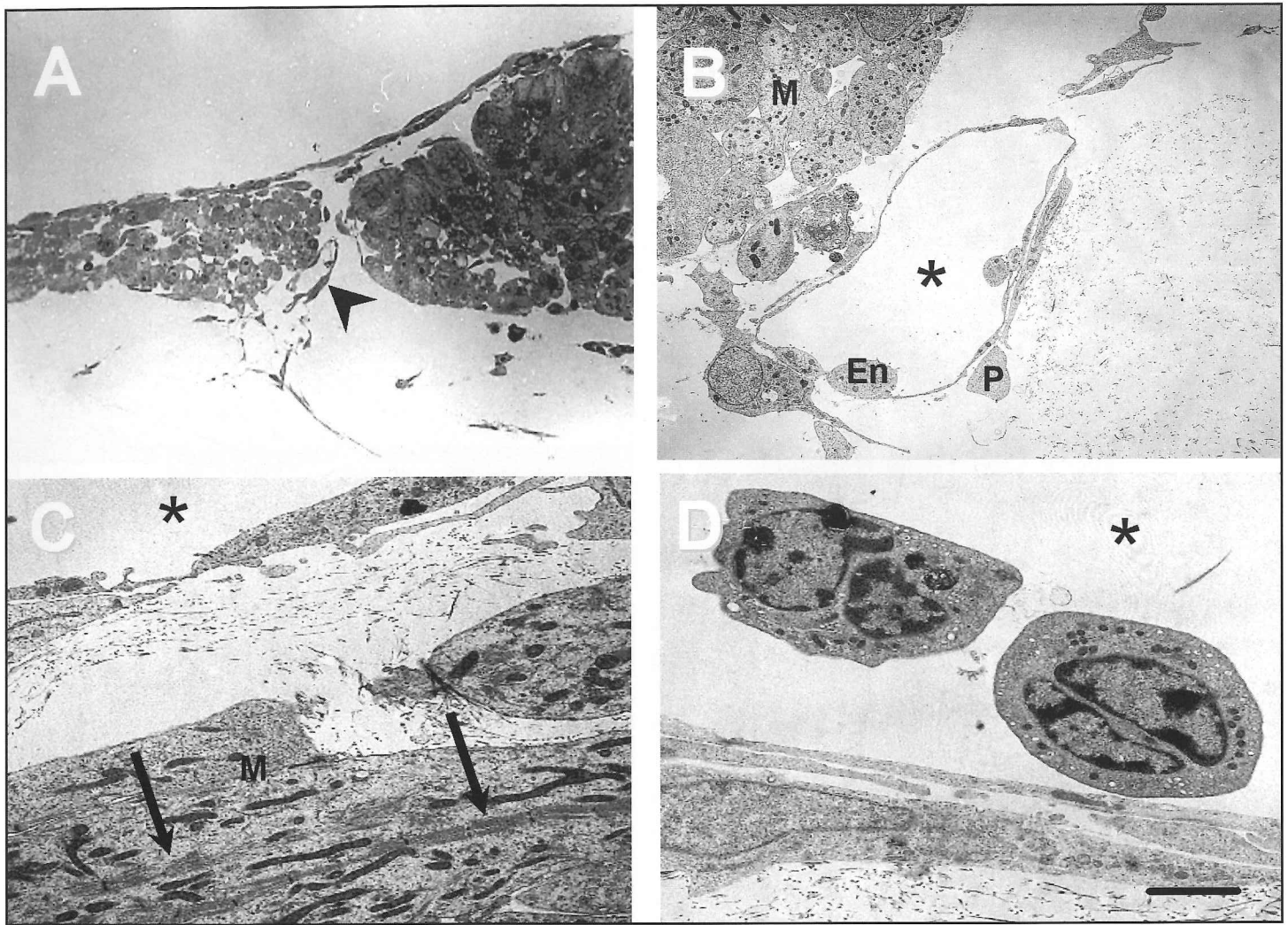


Figure 4. Representative transmission electron micrographs of chicken PE-derived cells in culture. In addition to endothelial cells and perivascular cells, PE-derived cells also demonstrated the ability to undergo myogenesis and produce cardiac myocytes in culture (A, B, and C). After 3 days in culture, many of the primary explants began to spontaneously and rhythmically contract, indicating the presence of cardiac muscle. Identification of myocytes was made by identifying myofibrils present in the cells at the ultrastructural level in either cross-section (B) or longitudinal section (C). Also present were cells that resembled polymorphonuclear leukocytes within the lumen of some vascular structures in culture (D). Arrow – longitudinally arranged myofibrils displaying a sarcomeric structure; arrowhead – vascular-like structure; asterisk – lumen of vessel; En – endothelial cell; P – pericyte or smooth muscle precursor. Scale Bar = 60 mm (A); 15 mm (B); 10 mm (C); 5 mm (D).

LITERATURE CITED

1. Aikawa, E. and Kawano, J. (1982) *Experientia* **38**(7), 816-818
2. Bogers, A. J., Gittenberger-de Groot, A. C., Poelmann, R. E., Peault, B. M., and Huysmans, H. A. (1989) *Anat Embryol (Berl)* **180**(5), 437-441
3. Yang, J. T., Rayburn, H., and Hynes, R. O. (1995) *Development* **121**(2), 549-560
4. Kwee, L., Baldwin, H. S., Shen, H. M., Stewart, C. L., Buck, C., Buck, C. A., and Labow, M. A. (1995) *Development* **121**(2), 489-503
5. Sengbusch, J. K., He, W., Pinco, K. A., and Yang, J. T. (2002) *J Cell Biol* **157**(5), 873-882
6. Bernanke, D. H. and Velkey, J. M. (2002) *Anat Rec* **269**(4), 198-208
7. Manner, J. (1992) *Anat Embryol (Berl)* **186**(4), 379-385
8. Gittenberger-de Groot, A. C., Vrancken Peeters, M. P., Mentink, M. M., Gourdie, R. G., and Poelmann, R. E. (1998) *Circ Res* **82**(10), 1043-1052
9. Viragh, S. and Challice, C. E. (1981) *Anat Rec* **201**(1), 157-168
10. Nahirney, P. C., Mikawa, T., and Fischman, D. A. (2003) *Dev Dyn* **227**(4), 511-523
11. Wada, A. M., Smith, T. K., Osler, M. E., Reese, D. E., and Bader, D. M. (2003) *Circ Res* **92**(5), 525-531
12. Ho, E. and Shimada, Y. (1978) *Dev Biol* **66**(2), 579-585
13. Hiruma, T. and Hirakow, R. (1989) *Am J Anat* **184**(2), 129-138
14. Viragh, S., Gittenberger-de Groot, A. C., Poelmann, R. E., and Kalman, F. (1993) *Anat Embryol (Berl)* **188**(4), 381-393
15. Hatcher, C. J. and Basson, C. T. (2003) *Circ Res* **92**(5), 477-479
16. Wada, A. M., Reese, D. E., and Bader, D. M. (2001) *Development* **128**(11), 2085-2093
17. Houser, J. W., Ackerman, G. A., and Knouff, R. A. (1961) *Anat Rec* **140**, 29-43
18. Pardanaud, L., Altmann, C., Kitos, P., Dieterlen-Lievre, F., and Buck, C. A. (1987) *Development* **100**(2), 339-349
19. Coffin, J. D. and Poole, T. J. (1988) *Development* **102**(4), 735-748
20. Mikawa, T., Borisov, A., Brown, A. M., and Fischman, D. A. (1992) *Dev Dyn* **193**(1), 11-23
21. Mikawa, T. and Gourdie, R. G. (1996) *Dev Biol* **174**(2), 221-232
22. Manner, J. (1999) *Anat Rec* **255**(2), 212-226
23. Ratajska, A., Torry, R. J., Kitten, G. T., Kolker, S. J., and Tomanek, R. J. (1995) *Dev Dyn* **203**(4), 399-407
24. Perez-Pomares, J. M., Carmona, R., Gonzalez-Iriarte, M., Atencia, G., Wessels, A., and Munoz-Chapuli, R. (2002) *Int J Dev Biol* **46**, 1005-1013
25. Nesbitt, T., Lemley, A., Davis, J., Yost, M. J., Goodwin, R. L., and Potts, J. D. (2006) *Microsc Microanal* **12**(5), 390-398
26. Bernanke, D. H. and Markwald, R. R. (1982) *Dev Biol* **91**(2), 235-245
27. Green J., Crossland R., and Langford J.K. (2007) *Tx J Micr* **38**(2), 100-106
28. Hamburger, V. and Hamilton, H. L. (1992) *Dev Dyn* **195**(4), 231-272
29. Spurr, A. R. (1969) *J. Ultrastruct. Res.* **26**, 31-43
30. Reynolds, E. S. (1963) *J. Cell Biol.* **17**, 208-212
31. Wessels, A. and Perez-Pomares, J. M. (2004) *Anat Rec A Discov Mol Cell Evol Biol* **276**(1), 43-57
32. Kattan, J., Dettman, R. W., and Bristow, J. (2004) *Dev Dyn* **230**(1), 34-43
33. Munoz-Chapuli, R., Macias, D., Gonzalez-Iriarte, M., Carmona, R., Atencia, G., and Perez-Pomares, J. M. (2002) *Rev Esp Cardiol* **55**(10), 1070-1082
34. Kruithof, B. P., van Wijk, B., Somi, S., Kruithof-de Julio, M., Perez Pomares, J. M., Weesie, F., Wessels, A., Moorman, A. F., and van den Hoff, M. J. (2006) *Dev Biol* **295**(2), 507-522
35. Nakajima, Y., Yamagishi, T., Hokari, S., and Nakamura, H. (2000) *Anat Rec* **258**(2), 119-127
36. Compton, L. A., Potash, D. A., Mundell, N. A., and Barnett, J. V. (2006) *Dev Dyn* **235**(1), 82-93
37. Van Den Akker, N. M., Lie-Venema, H., Maas, S., Eralp, I., DeRuiter, M. C., Poelmann, R. E., and Gittenberger-De Groot, A. C. (2005) *Dev Dyn* **233**(4), 1579-1588
38. Tomanek, R. J. and Zheng, W. (2002) *Tex Heart Inst J* **29**(4), 250-254

WANTED

- Your Papers
- Your Manuscripts
- Your Short Communications
- Your Photos
- Your Research Articles
- Your Abstracts

**We Want
To Publish You!**

ARSENIC-INDUCED STEATOSIS IN C57BL/6J MALE MICE CHRONICALLY EXPOSED THROUGH DRINKING WATER

JAIME B. VIGO¹, JOANNE T. ELLZEY^{1,*} THOMAS P. BAKER²,
JULIA O. BADER³ AND THOMAS G. OLIVER⁴

¹Analytical Cytology Core Facility, Biological Sciences, the University of Texas at El Paso, El Paso, Texas 79968-0519. ²Department of Pathology and Area Laboratory Services, Walter Reed Army Medical Center, 6900 Georgia Avenue NW, Washington, DC, 20307. ³Statistical Consulting Laboratory, University of Texas at El Paso, El Paso, Texas 79968. ⁴Department of Endocrinology, William Beaumont Army Medical Center, El Paso, TX.

Keywords: Arsenic, C57BL/6J mouse/mice, steatosis, inflammation, fibrosis, liver/hepatic, low fat diet, high fat diet, ultrastructure.

ABSTRACT

Epidemiological evidence suggests that chronic ingestion of arsenic through drinking water may have links with the onset of diabetes mellitus-Type 2. This investigation used an *in vivo* experimental setting to test the hypothesis that chronic ingestion of arsenic through the drinking water may induce diabetogenic effects in a mouse model fed with a low fat or a high fat diet. Four groups of C57BL/6J male mice (n=15/group) were fed with 4.5% (low) or 11% (high) fat diet, and exposed to drinking water containing 0 ppm or 22.5 ppm of sodium arsenite [As (III)] for 40 weeks. During the last 10 weeks, the fat content of the 11% fat diet groups was increased to 24% to accelerate increase in weight gain and to ensure reaching the obesity threshold (≥ 50 g) within the experimental timeline. Light and transmission electron microscopy studies revealed an arsenic-induced hepatic steatosis and inflammation in the As (III)-exposed low fat group compared to the control low-fat group. A similar diet-induced hepatic steatosis and inflammation were also observed in both of the high fat diet groups with no significantly different pathology observed between the arsenic-exposed and control groups. A significant diet-induced increase in the average accumulated weights starting at week 6 (diet by week interaction $p < 0.001$) and blood glucose of the groups fed with the high fat diet ($p < 0.001$) compared to the low fat diet groups were observed. Terminal blood insulin showed a significant diet-induced increase for the high fat fed groups compared to the low fat fed groups ($p = 0.02$). The organ to body weight ratio showed a significant diet effect for the liver ($p < 0.001$), a significant diet effect ($p = 0.005$) and a significant group effect ($p = 0.03$) for the kidney, and a significant diet effect ($p = 0.01$) for pancreas. There were significant group*diet*week interactions in both the amount of average water consumption and average cumulative food consumption. No significant differences were found for BUN. In conclusion, 40 weeks of exposure of C57BL/6J mice to 22.5 ppm of As (III) through drinking water did not provide evidence of diabetogenic effects but did provide evidence of steatosis in lean mice due to arsenic toxicity.

INTRODUCTION

Exposure to arsenic can occur from the environment through food and water consumption [41 and references within]. The two forms of arsenic, reduced [As (III)] and oxidized [As(V)], can be absorbed, and accumulated in diverse tissues and body fluids [40]. In the liver, the metabolism of arsenic involves enzymatic and non-enzymatic methylation, in which the most frequently ($\geq 90\%$) excreted metabolite in the urine of mammals is dimethylarsinic acid [DMA(V)]. The remaining ($\leq 10\%$) non-excreted arsenic accumulates in cells, which over time may lead to skin, bladder, kidney, liver, lung, and prostate cancers [41]. Other forms of arsenic toxicity in humans have been observed in blood, bone marrow, cardiac, central nervous system, gastrointestinal, gonadal, kidney, liver, pancreatic, and skin tissues [41]. The human liver may exhibit hepatic non-cirrhotic portal hypertension, fibrosis, and cirrhosis after exposure to therapeutic drugs containing As [41].

Epidemiological studies have suggested a correlation between chronic consumption of drinking water contaminated with arsenic and the incidence of Type 2-diabetes [41]. However, the literature provides insufficient scientific evidence to show cause and effect between arsenic and the onset of diabetes mellitus Type 2 [41]. Studies have demonstrated that the oxidative stress generated by arsenic may disrupt the signal transduction pathways of the nuclear transcriptional factors PPAR's, AP-1, and NF κ B [18, 42], as well as the pro-inflammatory cytokines IL-8 and TNF- α [2, 3, 4, 10, 12, 18, 42]. The interference of oxidative stress with signal transduction pathways may affect physiological processes associated with cell growth, metabolic syndrome X, glucose homeostasis, lipid metabolism, obesity, insulin resistance, inflammation, and diabetes-2 [22, 26, 27]. Recent scientific evidence has elucidated the physiological roles of the PPAR's in the ω -hydroxylation of fatty acids and the inhibition of pro-inflammatory transcription factors (NF κ B and AP-1), pro-inflammatory cytokines (IL-1, -6, -8, -12, and TNF- α), cell-adhesion molecules (ICAM-1 and VCAM-1), inducible nitric oxide synthase, pro-inflammatory nitric oxide (NO), and anti-apoptotic factors [2, 15, 22, 27, 41].

We designed an *in vivo* experimental setting to test the hypothesis that chronic ingestion of arsenite through drinking water may induce diabetogenic effects in a mouse model fed with a low fat or a high fat diet. In order to achieve this goal, the wild-type mouse strain C57BL/6J was selected. This strain has been widely used in studies of obesity and diabetes due to its susceptibility to diet-

*Corresponding Author:

Joanne T. Ellzey

Analytical Cytology Core Facility, Biological Sciences

The University of Texas at El Paso, El Paso, Texas 79968-0519

E-mail: jellzey@utep.edu

Phone: (915)-747-6880, FAX: (915)-747-5808

induced obesity, insulin resistance, and type-2 diabetes. Hyperglycemia and hyperinsulinemia may occur in this strain when a high fat diet ($\geq 15\%$ fat) is used to induce obesity (body weight $\geq 50\text{g}$; Jackson Laboratory Mice Data Sheet). Therefore, two feeding methods were used in this study to determine the effects of arsenic toxicity based on the percent of fat content: low fat 4.5%, and high fat 11% or 24%. The arsenic form and dose were chosen from studies of metallothionein I and II null and wild type SV129 mice exposed to 22.5 ppm of As^{+3} for a time period of up to 48 weeks. Upon arsenic exposure, these models showed liver pathology including fatty infiltration (steatosis), inflammation, and focal necrosis [41].

MATERIALS AND METHODS

Experimental Design – All mice used were males of the C57BL/6J strain, obtained at 6 weeks of age from The Jackson Laboratory (Bar Harbor, ME, USA). This study complied with the U.S. Public Health Policy on the care and use of animals. Protocols for experiments were approved by the Institutional Animal Care and Use Committee (IACUC) at William Beaumont Army Medical Center (WBAMC) and the University of Texas at El Paso (UTEP). Mice were allowed to acclimatize for 10 days upon arrival in cages of five mice per cage with free access to food and water under a 12-hour photoperiod at an average temperature of 22–26°C and 70% average relative humidity. The cages were 1/2 inch filled with 1/8 inch Harlan Teklad All Natural 100% Corncob Bedding material, which was replaced on a weekly basis. Upon completion of the acclimation period, mice were randomly divided into four groups. Two groups were fed with rodent chow containing 4.5% fat (Lab Diet 5001) and the other two groups were fed with 11% fat (Lab Diet 5015; maximum fat content commercially available at the initiation of the study). The four mice groups were entitled: control low fat diet (CL), arsenic-exposed low fat diet (AL), control high fat diet (CH), and arsenic-exposed high fat diet (AH). Mice belonging to AL and AH groups were exposed to 22.5 ppm of arsenic (as determined by inductively coupled plasma (ICP) spectroscopy analysis) as sodium arsenite through drinking water over a period of 40 weeks. At week 30, the fat content of the high fat diet group chow was changed to 24% fat (Lab Diet 58NX) (Purina Mills, Richmond, IN) to accelerate the increase in weight gain and to ensure reaching the obesity threshold ($\geq 50\text{g}$) within the experimental timeline. Water consumption per group was measured with a volumetric cylinder and by adding initially 100 mL of control or experimental drinking water to the cages water bottles and measuring the amount left after 1 week. Food consumption per cage was measured with a calibrated scale and by adding initially 100 g of chow and measuring the amount left after 1 week.

Blood Glucose and Blood Urea Nitrogen (BUN) Analyses – Glucose measurements were taken after a 4-hours fasting on a bi-weekly basis. Upon selection of mice cages, the 5 mice in a cage were placed in a custom-designed 5-compartment anesthesia-induction chamber. The anesthetic vaporizer machinery, supplying anesthesia to the chamber, was set to 3L of oxygen/min and 2.5 vols/min of isoflurane to anesthetize one mouse at a time. Numb mice were placed upside down on a vented warming table and continuously kept under anesthesia through an anesthetic mask. Mice tails were introduced into a warm water cup for about 15 seconds to promote dilation of the central vein. Upon localization of the dilated central vein of the tail, the vein was poked with a 25-gauge needle at an angle of 45° to allow blood to flow out of the vein. Blood levels of glucose were measured with a Freestyle® blood glucose meter (TheraSense Inc. Alameda, CA). Blood urea nitrogen levels (BUN) were taken with Asostix® strips obtained from the Bayer Corporation, Elkhart, IN. After measuring glucose and BUN, the tails were cleaned and disinfected with sterile 70%

isopropyl alcohol gauze, and the mice were allowed to recover in a designated recovery cage. At the termination of the experiment, a submandibular blood sample ($2.0 \pm 0.5\text{ mL}$) was collected from each mouse with a Goldenrod™ Animal Lancet (MEDipoint, Inc, Mineola, NY) to measure the levels of blood insulin. Upon terminal blood collection, the kidney, liver, and pancreas organs of each mouse were excised and preserved for pathological studies. Average values for each group were taken from an initial total of 15 mice per group divided into 5-mice per cage. The measured variables included weekly cumulative body weights, weekly water consumption, bi-weekly blood glucose, bi-weekly BUN, terminal blood insulin, and terminal liver-, and kidney-to-body-weight ratios as shown in Table 1.

Light Microscopy – Kidney, liver and pancreas tissue from each mouse were fixed in 10% formaldehyde, embedded in paraffin, and stained with hematoxylin and eosin (H&E), Masson's Trichrome, or Periodic Acid Schiff (PAS). The H&E stain was used to observe the overall histology of the tissues and to document pathology. The PAS stain with diastase was used to look for diabetic changes in the kidney, primarily for amyloid deposition. The Masson's Trichrome stain was used to observe fibrosis. Pathology was graded using a semiquantitative 1-3 grading system (mild, moderate, marked).

Transmission Electron Microscopy (TEM) – Small pieces of tissue (1mm^3) were fixed in 2.0% (wt/vol) paraformaldehyde and 2.5% (vol/vol) glutaraldehyde in 0.12 M Millong's phosphate buffer, pH 7.4 for 2.5 hours at room temperature on a rotary agitator. Specimens were washed 3 times of 15-minutes with cold 0.06 M phosphate buffer and then post-fixed with 1% (wt/vol) osmium tetroxide, 0.05 M potassium ferricyanide in 0.12 M phosphate buffer for 1 hour on ice. Specimens were then washed in 0.06 M phosphate buffer followed by 3 times of 15-minute washes with distilled water and then en block staining overnight with 0.5% (wt/vol) aqueous uranyl acetate at 4°C. Specimens were then dehydrated with ethanol (75%, 95%, 100%) followed by 100% acetone. Specimens were infiltrated with and embedded in Poly Bed 812 (Polysciences, Inc., Warrington, PA). Thick sections ($1\text{ }\mu\text{m}$) were stained with Toluidine Blue and Fuschin to determine suitable areas to be thin sectioned (60–90 nm). Thin sections were post stained with the uranyl acetate followed by Reynolds Lead Citrate (Reynolds, 1963). Grids were examined and photographed in a Zeiss EM-10 transmission electron microscope at an accelerating voltage of 60 or 80 kV.

Statistical Analyses – Statistical analyses included the General Linear Mixed Models (GLMM) for repeated measures with factors group (Arsenic versus Control), diet (Low Fat versus High Fat) and week, and Tukey's post-hoc pairwise comparison tests, using the Statistical Analysis System (SAS version 9.1.3). If a significant effect in time or treatment group was found with the GLMM, the data were subjected to the post-hoc procedure, Tukey's test.

RESULTS

Metabolically Diet-induced Effects of Arsenic Exposure – As shown in Table 1, the combined results obtained with the high fat groups starting at week 6 showed a significant increase in cumulative body weights compared to results obtained with the low fat groups, indicating a significant diet*time interaction ($p < 0.001$). At week 40, both control and arsenic-exposed groups fed with high fat diet reached the level of obesity ($\geq 50\text{g}$). The average water consumption showed a significant group*diet*week interaction ($p < 0.001$). The Tukey's post-hoc procedure showed significant group effect in time for the low fat diet groups, but not for the high fat diet ones. The average cumulative food consumption showed a significant group*diet*week interaction ($p < 0.001$),

and Tukey's post-hoc procedure showed significant group effect across the weeks 9 to 24 for the high fat diet, but not for the low fat diet. The combined overall average bi-weekly blood glucose of the high fat groups showed a significant increase ($p < 0.001$) when compared to the low fat groups. The elevation of blood glucose in the high fat-fed groups (193 ± 17 mg/dL for the control vs. 203 ± 41 mg/dL for the As (III)-exposed) to prediabetic blood glucose levels for a mouse (123 to 225 mg/dL)^[20] was an expected diet-induced effect. The terminal blood insulin showed a significant diet-induced increase for the high fat fed groups (control 4.5 ± 3.3 ng/ml and arsenic-exposed 2.4 ± 1.4 ng/ml) compared to the low fat fed groups (control 3.3 ± 1.4 ng/ml and arsenic-exposed 2.3 ± 1.6 ng/ml, $p = 0.02$). The organ to body weight ratio showed a significant diet effect for the liver ($p = 0.001$, higher for high fat diet than for low fat diet), as well as a significant diet effect for kidney ($p = 0.005$, higher for low fat diet than for high fat diet). No significant differences in diet or group were found for the bi-weekly BUN. No significant differences in diet or group among all measured variables were found in any of the 6-week-harvested mice.

Effects of Arsenic Exposure on the Liver Pathology and Ultrastructure – Table 2 shows a summary of the pathological effects observed per group. The hepatic pathology for the arsenic-exposed low fat diet group demonstrated 33.3% mild macrovesicular steatosis, and 6.7% moderate macrovesicular steatosis. A total of 60% of the arsenic-exposed low fat diet mice had normal liver histology. In contrast, the control low fat group demonstrated 14.3% of mild inflammation, but no mice with hepatic steatosis. A total of 85.7% of the mice in the control low fat diet group showed normal liver. The pathological effects of a high fat diet were demonstrated in the groups fed with the 11% fat diet followed by 24% fat diet. The liver pathology for the control high fat group showed steatohepatitis; 33.3% mice showed marked microvesicular and macrovesicular steatosis, mild inflammation, and mild necrosis, 26.7% marked microvesicular and macrovesicular steatosis and mild inflammation, 13.3% microvesicular and macrovesicular steatosis, 6.7% mild inflammation, and 20% showed normal liver histology. The arsenic-exposed high fat group showed a similar, not significantly different pathology from the control high fat group. In this group, as in the control high fat group, the steatohepatitis was characterized by 33.3% of the mice showing marked microvesicular and macrovesicular steatosis, mild inflammation, and mild necrosis. However, 40% showed marked microvesicular and macrovesicular steatosis, 6.7% mild microvesicular and macrovesicular steatosis and mild inflammation, 6.7% microvesicular and macrovesicular steatosis, and 13.3% remained normal. Only two out of fifteen mice (13.3%) had normal liver histology.

A summary of liver histology for all groups (CL, AL, CH, and AH) is shown in figures 1-5. The CL mouse (Fig.1) shows the normal features of hepatic tissue including the central vein, interlobular vein, sinusoids, and hepatocytes. Figure 2, representative of AL mice, shows arsenic-induced microvesicular and macrovesicular steatosis, represented as white lipid inclusions within hepatocytes. Figure 3, representative of CH mice, shows the high fat diet-induced microvesicular and macrovesicular steatosis effect accompanied by inflammation. Figure 4, representing an AH mouse, shows the high fat diet-induced microvesicular and macrovesicular steatosis effect accompanied by inflammation. The pathology of the AH group was similar to the pathology of the CH group. Figure 5, also from an AH mouse, shows the extreme case of microvesicular and macrovesicular steatosis with inflammation and necrosis.

Although light microscopy revealed normal liver histology in the control low fat diet mice, under the electron microscope, lipid was more noticeable in hepatocytes of numerous control low fat diet mice than characteristically seen in BALBc or C3H mouse hepatocytes. In Figure 6, representative of CL group, the lipids are noticeable in the top hepatocyte. Normal lipid droplets appear in lipocytes within the sinusoids (center of the picture). In Figure 7, representative of AL group, the arsenic-induced steatosis can be observed as several lipid inclusions within hepatocytes. In Figures 8 and 9, representing the CH and AH groups, respectively, a more severe case of steatosis can be observed, in which the cytoplasmic region appears occupied by large lipid inclusions.

DISCUSSION AND CONCLUSIONS

Light microscopy results showed that 12/14 mice in the CL group had normal liver histology. In the electron micrographs of CL mice, lipids are more noticeable than in BALBc or C3H mouse hepatocytes. Thus, the high resolution of transmission electron microscopy can detect low levels of lipid not noticeable in light microscopy. The increase in liver lipid content may be due to the prediabetic level of glucose in the blood of all of the C57BL/6J mice in our study. The pathology of microvesicular and macrovesicular steatosis observed in the AL group provides evidence that arsenic toxicity can induce hepatic steatosis in a mouse model fed with a low fat diet (4.5% fat content). This unusual association between lean body mass and liver steatosis has been reported before in the literature in mice fed a diet containing a fatty acid [10-trans, 12-cis-conjugated linoleic acid (CLA2)] that can induce steatosis in a lean body^[5,6]. However, the hepatic condition known as non-alcoholic fatty liver disease (NAFLD) is common in obesity induced by a high fat diet, a physiological effect that explains the observed hepatic steatosis in the mice groups fed with the high

Table 1: Average values per group of cumulative weight, water consumption, food consumption, blood glucose, terminal insulin, terminal liver to body weight ratio, and terminal kidney to body weight ratio at week 40. CL: control low fat, AL: arsenic low fat, CH: control high fat, AH arsenic high fat.

GROUP	AVERAGE CUMMULATIVE WEIGHT (g)	AVERAGE WATER CONSUMPTION (mL)	AVERAGE FOOD CONSUMPTION (g)	AVERAGE BLOOD GLUCOSE (mg/dL)	AVERAGE TERMINAL INSULIN (ng/mL)	AVERAGE TERMINAL LIVER TO BODY WEIGHT RATIO
CL	34.01 ± 1.28	30.0 ± 1.06	27.73 ± 1.08	175 ± 20	3.3 ± 1.4	0.046 ± 0.002
AL	32.75 ± 2.77	23.26 ± 0.67	26.84 ± 1.07	170 ± 15	2.3 ± 2.6	0.047 ± 0.004
CH	51.25 ± 4.72	24.73 ± 2.28	23.13 ± 1.58	193 ± 17	4.5 ± 3.3	0.069 ± 0.015
AH	50.5 ± 4.39	18.72 ± 0.37	24.99 ± 1.57	203 ± 41	2.4 ± 1.4	0.068 ± 0.013

Table 2: Hepatic pathological results for male C57BL/6J arsenic-treated mice compared to controls. CL: control low fat, AL: arsenic low fat, CH: control high fat, AH arsenic high fat.

GROUP	SAMPLE SIZE	NORMAL LIVER	MILD INFLAMMATION	MICROVESICULAR & MACROVESICULAR STEATOSIS			MICROVESICULAR & MACROVESICULAR STEATOSIS WITH INFLAMMATION
				MILD	MODERATE	MARKED	
CL	14	12	2	0	0	0	0
AL	15	9	0	5	1	0	0
CH	15	3	1	0	0	2	4
AH	15	2	0	1	0	6	1

fat diet in this investigation. According to the literature, the obesity induced by a high fat diet may be associated with increase in free fatty acids, dyslipidemia, metabolic syndrome X, insulin resistance, nonalcoholic steatohepatitis (NASH), diabetes-2, and cirrhosis [7,8,13,23,28,29-32,34,37,39,40]. These disorders develop from modulating aberrant cytokine and insulin signaling. In NASH, generated oxidative stress leads to inflammation through mechanisms that remain unclear [24,31]. Elevated levels of cytokines, such as proinflammatory TNF- α , lead to increased hepatic fatty acid synthesis, whereas increased hepatic β -oxidation of phospholipids is associated with decreased levels of certain proinflammatory cytokines [9,17,38,39,43]. Decreased β -fatty acid oxidation may cause fat accumulation and persistent accumulation of hepatic triglycerides may induce insulin resistance [6,14,25]. For example, in insulin-resistant and hypertriglyceridemic apoB/BATless mice, the hepatic mRNA levels of lipogenic enzymes such as acetyl-CoA carboxylase, fatty-acid synthase, and stearoyl-CoA desaturase-1 are increased compared to apoB control mice, suggesting that hepatic steatosis is associated with an elevated degree of hepatic lipogenesis [11,33]. In general, lipodystrophy is characterized by a decrease in the numbers of adipocytes, increased insulin resistance, leptin deficiency, and hepatic steatosis [1].

Control of lipogenesis and hepatic steatosis may be achieved through the modulation of nuclear receptors, cytokines, and proteins involved in fatty acid biochemistry. For example, the nuclear receptors peroxisome proliferator-activated receptor (PPAR)- α and PPAR- γ isoforms are involved in the pathogenesis of hepatic steatosis by modulating fatty acid metabolism [11,16,37,44]. Disruption of SREBP-1 in ob/ob mice decreases the storage of hepatic triglyceride and the levels of plasma alanine aminotransferase (ALT), thereby improving insulin resistance and hepatic steatosis [40,52]. The up-regulation of PPAR- γ in hepatocytes exacerbates liver steatosis [28,36,43,44]. In particular, PPAR- γ is implicated in liver steatosis induced by high fat diet [19].

Hepatic adiponectin is an adipocyte-derived polypeptide active in endothelial cells of portal vessels and sinusoids that may alleviate steatosis, insulin resistance, inflammation, and elevated

levels of serum alanine aminotransferase (ALT) in mice [21,42]. The mechanism occurs by decreasing the activities of the fatty acid synthesis enzymes acetyl-CoA carboxylase and fatty acid synthase and suppression of the production and plasma levels of pro-inflammatory TNF- α [21,43].

In conclusion, the data of this study do not support the hypothesis that chronic ingestion of arsenic (22.5 ppm) through the drinking water can induce diabetogenic effects in C57BL/6J mice when fed a low or high fat diet for a period of 9 months. However, the data do provide evidence of arsenic-induced steatosis and inflammation in lean C57BL/6J mice fed with a low fat diet, a pathological effect possibly due to the oxidative stress generated by arsenic toxicity on the signal transduction pathways of nuclear transcriptional factors and cytokines reported in the literature. The results suggest that the toxicity of arsenic leads to increasing levels of hepatic lipogenesis. The high fat diet with or without arsenic produces greater pathology than a low fat diet resulting in microvesicular and macrovesicular steatosis with inflammation and necrosis of liver cells.

A disadvantage of the mouse model used in this study was the inadequate amount of blood available per mouse for measuring the parameters characteristic of diabetes mellitus. Furthermore, rodents may tolerate much higher doses of arsenic than humans due to an increased ability to metabolize and excrete arsenic [37].

ACKNOWLEDGEMENTS

The authors acknowledge the collaboration of the Department of Defense Veterinary Food Analysis and Diagnostic Laboratory in Fort Sam Houston, Texas. The electron microscopy results were obtained in the Analytical Cytology Core Facility, Border Biomedical Research Center. The study was supported by the NIH-RCMI #5G12RR008124, a Health Oriented Topics grant from the Center for Border Health Research, Paso del Norte Health Foundation and the Clinical Investigations Department, William Beaumont Army Medical Center, El Paso, Texas.

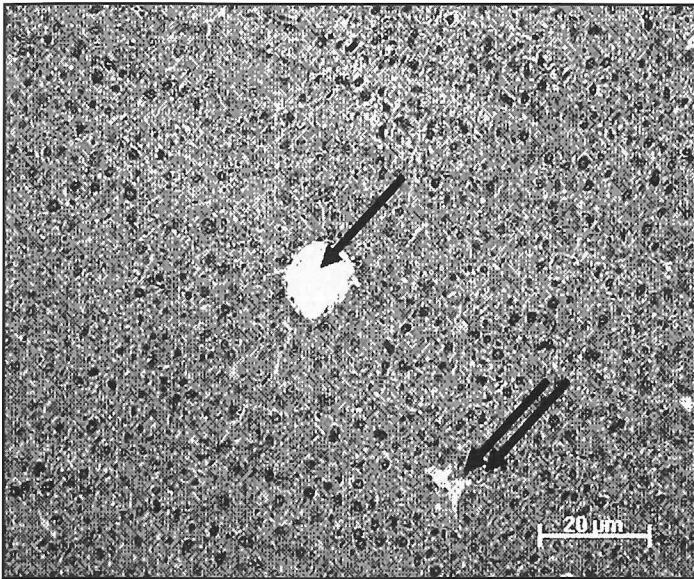


Figure 1: Representative light micrograph (X200) of a CL-mouse liver section representing the normal histological view of cords of hepatocytes around the central vein (single arrow) and interlobular vein (double arrow).

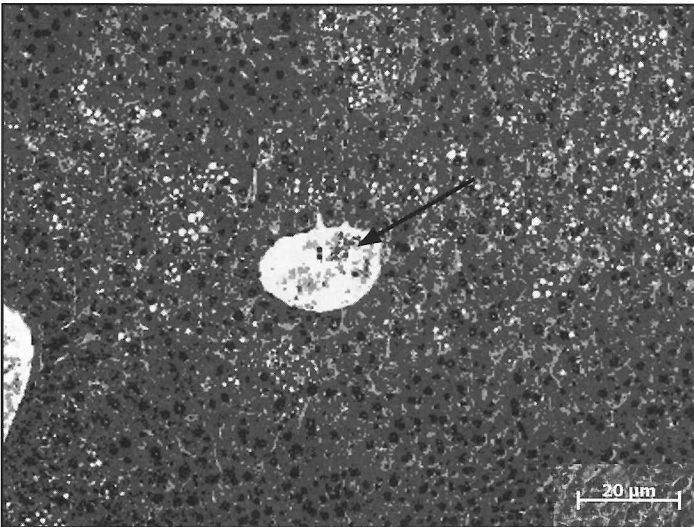


Figure 2: Representative light micrograph (X200) of an AL-mouse liver lobule showing steatosis (white inclusions) in the hepatocytes of the cords around the central vein (arrow).

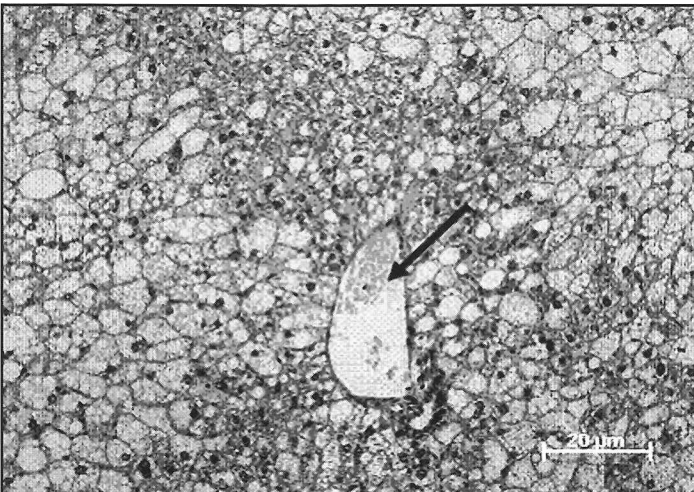


Figure 3: Representative light micrograph (X200) of a CH-mouse liver lobule showing severe steatosis (white inclusions) in the hepatocytes of the cords around the central vein (arrow).

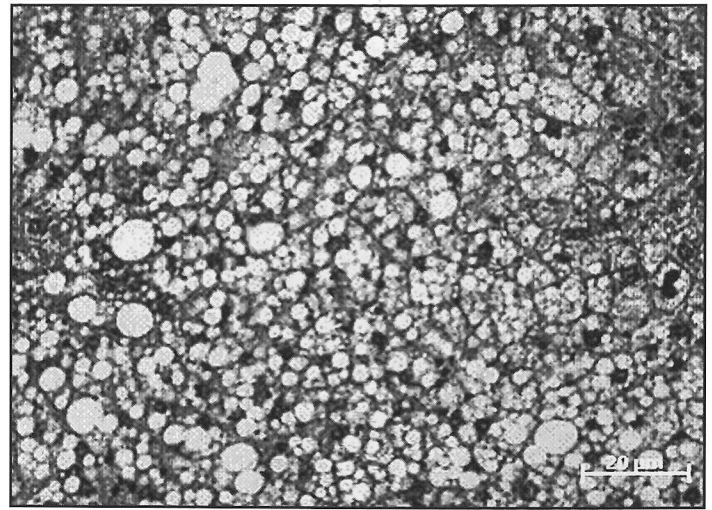


Figure 4: Representative light micrograph (X200, PAS stain) of an AH-mouse hepatic parenchyma demonstrating marked macrovesicular and microvesicular steatosis (white inclusions). The steatosis almost completely obscures the underlying hepatic parenchyma.

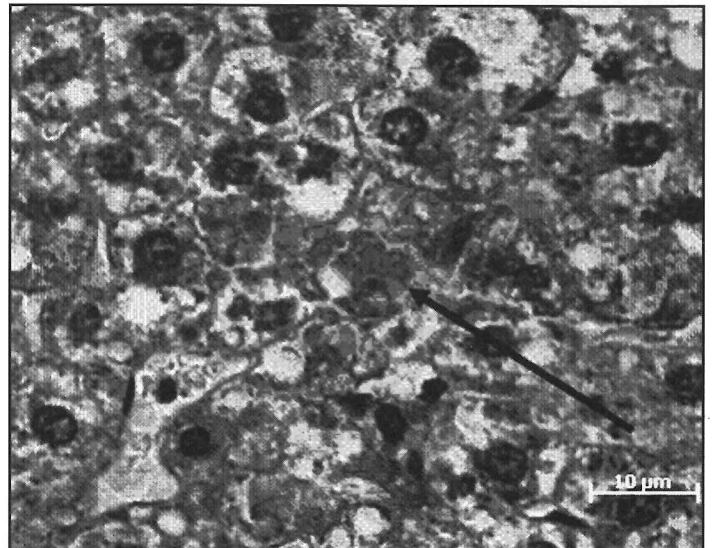


Figure 5: Representative light micrograph (X400, PAS stain) of an AH-mouse hepatic parenchyma demonstrating single cell necrosis (arrow).

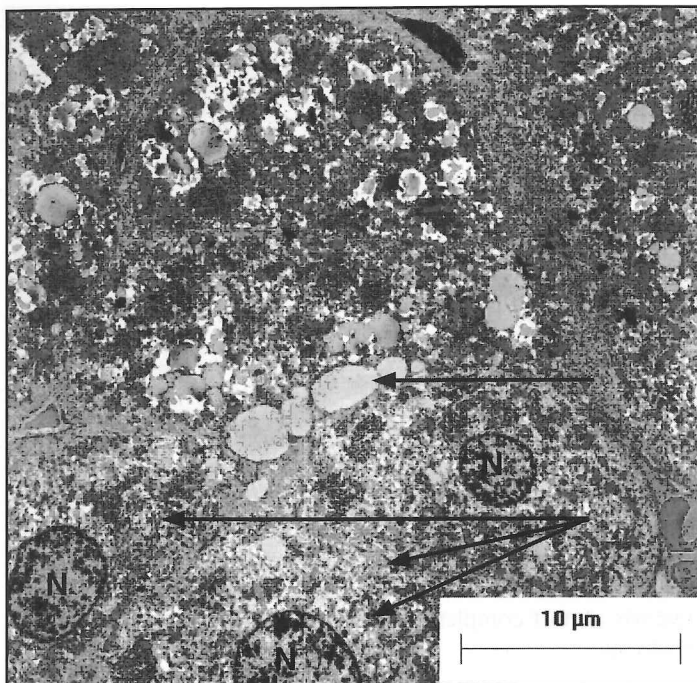


Figure 6: Representative TEM of a CL-mouse liver tissue showing the beginning of lipid accumulation (arrows) within hepatocytes (X1,600).

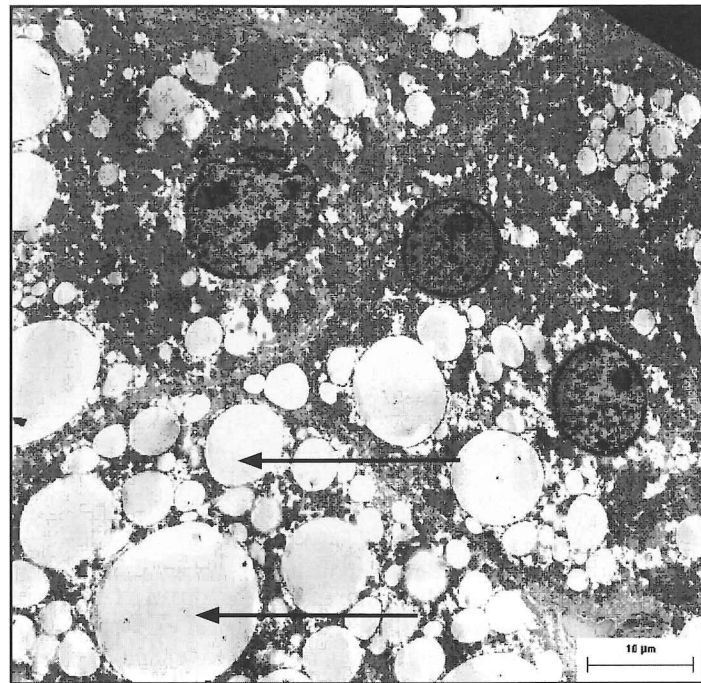


Figure 8: Representative TEM of the control high fat mouse liver tissue. Hepatocytes exhibit macrovesicular and microvesicular steatosis (arrows) (X1,600).

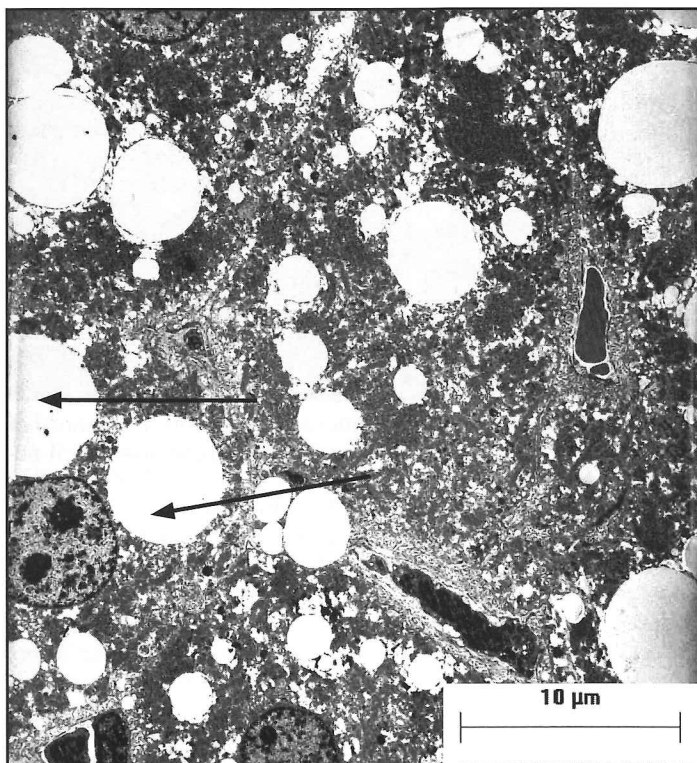


Figure 7: Representative TEM of the 22.5ppm As (III)-exposed low fat diet mouse liver. Hepatocytes exhibit macrovesicular and microvesicular steatosis (arrows) (X1,600).

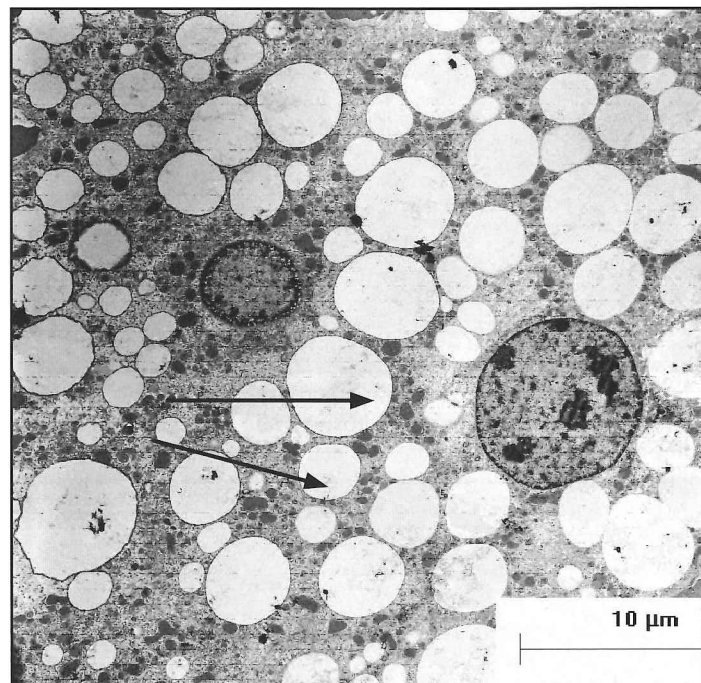


Figure 9: Representative TEM of the 22.5ppm As (III)-exposed high fat diet mouse liver. Hepatocytes exhibit steatosis (arrows) (X1,600).

REFERENCES

- Asilmaz, E., P. Cohen, M. Miyazaki, P. Dobrzyn, K. Ueki, G. Fayzikhodjaeva, A. A. Soukas, Alexander A.; R. C. Kahn, J. M. Ntambi, N. D. Socci, and J. M. Friedman. Site and mechanism of leptin action in a rodent form of congenital lipodystrophy. *Journal of Clinical Investigation*, 113(3) (2004) 414-424.
- Black, P. The inflammatory response is an integral part of the stress response: Implications for atherosclerosis, insulin resistance, type II diabetes and metabolic syndrome X. *Brain, Behavior, and Immunity*, 17 (2003) 350-364.
- Carey, A., B. Lamont, S. Andrikopoulos, I. Koukoulas, J. Proietto, and M. Febbraio. Interleukin-6 gene expression is increased in insulin-resistant rat skeletal muscle following insulin stimulation. *Biochemical and Biophysical Research Communications*, 302 (2003) 837-840.
- Dandona, P., A. Aljada, and A. Bandyopadhyay. Inflammation: the link between insulin resistance, obesity and diabetes. *Trends in Immunology*, 25(1) (2004) 4-7.
- Degrace, P., L. Demizieux, J. Gresti, J.-M. Chardigny, J.-L. Sebedio, and P. Clouet. Association of liver steatosis with lipid oversecretion and hypertriglyceridemia in C57BL/6J mice fed trans-10,cis-12-linoleic acid. *Letters*. 546(2-3) (2003) 335-339.
- Degrace, P.; L. Demizieux, J. Gresti, J. M. Chardigny, J. L. Sebedio, and P. Clouet. Hepatic steatosis is not due to impaired fatty acid oxidation capacities in C57BL/6J mice fed the conjugated trans-10,cis-12-isomer of linoleic acid. *Journal of Nutrition*, 134(4) (2004) 861-867.
- den Boer, M. A. M., P. J. Voshol, J. P. Schroeder-van der Elst, E. Korshennikova, M. D. Ouwers, D. F. Kuipers, L. M. Havekes, and J. A. Romijn. Endogenous interleukin-10 protects against hepatic steatosis but does not improve insulin sensitivity during high-fat feeding in mice. *Endocrinology*, 147(10) (2006) 4553-4558.
- Diehl, A. M. Obesity and alcoholic liver disease. *Alcohol*, 34 (2004) 81-87.
- Eliassen, K. A., B. P. Brodal, A. Svindland, H. Osmundsen, H. Roenning, S. Djurovic, and K. Berg. Activity of peroxisomal enzymes, and levels of polyamines in LPA-transgenic mice on two different diets. *Lipids in Health and Disease*, 4(23) (2006) No pages given.
- Fischer, C., L. Perstrup, A. Berntsen, P. Eskildsen, and B. Pedersen. Elevated plasma interleukin-18 is a marker of insulin-resistance in type 2 diabetic and non-diabetic humans. *Clinical Immunology*, 117(2) (2005) 152-160.
- Gavrilova, O., M. Haluzik, K. Matsusue, J. J. Cutson, L. Johnson, K. R. Dietz, C. J. Nicol, C. Vinson, F. J. Gonzalez, and M. L. Reitman. Liver peroxisome proliferator-activated receptor γ contributes to hepatic steatosis, triglyceride clearance, and regulation of body fat mass. *Journal of Biological Chemistry*. 278(36) (2003) 34268-34276.
- Gentry, P., T. Covington, S. Mann, A. Shipp, J. Yager, and H. Clewell. Physiologically based pharmacokinetic modeling of arsenic in the mouse. *Journal of Toxicology and Environmental Health A*, 67 (2004) 43-71.
- Grefhorst, A., J. Hoekstra, T. Derks, G. J. Terry, M. D. Ouwers, J. F. W. Baller, R. H. Havinga, M. Louis, J. A. Romijn, and F. Kuipers. Differential effects of pharmacological liver X receptor activation on hepatic and peripheral insulin sensitivity in lean and ob/ob mice. *American Journal of Physiology*, 289(5, Pt. 1) (2005) E829-E838.
- Grefhorst, A., T. H. van Dijk, A. Hammer, F. H. van der Sluijs, R. Havinga, L. M. Havekes, J. A. Romijn, P. H. Groot, D.-K. Reijngoud, and F. Kuipers. Differential effects of pharmacological liver X-receptor activation on hepatic and peripheral insulin sensitivity in lean and ob/ob mice. *American Journal of Physiology*, 289(3, Pt. 1) (2005) G592-G598.
- Hara K., O. Terumasa, K. Tobe, K. Yasuda, Y. Mori, H. Kadowaki, R. Hagura, Y. Akanuma, S. Kimura, C. Ito, and T. Kadowaki. The Pro12Ala polymorphism in PPAR-2 may confer resistance to type 2 diabetes. *Biochemical and Biophysical Research Communications*, 271 (2000) 212-216.
- Harano, Y., K. Yasui, T. Toyama, T. Nakajima, H. Mitsuyoshi, M. Mimani, T. Hirasawa, Y. Itoh, and T. Okanoue. Fenofibrate, a peroxisome proliferator-activated receptor α agonist, reduces hepatic steatosis and lipid peroxidation in fatty liver Shionogi mice with hereditary fatty liver. *Liver International*, 26(5) (2006) 613-620.
- Hookman P., and J. S. Barkin. Current biochemical studies of nonalcoholic fatty liver disease and nonalcoholic steatohepatitis suggest a new therapeutic approach. *The American Journal of Gastroenterology*, 98(9) (2003) 2093-7.
- Hu Y., X. Jin, and E. Snow. Effect of arsenic on transcription factor AP-1 and NF- κ B. *Toxicology Letters*, 133(2002) 33-45.
- Inoue, M., T. Ohtake, N. Takahashi, M. Nagamine, S. Tanno, Y. Kohgo, and T. Okumura. Increased expression of PPAR in high fat diet-induced liver steatosis in mice. *Biochemical and Biophysical Research Communications*, 336(1) (2005) 215-222.
- Jacoby, R., J. Fox, and M. Davisson. *Clinical Chemistry Reference Ranges for Adult Mice in Laboratory Animal Medicine*, 2nd Edition. James G. Fox, et al., editors. New York: Academic Press, (2002) 44.
- Kaser, S., A. Moschen, A. Cayon, A. Kaser, J. Crespo, F. Pons-Romero, C. F. Ebenbichler, J. R. Patsch, and H. Tilg. Adiponectin and its receptors in non-alcoholic steatohepatitis. *Gut*. 54(1) (2005) 117-121.
- Kota, P., H. Hsun-Wei, and B. Roufogalis. An overview on biological mechanisms of PPAR's. *Pharmacological Research* 51 (2005) 85-94.
- Laurent, A., C. Nicco, J. T. V. Nhieu, D. Borderie, C. Chereau, F. Conti, P. Jaffray, O. Soubrane, Y. Calmus, B. Weill, and F. Batteux. Pivotal role of superoxide anion and beneficial effect of antioxidant molecules in murine steatohepatitis. *Hepatology*, 39(5) (2004) 1277-1285.
- Leclercq, I. A.; G. C. Farrell, C. Sempoux, A. dela Pena, and Y. Horsmans. Curcumin inhibits NF- κ B activation and reduces the severity of experimental steatohepatitis in mice. *Journal of Hepatology*, 41(6) (2004) 926-934.
- Letteron, P., A. Sutton, A. Mansouri, B. Fromenty, and D. Pessayre. Inhibition of microsomal triglyceride transfer protein: another mechanism for drug-induced steatosis in mice. *Hepatology*, 38(1) (2003) 133-140.
- Luquet, S., C. Gaudel, D. Holst, J. Lopez-Soriano, C. Jehl-Pietri, A. Fredenrich, and P. Grimaldi. Roles of PPAR delta in lipid absorption and metabolism: a new target for the treatment of type 2 diabetes. *Biochimica et Biophysica Acta* 1740 (2005) 313- 317.

27. Moraes, L., L. Piqueras, and D. Bishop-Bailey. Peroxisome proliferator-activated receptors and inflammation. *Pharmacology and Therapeutics* 110(3) (2006) 371-385.
28. Motomura, W., M. Inoue, T. Ohtake, N. Takahashi, M. Nagamine, Miho, S. Tanno, Y. Kohgo, and T. Okumura. Up-regulation of ADRP in fatty liver in human and liver steatosis in mice fed with high fat diet. *Biochemical and Biophysical Research Communications*, 340(4) (2006) 1111-1118.
29. Park, S. H., S. G. Lee, S. K. Kang, K. Sung Keel, and S. H. Chung. *Acanthopanax senticosus* reverses fatty liver disease and hyperglycemia in ob/ob mice. *Archives of Pharmacological Research*, 29(9) (2006) 768-776.
30. Roden, M. Mechanisms of Disease: hepatic steatosis in type 2 diabetes-pathogenesis and clinical relevance. *Nature Clinical Practice Endocrinology and Metabolism*, 2(6) (2006) 335-348.
31. Sahai, A., P. Malladi, H. Melin-Aldana, R. M. Green, and P. F. Whittington. Upregulation of osteopontin expression is involved in the development of nonalcoholic steatohepatitis in a dietary murine model. *American Journal of Physiology*, 287(1, Pt. 1) (2004) G264-G273.
32. Schwabe, R. F. Endocannabinoids promote hepatic lipogenesis and steatosis through CB1 receptors. *Hepatology*, 42(4) (2005) 959-961.
33. Sekiya, M., N. Yahagi, T. Matsuzaka, Y. Najima, M. Nakakuki, R. Nagai, S. Ishibashi, J.-I. Osuga, N. Yamada, and H. Shimano. Polyunsaturated fatty acids ameliorate hepatic steatosis in obese mice by SREBP-1 suppression. *Hepatology*, 38(6) (2003) 1529-1539.
34. Steneberg, P., N. Rubins, R. Bartoov-Shifman, M. D. Walker, and H. Edlund. The FFA receptor GPR40 links hyperinsulinemia, hepatic steatosis, and impaired glucose homeostasis in mouse. *Cell Metabolism*, 1(4) (2005) 245-258.
35. Styblo, M., L. M. Del Razo, E. L. LeCluise, G. A. Hamilton, C. Wang, W. R. Cullen and D. J. Thomas. Metabolism of arsenic primary cultures of human and rat hepatocytes. *Chem. Res. Toxicology* 12 (1999) 560-565.
36. Takahashi, N., Y. Qi, H. R. Patel, and R. S. Ahima. A novel aminosterol reverses diabetes and fatty liver disease in obese mice. *Journal of Hepatology*, 41(3) (2004) 391-398.
37. Tanaka, T., H. Masuzaki, K. Ebihara, Y. Ogawa, S. Yasue, H. Yukioka, H. Chusho, F. Miyanaga, T. Miyazawa, M. Fujimoto, T. Kusakabe, N. Kobayashi, T. Hayashi, K. Hosoda, and K. Nakao. Transgenic expression of mutant peroxisome proliferator-activated receptor- γ in liver precipitates fasting-induced steatosis but protects against high-fat diet-induced steatosis in mice. *Metabolism, Clinical and Experimental*, 54(11) (2005) 1490-1498.
38. Tomita, K., G. Tamiya, S. Ando, K. Ohsumi, T. Chiyo, A. Mizutani, N. Kitamura, K. Toda, T. Kaneko, Y. Horie, J.-Y. Han, S. Kato, S.; M. Shimoda, Y. Oike, M. Tomizawa, S. Makino, T. Ohkura, H. Saito, N. Kumagai, H. Nagata, H., H. Ishii, and T. Hibi. Tumour necrosis factor signalling through activation of Kupffer cells plays an essential role in liver fibrosis of non-alcoholic steatohepatitis in mice. *Gut*, 55(3) (2006) 415-424.
39. Ueki, K., T. Kadowaki, and R. C. Kahn. Role of suppressors of cytokine signaling SOCS-1 and SOCS-3 in hepatic steatosis and the metabolic syndrome. *Hepatology Research*, 33(2) (2005) 185-192.
40. Ueki, K., T. Kondo, Y.-H. Tseng, and R. C. Kahn. Central role of suppressors of cytokine signaling proteins in hepatic steatosis, insulin resistance, and the metabolic syndrome in the mouse. *Proceedings of the National Academy of Sciences of the United States of America*, 101(28) (2004) 10422-10427.
41. Vigo, J. B., and J. T. Ellzey. Effects of arsenic toxicity at the cellular level: A Review. *Texas Journal of Microscopy*, 37(2) (2006) 45-49.
42. Walton, F., A. Harmon, D. Paul, Z. Drobna, Y. Patel, and M. Styblo. Inhibition of insulin-dependent glucose uptake by trivalent arsenicals: possible mechanisms of arsenic-induced diabetes. *Toxicology and Applied Pharmacology*, 198(3) (2004) 424-433.
43. Xu, A., Y. Wang, H. Keshaw, L. Y. Xu, K. S. Lam, and G. J. S. Cooper. The fat-derived hormone adiponectin alleviates alcoholic and nonalcoholic fatty liver diseases in mice. *Journal of Clinical Investigation*, 112(1) (2003) 91-100.
44. Yu, S., K. Matsusue, P. Kashireddy, W. Q. Cao, V. Yeldandi, A. Yeldandi, M. S. Rao, F. J. Gonzalez, and J. K. Reddy. Adipocyte-specific gene expression and adipogenic steatosis in the mouse liver due to peroxisome proliferator-activated receptor- γ 1 (PPAR- γ 1) overexpression. *Journal of Biological Chemistry*. 278(1) (2003) 498-505.

ADVERTISER'S INDEX

Advertiser	Page Located	Advertiser	Page Located
Diatome U.S.	96	Micro Star Technologies, Inc.	107
Electron Microscopy Sciences.....	138	Ted Pella Inc.	125
FEI Company.....	139	Tousimis Research Co.	140
Gatan, Inc.	94	Zeiss.....	137
Hitachi High Technologies America	135		

Next Generation Silicon Nitride Support Films for TEM

Advantages:

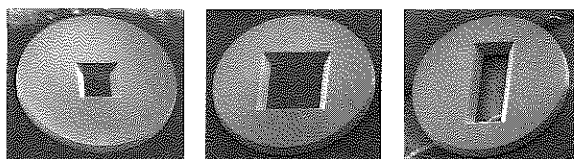
- 3.0 mm circular frame for standard TEM holders
- EasyGrip™ edge for ease of handling
- Resilient and chemically inert planar substrate
- Usable across a range of microscopy platforms (SEM, AFM, TEM through to optical)
- Free from debris or broken edges

Applications:

- High temperature experiments
- Observation of deposited thin films
- Direct cell growth including electron tomography
- Imaging and analysis of nanoparticles, nanofibers and nanotubes

Specifications:

- Window sizes: 0.5 x 0.5; 1.0 x 1.0 and 1.5 x 0.5mm



0.5 x 0.5mm

1.0 x 1.0mm

1.5 x 0.5mm

- Special size for electron tomography, 0.5mm x 1.5mm, allowing extended area imaging at high tilt
- 200 micrometer silicon substrate with 50nm ultra-low stress silicon nitride

21500-10 Silicon Nitride Membrane, 0.5 x 0.5mm, 50nm thickness, pkg/10

21500-100 Silicon Nitride Membrane, 0.5 x 0.5mm, 50nm thickness, pkg/100

21502-10 Silicon Nitride Membrane, 1.0 x 1.0mm, 50nm thickness, pkg/10

21502-100 Silicon Nitride Membrane, 1.0 x 1.0mm, 50nm thickness, pkg/100

21504-10 Silicon Nitride Membrane, 1.5 x 0.5mm, 50nm thickness, pkg/10

21502-100 Silicon Nitride Membrane, 1.5 x 0.5mm, 50nm thickness, pkg/100

PELCO® Silicon Aperture Frames (without support film)

The PELCO® Silicon Aperture Frames are 3mm disk type frames with a thickness of 200µm and square or rectangular apertures. They have found a variety of applications:

- Support frame to attach TEM lamellas made with FIB
- Support frame for thin films, foils, wires and fibers
- Mask for thin film research (deposition mask)

21540-10 PELCO® Silicon Aperture Frame (no support film) 0.5 x 0.5mm, pkg/10

21541-10 PELCO® Silicon Aperture Frame (no support film) 1.0 x 1.0mm, pkg/10

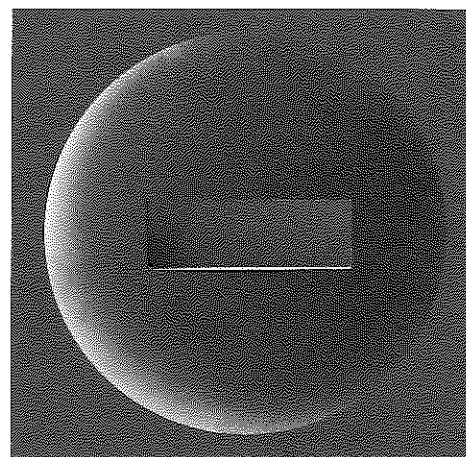
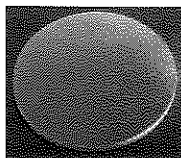
21542-10 PELCO® Silicon Aperture Frame (no support film) 1.5 x 0.5mm, pkg/10

Silicon Nitride Coated 3mm Disks (blanks)

These 3mm silicon disks have a 50nm ultra low stress silicon nitride layer (Si_3N_4) on both sides and can be used for a number of applications:

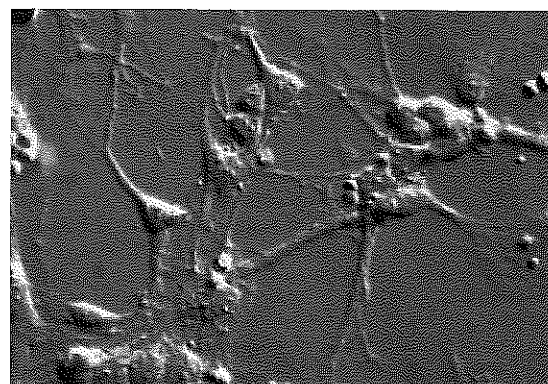
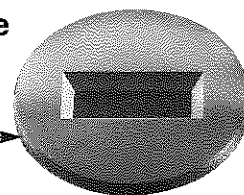
- Specimen mounts for SEM and FESEM applications
- Specimen disks for AFM applications which need a Si_3N_4 background
- Blanks to build the PELCO® Liquid Cell™ together with the PELCO® Silicon Nitride Membrane

21555-10 PELCO® Silicon Nitride 3mm Disks, pkg/10



Circular Shape

EasyGrip™
Edge



DIC image of hippocampus neurons grown on a silicon nitride substrate by Prof. M. Stowell, et. al., MCDB, CU-Boulder, Colorado

www.tedpella.com/grids_html/silicon-nitride.htm

TED PELLA, INC.
Microscopy Products for Science and Industry

4595 Mountain Lakes Blvd., Redding, CA 96003
Phone: 800-237-3526 • FAX: 530-243-3761
sales@tedpella.com • www.tedpella.com

Abstracts

BIOLOGICAL SCIENCES

Fall 2007

MICROSCOPIC SURVEY ON BIODIVERSITY OF AQUATIC COMMUNITY IN CETA CANYON. KAITLYN BALLEW, JOEL BABITZKE, WILLIAM J. ROGERS and NABARUN GHOSH, Department of Life, Earth and Environmental Sciences, West Texas A&M University, Canyon, TX 79016

Ceta Canyon, founded in 1918, serves as a major retreat center hosting many events like camping and excursions. Improvements in the last decade have greatly enhanced the capacity and versatility of this reserve in serving all types of groups. Reports are meager on biodiversity of the local streams, ponds and the waterfall in Ceta Canyon. Samples of phytoplankton, zooplankton, aquatic angiosperms and arthropods were collected using various types of nets, such as the Surber stream sampler, phytoplankton nets, and sweep nets. Collection was done all along the shoreline through a stream that runs through the center of the Ceta Canyon. The collected samples were placed in labeled vials for further observation, identification and analysis. Prepared slides from samples were observed at different magnifications with an Olympus BX40 microscope equipped with FITC (fluorescein-isothiocyanate) and TRITC (tetramethylrhodamine) fluorescent filters, a mercury lamp source, an Olympus DP-70 digital camera connected to the computer. The micrographs were captured with DP Manager and were analyzed using the Image Pro 6.0 software. Twenty-five organisms were viewed and photographed using bright field, FITC, and TRITC filter settings. A high-pressure mercury lamp was used to excite the storage molecules or proteins of the organisms. The micro-arthropods were viewed and photographed with an Olympus SZ-40 stereomicroscope attached to a DVC camera that helped us identify the specimens. Besides a rich planktonic diversity, common freshwater insects like dragonflies, damselflies (Odonata), stoneflies (Plecoptera), caddisflies (Trichoptera), and mayflies (Ephemeroptera) were found. The organisms varied in taxonomic composition and density in the three parts of the stream namely riffle, run and pool.

MICROSCOPIC EVALUATION OF ROUNDUP EFFECT ON A FRESHWATER PLANKTONIC COMMUNITY. JENNIFER COLLINS, WILLIAM J. ROGERS and NABARUN GHOSH, Department of Life, Earth and Environmental Sciences, West Texas A&M University, Canyon, TX 79016.

Prymnesium parvum, a flagellated unicellular golden alga, is a mixotroph with the ability to exist as a photosynthetic autotroph or heterotroph predator. For yet unknown reasons, the algae bloom and shift from autotrophic to heterotrophic states. In the respiration mode, the organism releases toxins that attach to fish gill surfaces, thus causing the loss of millions of fish every year in Texas. The objective of this study was to determine if the herbicide Roundup, commonly used on Roundup ready cotton, causes the shift in a photosynthetic/aerobic freshwater planktonic community. Water was sampled from Colorado City Lake in 32-ounce jars (double blind method design). Eight jars were used for each experimental group: control with no Roundup, 1 ppm, 10 ppm, and 100 ppm Roundup. Samples were kept under a 12-12 hours photoperiod over a seven-day period. The concentration of golden

algae and *Chlamydomonas* sp., obligate photosynthetic organisms (indicator organism in the experiment), were assessed. Plankton counts were conducted at 24 hours, 48 hours, 96 hours, and 168 hours from the beginning of the experiment using a Sedgwick-Rafter cell counter under a BX-40 Olympus microscope attached to a DP-70 digital camera. A 1 ml sample was collected, at the specified time interval, and then counted using a Palmer Counting Cell at 50-500 magnification. The results on golden algae were inconclusive. The golden algae seemed to survive over the different time intervals and Roundup concentrations. *Chlamydomonas* counts at the 1ppm Roundup concentration were not significantly different ($\alpha=0.05$) from the control, but they dropped significantly at 10 ppm and 100 ppm Roundup. Assuming that the golden algae population remained the same and that the *Chlamydomonas* population decreased by over five fold, we believe a shift in the planktonic community can occur at 10 and 100 ppm. Funding Source: REU Program Summer Grant, 2007.

IMMUNOCYTOCHEMICAL LOCALIZATION OF SITES OF ETHYLENE PRODUCTION IN PIERCE'S DISEASE IN GRAPE PETIOLES. E. ANN ELLIS¹, B. GREG COBB², and GEORGE R. MCEACHERN², ¹Microscopy and Imaging Center and ²Dept. of Horticultural Sciences, Faculty of Molecular and Environmental Plant Sciences, Texas A&M University, College Station, TX 77843.

Pierce's disease, an economically important plant pathogen, infects the xylem of wine producing grapes in the southeastern states, Texas and California. Previous transmission electron microscopy studies of Pierce's disease demonstrated the bacterium *Xylella fastidiosa* in the xylem of grape (*Vitis vinifera*) petioles. Tyloses and gums produced in infected xylem result in partial vascular occlusion, possible water stress and senescence of the leaves. The phytohormone ethylene modulates many processes in plant morphogenesis and pathology and can be produced by both higher plants and microorganisms. A number of studies have indicated a role for ethylene production by microorganisms in plant pathology. In addition, control plants treated with ethylene exhibit foliar symptoms of Pierce's disease. The enzyme 1-aminocyclopropane-1-carboxylate oxidase (ACC oxidase) is a marker for sites of ethylene production. This study used colloidal gold based immunocytochemical localization of ACC oxidase in petioles of grape leaves infected with *X. fastidiosa* to determine sites of ethylene production in Pierce's disease. ACC oxidase localized in the bacteria, adjacent to the bacteria in the xylem and accumulated in xylem cell walls. There were decreased levels of ACC oxidase in the cytoplasm of parenchyma cells and adjacent vacuoles and cell walls. Localization of the enzyme in cell walls and vacuoles probably indicates cell wall absorption of the secreted enzyme. This work provides evidence for a role for ethylene generated by ACC oxidase in the etiology of Pierce's disease.

A NON-DESTRUCTIVE METHOD OF EXAMINING TREE RINGS WITH A HANDHELD MICROSCOPE CAMERA.

TINA HALUPNIK, Department of Biology, University of Texas at Arlington, Arlington, Texas 76019.

The ProScope HR device is an affordable handheld microscope camera, useful in a wide range of fields, both amateur and professional. Actively powered via a PC USB connection, magnified images up to 400X can be viewed in real time on the computer, before being captured as stills, movies, or time-lapse sequences. LED lights are built into most of the lenses, to illuminate the subject. I have recently found the ProScope HR to be a useful tool for examining tree rings. Previously, when researchers wanted to microscopically examine tree rings, long cylindrical cores of wood would be removed from living trees in the field, then specially prepared to be examined with compound light microscopes. This method of examining tree rings is not feasible if only a large, intact section of trunk is available and it is either not possible or desirable to cut into the sample for cores. Dr. Howard J. Arnett's intact slab of Prometheus, an ancient bristlecone pine (*Pinus longaeva*), is an example of a piece of wood that should not be sectioned. Since the ring data spans 4900 years of life, the value of this segment of Prometheus lies in its intact condition. Using the ProScope, I have captured 30X, 100X, and 400X micrographs of Prometheus, with enough detail to accurately measure the features of the rings. These micrographs also reveal some issues that need to be addressed. Increased magnification reveals surface marks that obscure the cells. These marks need to be removed. Furthermore, since the microscope performs best when contacting the sample surface, uneven surfaces produce uneven areas of image sharpness. Despite this, when tree samples prove too large to examine with conventional compound microscopes, a handheld USB microscope camera like the ProScope can produce satisfactory micrographs without damaging the wood.

INVESTIGATION OF *SARRACENIA ALATA* (WOOD). RACHAEL N. JONES and DENNIS A. GRAVATT, Department of Biology, Stephen F. Austin State University, Nacogdoches, TX 75962.

Sarracenia alata Wood (pitcher plant or yellow trumpet) is typically found in saturated, acidic, nutrient deprived soils. The populations used in this study are located in the Angelina National Forest near Boykin Springs Park, Angelina County, Texas. They are located in herbaceous seeps embedded within dry sandy uplands. The leaves of *S. alata* are comprised of the hood, peristome, ala, and pitcher. Internally, we found that the leaves can be delineated into four zones: zone 1 refers to the hood; zone 2 contains the peristome; zone 3 includes the top portion of the pitcher; and zone 4 is the bottom portion of the pitcher. Samples from internal and external portions from all four zones were collected, preserved, fixed, and prepared for SEM. Key identifying features for each zone were noted. Trichome and stomatal morphology were described for each of the four zones. The trichome morphology was found to differ amongst the zones, and the stomata were embedded within stomatal crypts. However, there was a lack of nectar glands in the peristome as previously reported with other *Sarracenia* species. This study will serve as foundational work for future studies of *S. alata*.

ANTIGEN RETRIEVAL IN FtsZ LOCALIZATION IN *ARABIDOPSIS THALIANA*. CAROL B. JOHNSON and E. ANN ELLIS, Microscopy and Imaging Center and Department of Biology, Texas A&M University, College Station, TX 77843.

Filamentous temperature sensitive Z ring (FtsZ) protein is a cytoskeletal GTPase and structural homologue of tubulin that is important in chloroplast division. Previous immunofluorescence studies in *Arabidopsis thaliana* demonstrated two forms, FtsZ-1 and FtsZ-2, which are involved in ring formation at the site of

division of chloroplasts in higher plants. This study investigated the appropriate immunolabeling conditions for ultrastructural localization of these proteins. Antigen retrieval with heat and high pH was necessary in order to improve immunolabeling at the light microscope level. Conventional immunocytochemical localization (no antigen retrieval) used rabbit anti-FtsZ-1 and rabbit anti-FtsZ-2-1 primary antibodies with goat-anti-rabbit IgG secondary antibodies labeled with 12 nm colloidal gold. Antigen retrieval with urea at high pH (pH 9.5) was used in an attempt to improve immunolabeling at the ultrastructural level. Micrographs of the conventional localization of FtsZ-1 revealed localization in the stroma of the chloroplasts. Micrographs of conventional localization of FtsZ-2-1 showed localization in the inner chloroplast membrane and in the stroma. Antigen retrieval localization of FtsZ-2-1 is visible in the thylakoid membranes, in the stroma, and in the cytoplasm and cell walls. A comparison of the two localization methods indicates that the level of labeling was higher with the antigen retrieval method. However, more non-specific labeling was observed. The increased non-specific labeling with antigen retrieval suggests that a higher dilution of primary antibody might give more specific localization.

CHANGES IN TRACHEID LENGTH OF PROMETHEUS (*PINUS LONGAEVA*). KELSEY A. PENDLEY and HOWARD J. ARNETT. The Department of Biology and The Center for Electron Microscopy, The University of Texas at Arlington, Arlington, TX 76019.

Pinus longaeva trees (bristlecone pines) are the oldest known living trees. Because of their extreme age, they may be able to reveal information about past glacial periods such as the Little Ice Age. We conducted an investigation to see if tracheid length in bristlecones and temperatures of the Medieval Warming Period and the Little Ice Age correlate. Tracheid length data for this study was obtained from Baas *et al.* (1986) and temperature reconstructions were provided by Robert A. Rhode. Using those data, we found no correlation between tracheid length and temperature. The literature indicates that some tree species typically display signs of tracheid senescence with age. Example species include: *Fagus sylvatica*, *Pseudotsuga taxifolia*, *Pinus sylvestris*, and *Picea abies* (Dinwoodie, 1961). However, one study conducted on trees of *P. longaeva* concluded that tracheids of this species continue to steadily increase in length through time (2200 years) (Baas *et al.*, 1986). Further research on the species *P. longaeva* supports the idea that bristlecone pines do not senesce (Lanner and Connor, 2001). The first 400 of 4901 years of the oldest known bristlecone pine, Prometheus, were macerated using Franklin's method. The tracheids in each sample were measured using NIS-Elements and evaluated. The tracheids displayed a strong juvenile growth phase followed by a period that appeared to level off. Our hypothesis is that the tracheids of Prometheus will match the results of the Baas *et al.* (1986) study. Further macerations of the remaining 4500 years will be necessary to determine if our hypothesis is correct.

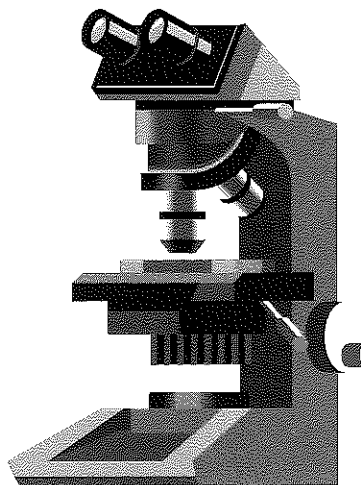
Baas, P., Schmid, R., and van Heuven, B.J. (1986). Wood anatomy of *Pinus longaeva* (bristlecone pine) and the sustained length-on-age increase of its tracheids. IAWA Bulletin, 7 (3), 221-228.
Dinwoodie, J.M. (1961). Tracheid and fibre length in timber; a review of literature. Forestry 34, 125-144.
Lanner, R.M. and Connor, K.F. (2001). Does bristlecone pine senesce? Experimental Gerontology 36, 675-685.

INVESTIGATING THE EFFECTS OF ESTROGEN ON ZEBRA FINCH EGGSHELL THICKNESS AND MAMMILLARY CONE COUNT. H. POURARSALAN and S.L. WEST-MORELAND, Dept. of Biology and The Center for Electron Microscopy, University of Texas at Arlington, Arlington, TX 76019.

Female Zebra finch chicks were exposed to estrogen in their daily consumption of seeds. We hypothesized that estrogen will cause eggshell thinning and higher mammillary cone density in Zebra Finch eggs. Jim Millam at University of California at Davis orally administered the experimental female chicks with estradiol benzoate in accordance to the normal consumption of it in nature and with canola oil for 7 days when they were 5-11 days old. Control females were administered canola oil only. The females were allowed to form mating pairs with males at 110 days and 25 eggs were collected: 15 control and 10 experimental. Three samples were removed from each eggshell and SEM images were taken at 500X. Thickness of the eggshells was determined using Image ProPlus. It was found that the eggshells from treated chicks were significantly thinner than the control ($p=0.02$). We then investigated the relationship between eggshell thickness and mammillary cone density. We marked the cone tips on the photos using Microsoft Photoshop and counted the tips using Image Pro Plus. The mean value for the thickness of eggshells from treated chicks was 65.97 micrometers (s.d.=11.2) while the mean value for control was 63 micrometers (s.d.=14.6). Although this difference was not significant ($p=0.228$), it shows a trend that the thicker the eggshell, the lower the mammillary cone density. Both experiments supported our original hypotheses regarding the effect of estradiol benzoate on eggshell thickness and shell morphology.

AN ELECTRON MICROSCOPY STUDY OF THE SALT GLANDS IN *ZOYSIA MATRELLA*. ¹SHEETAL RAO, ²E. ANN ELLIS, ²MICHAEL W. PENDLETON, and ¹MARLA BINZEL, ¹Department of Horticultural Sciences and ²Microscopy and Imaging Center, Texas A&M University, College Station, TX 77843.

Some salt tolerant plants are characterized by the presence of functional salt glands on their leaves. In *Zoysia matrella*, salt glands are modified trichomes, which facilitate excretion of excess salt. The overall objective of this research focused on studying the mechanism of salt tolerance in *Zoysia matrella*, a warm-season, highly salt-tolerant, turf grass. Scanning electron microscopy (SEM) and TEM studies of functional salt glands were done on plants grown in the greenhouse and watered with either deionized water (control) or high concentrations of sodium chloride (300 mM NaCl). SEM was used to visualize salt glands located on both the adaxial and abaxial leaf surfaces, and concentrated in rows parallel to stomata. In leaves from salinized plants, salt crystals were deposited next to the salt glands on the adaxial side indicating active salt secretion from glands. There were no salt crystals on leaves of control plants or on the abaxial side of salinized leaves. Energy dispersive spectroscopy (EDS) analysis of the leaf surface confirmed the presence of sodium and chlorine around the secreting salt gland. An opening near the tip of the salt gland is assumed to be the gland pore through which excess salt is excreted onto the leaf surface. TEM revealed a very thick cuticle around the salt glands. A large flask-shaped cell was prominent in all leaf sections from control as well as salt-treated plants. There was intense staining of the plasma membrane in the base of the salt gland and also in some of the epidermal cells adjacent to the salt gland. Phosphotungstic acid-chromic acid, a specific stain for plant plasma membranes, showed distinct invaginations of the plasma membrane in the salt gland. These invaginations presumably provide increased membrane surface area for salt pumping, thus increasing the secretory capability of the cells involved in salt secretion. This observation is consistent with previous studies in other species.



STRUCTURE AND SIGNIFICANCE OF TERMITE REACTION WOOD IN THE LIFE HISTORY OF THE JOSHUA TREE (*Yucca brevifolia*)

HOWARD J. ARNOTT

The Department of Biology and The Center for Electron Microscopy,
The University of Texas at Arlington, Arlington, TX, 76019

In 1951, on a field trip in the Mojave Desert with Dr. George R. Johnstone, Professor of Botany at the University of Southern California, I was introduced to the dense wood in the stem of the Joshua tree (*Yucca brevifolia* Engelm., *Agavaceae*). I still remember Dr. Johnstone's comment as he cut up a "chunk" of this dense wood. He said, "In this piece there are all the sclereids that anyone could ever want." In 2006, Catherine Arnott-Thornton and I chanced upon this dense wood again in several parts of the Mojave Desert. One occasion was at Saddleback Butte State Park, some 15 miles east of Lancaster, California; Joshua trees and creosote bushes (*Larrea tridentata*) are the dominant species found in the park. I have described this trip in my autobiography Part IV (Arnott, 2007, *Tx. J. Micr.* 38:1).

The stems of several downed Joshua Trees in the park contained dense wood similar to that seen earlier. The dense wood seems to be caused by an invasion of termites in the stem of the tree. It appears that the stem produces this dense tissue in an endeavor to wall off or impound the penetration of the termite colony. In producing this *termite reaction wood*, the tree often causes its own death by cutting off the supply of water to the upper part of the tree. The subject of this article is the nature of the termite reaction wood.

I collected small samples of termite reaction wood from dead trees west of Saddleback Butte State Park and from two dead trees just outside Death Valley National Monument. In every Joshua tree site that I inspected I was able to find termite reaction wood. However, the best sample I found was collected in 2006 along Wilson Farm Road, 0.2 miles south of Maricopa Road, in San Bernardino County, California. This piece was found on the ground near several Joshua trees; it was almost 60 cm. in length and about 18cm. in diameter. Some of this material was retained in the collection at the Laboratory for Tree-Ring Research at the University of Arizona in Tucson as a voucher. Sections were subsequently sanded to produce a surface that could be observed with the light microscope using reflected light. I was not able to make microtome sections of this material; however, occasional hand sections were adequate to be observed in transmission light.

Dead Joshua trees are readily seen on the Mojave Desert and can be observed on the ground or by aerial reconnaissance. Using *Windows Live Local* in regions where high resolution photos prevail, it is easy to spot dead Joshua trees as they have a common signature. The tree shown in Figure 1, photographed from the ground in 2006 was easily seen in Live Local aerial views of 2007. (As an aside, I want to point out that the nature of the creosote bush clones are easily seen in these aerial photographs; both "C" and circular bull's eye profiles can be enumerated). Most of the Joshua trees that I have observed on the ground had termite

colonies. Termite reaction wood can be found usually near the base of the trees. However, the termite reaction wood may be formed higher in the trunk as seen in Fig. 1. Wherever termite reaction wood is found, at the base or higher, the tree will subsequently die and eventually fall over. The reaction wood can be seen in stems that have undergone weathering; the bark and external tissues will weather much sooner than the termite reaction wood which is very dense and resistant. Sometimes it is necessary to "dissect" the stem to reveal the reaction wood. I have found large sections of termite reaction wood (see paragraph 3 above) at some distance from the plants in which they were formed as well as in the plant trunks (Figs. 1-4). The outside of the reaction wood weathers in the sunshine to a grey color; if the piece is inverted, it will be dark colored, often with a strong red tint. These pieces often show openings which represent termite channels (Fig. 4). Sometimes these openings are at the end of short tubular branches, which extend from the surface of the termite reaction wood; in other cases they are merely round holes on the surface of the wood (Figs. 3-4). It is worth noting that termites no longer occupy dead Joshua tree trunks on the ground.

When a cylindrical specimen like that in Figs. 2 and 3 was cut in cross section, it was observed that the termite reaction wood was filled with crevices or channels (Fig. 4, 5). Often these channels are filled with dirt and other debris left by the termites (Fig. 4). The dirt and debris can be removed using compressed air. Observation of clean sections showed crevices, which appeared to be randomly formed, but were in fact carefully "crafted" by stem growth (Fig. 5). When cross sections of a polished specimen of termite reaction wood were examined, several different zones could be identified. However, it is of first importance to note that most vascular bundles ran perpendicular to the cut surface. This is, of course, what one would expect to see in a normal yucca stem. The zones alluded to above speak about the way the plant has reacted to the termite channels. In different zones, the vascular bundles may be completely "embedded" in a tissue (matrix). This tissue appeared to be a mixture of sclerenchyma and parenchyma cells. In other zones, the vascular bundles were partly or completely free from this cellular matrix (Fig. 5, 13). Careful examination of Fig. 5 shows distinctive areas within the termite reaction wood. Clearly, there are tissues that show a direct relationship to the termite channels (fissures). Zones of radial development are associated with these channels. This seems to indicate that the reaction wood is formed over a period of time and that the cells of the reaction wood are formed by a cambium similar to that usually found in tree yuccas. The reaction wood differs from normal "wood" in Joshua tree stem in that the vascular bundles are well separated and the "wood" might be termed soft and spongy.

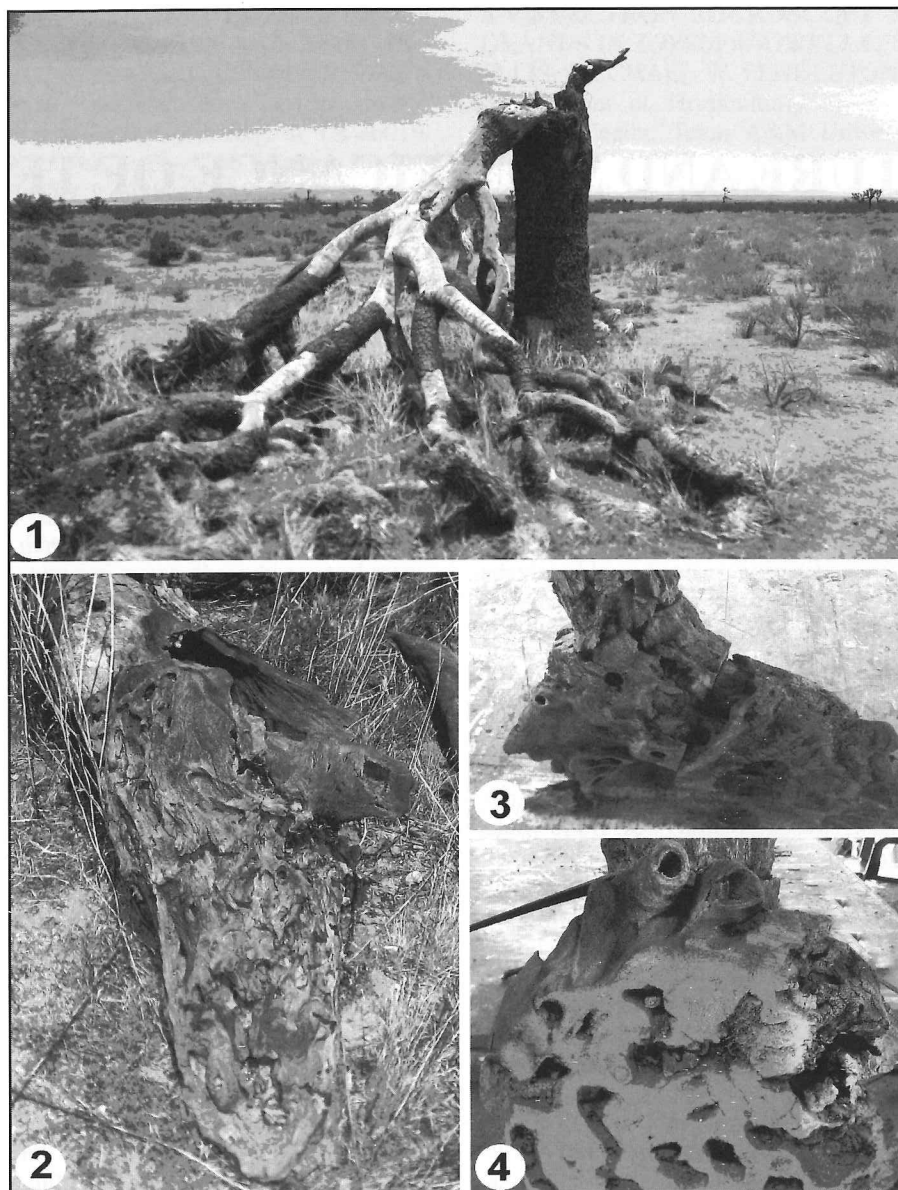


Figure 1. A dead Joshua tree located west of Buttermer Rd. and just north of the California Aqueduct, San Bernardino County, California. This tree had termite reaction wood just below the break. The same tree was observed in aerial photos on Windows Live Local. **Figure 2.** Large piece of termite reaction wood from *Yucca brevifolia* collected in San Bernardino County, California. (See text for details about this piece). **Figure 3.** Same piece as in Fig. 2. A preliminary cut has already been made. Note the termite channels. **Figure 4.** Cross section of the piece of termite reaction wood shown in Figs. 2, 3. The section has many termite galleries, which still contain debris. Note several external termite apertures. On the upper surface of this piece there are two weathered termite entrance ports which are tubular.

The cross sectional anatomy of the termite reaction wood is shown in Figs. 6 and 7. In a zone where growth appears to be radial, ray-like structures can be observed between the cross sections of vascular bundles (Figs. 5, 6). Between the vascular bundles, which are usually very dense and formed more or less as in other monocot stems, a cellular matrix can be seen. The exact nature of these bundles can not be elucidated until they can be properly sectioned and studied by TEM and SEM. It was not possible to establish how much of the bundles was xylem, phloem, or even fibers. Observations of longitudinal sections of the wood show vascular bundles that branch and anastomose forming a strong three-dimensional network (Figs. 8, 9). Between the vascular bundles, a coherent tissue of parenchyma/sclerenchyma cells forms a solid matrix (Fig. 9). The individual cells of this matrix can be seen in Fig. 10-12. Many of these cells are polygonal in

section. Often they have a thick cell wall and are probably the sclereids mentioned by Johnstone (mentioned above). Fig. 13 shows a zone in the reaction wood where the vascular bundles are free. The nature of these free vascular bundles is not clear. Two explanations are possible: 1) for some reason the cellular matrix has not been formed, and 2) termites may have browsed on this tissue, eating the relatively soft matrix cells and leaving the free vascular bundles. The latter seems somewhat far fetched.

A preliminary view of the termite reaction wood macerations can be seen in Figs. 12-16. Elongate cells that appear to be tracheary elements (probably tracheids) are easily observed in the macerations. The irregular or kinked-shaped elongate cells are about 1.3 mm in length and have oblique wall pitting (Fig. 14). The tracheid cell walls are very birefringent under polarized light (Fig. 16). Between the tracheids, many small

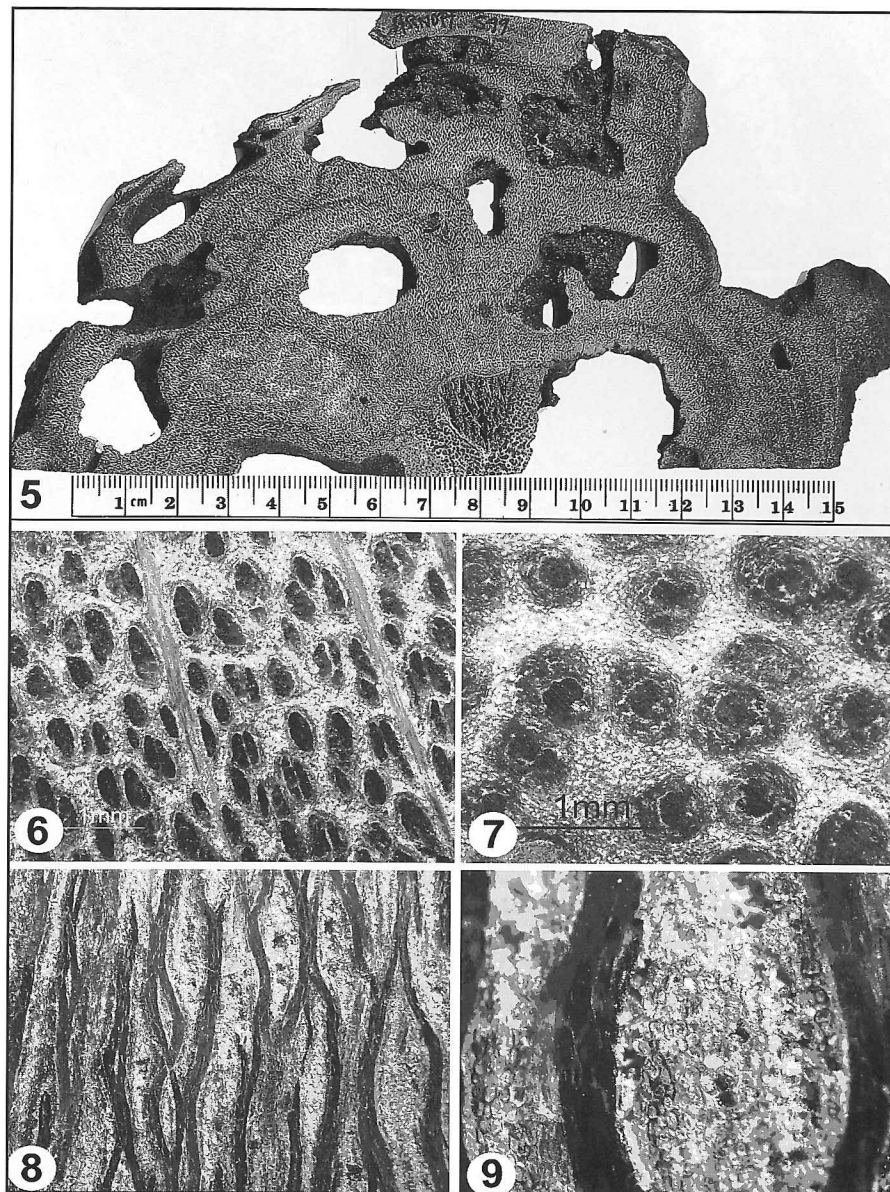
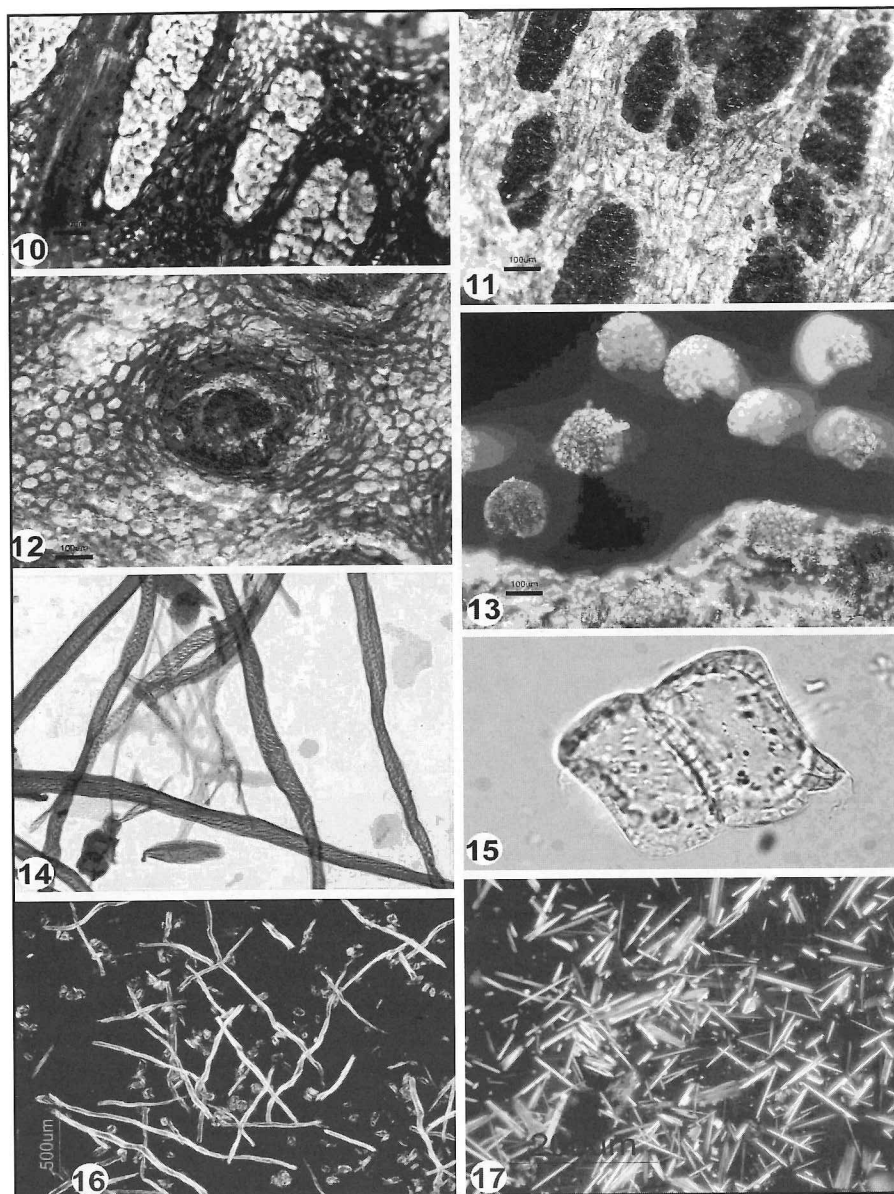


Figure 5. Sanded and polished cross section of termite reaction wood. Several termite galleries are visible. Note the tangential and radial components exhibited by this section. **Figures 6 and 7.** Transverse sections of termite reaction wood showing details of the vascular bundles and the cellular matrix between them. In this preparation it is difficult to distinguish if both xylem and phloem are present in each bundle. However, each bundle is clearly surrounded by a distinct bundle sheath. Cells of the bundle sheath and the matrix seem to intergrade. **Figures 8 and 9.** Longitudinal sections of the termite reaction wood showing the dense nature of the vascular bundles. Fig. 8 shows the network of vascular bundles characteristic of monocot stems.

parenchyma/sclerenchyma cells can be found. Two typical brachysclereids with thick pitted cell wall are seen in Fig. 15. The ubiquitous calcium oxalate crystals, found in so many tissues of yucca, are also found in the termite reaction wood (Fig. 17). Careful examination of that tissue using polarized light revealed crystal idioblasts among the matrix cells. Judging by the isolated crystals there are probably both raphides and styloids cells present in the matrix. No phloem cells were observed.

Clearly, the termite reaction wood found in the stem of *Yucca brevifolia* is complicated, probably vastly more complex than the typical wood of pine trees. A complete understanding of these tissues will require more examination, especially investigation of the reaction wood as it develops, meaning sampling living trees, particularly trees that are in the process of forming this tissue. It seems that there are plenty of bits and pieces for those interested in the structure of monocot wood. Truly, monocot wood is on the frontier.

I thank Rex Adams of the Laboratory of Tree-Ring Research at the University of Arizona in Tucson for sectioning the piece found in 2006 along Wilson Farm Road, 0.2 miles south of Maricopa Road, in San Bernardino County, California, into 1 cm thick sections. I also thank Kelsey Carnahan, a student in my lab, for preparing macerations of the termite reaction wood, which were important in determining its cellular structure.



Figures 10 and 11. Details of the vascular bundles as seen in transverse section. Fig. 10 represents a thin hand section showing vascular bundle details. Fig. 11 shows the characteristic dark color found in many vascular bundles. **Figure 12.** Transverse section showing details of the cellular nature of a vascular bundle. The bundle sheath is clear and surrounded by parenchyma/sclerenchyma cells. A series of radial files is present in the lower part of the center of the bundle. **Figure 13.** Seven vascular bundles in an unconsolidated cavity similar to those seen in Fig. 5. **Figures 14-16.** Macerated termite reaction wood. Figure 14. Isolated tracheids stained with saffrin. The tracheids have oblique oriented slot-like pits. Figure 15. Two isolate macrosclereids with thick walls and simple pits. Figure 16. Tracheids and matrix cells from termite reaction wood seen under crossed polarizers. The twisted or irregular character of these tracheids can easily be seen. **Figure 17.** Crystals of calcium oxalate (styloids and raphides) isolated from termite reaction wood under polarized light.

MATERIAL SCIENCES

FALL 2007

AN ANALYSIS OF GENUINE WORLD WAR II GERMAN MILITARIA. MICHAEL W. PENDLETON*, *Microscopy and Imaging Center, Texas A&M Univ., College Station, TX 77843-2257 and BONNIE B. PENDLETON**, **Dept. of Agric. Sciences, West Texas A&M Univ., Canyon, TX 79016-0001.

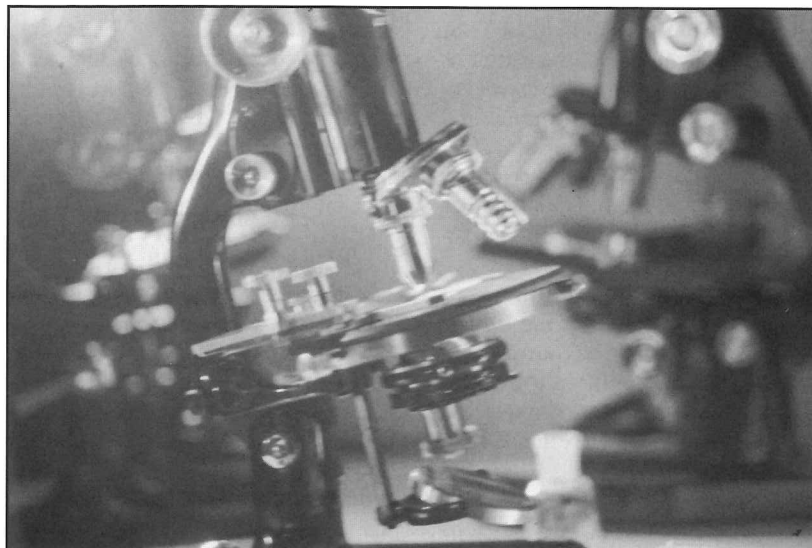
The study of World War II German militaria (medals, weapons, uniforms, etc.) is a topic of research for collectors and museum curators. If the demand for these war relics is great enough, the price for such items exceeds the manufacturing cost and the production of fake militaria becomes profitable. This is one reason that the production of counterfeit World War II German militaria has become common (Cowdery, 1993). Scanning electron microscopy (SEM) and energy-dispersive X-ray spectroscopy (EDS) have been utilized to distinguish between real and fake World War II Iron Cross medals (Aneja *et al.*, 2007). Real Iron Cross medals were painted with black paint produced by burning animal bones while the fake medals were painted with modern silicon based paint. The silver content was far greater in the real medals than was present in the fake medals. For this study, a silver bust of a German soldier obtained by an American serviceman while in Germany during World War II was analyzed by SEM and EDS to determine the type of base metal and plating. Because the provenience of this bust is based on family oral tradition, it is assumed to be genuine and therefore the results of the analysis presented in this study are useful in order to distinguish between real and fake soldier busts. The base metal of the German soldier bust was found to be lead while silver was used to plate the entire outer surface, including the helmet and face.

GEOLOGICAL SCIENCES

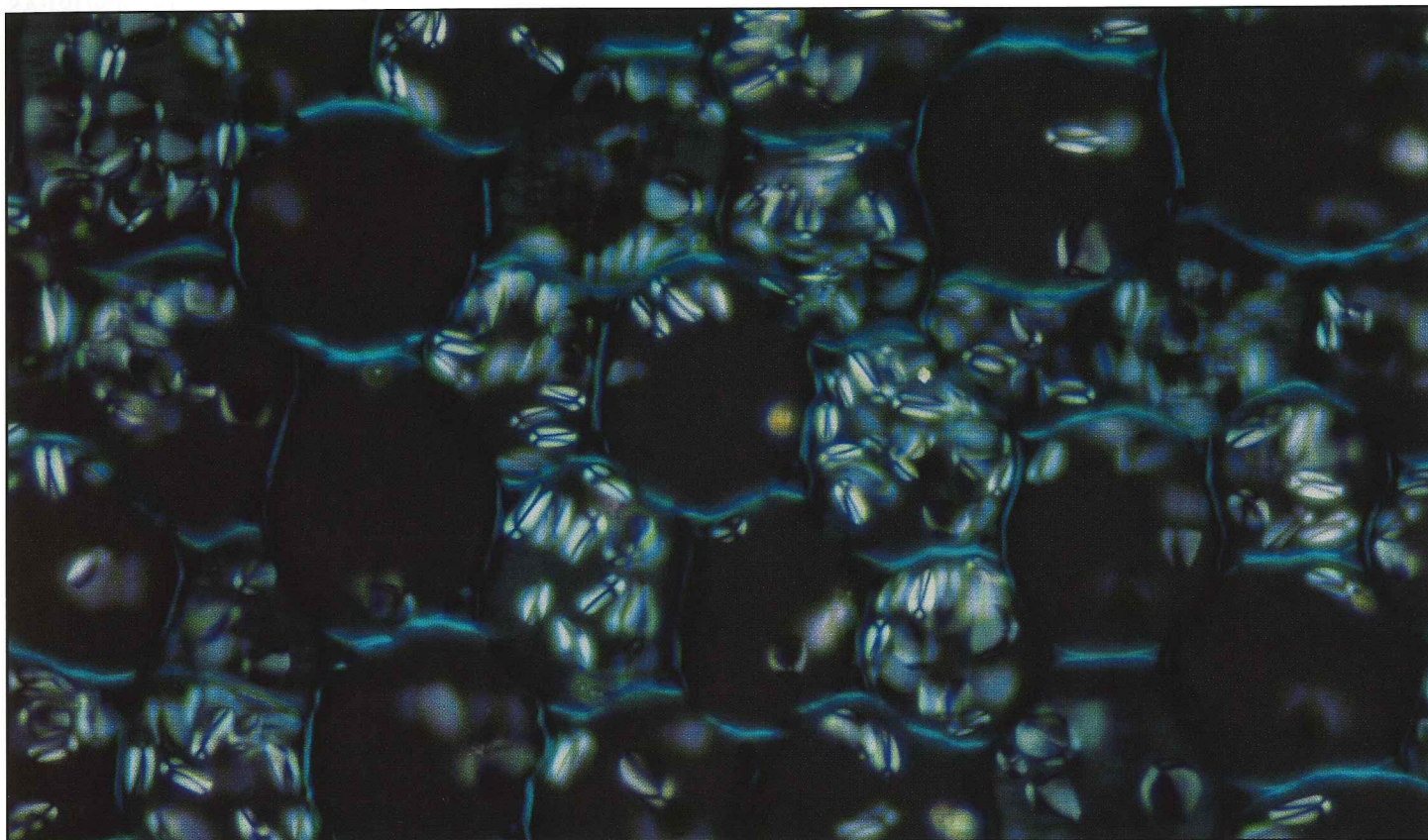
FALL 2007

CHARACTERIZATION OF MICROFABRIC AND MINERALOGY OF MARINE SEDIMENTS BY ELECTRON MICROSCOPY. DEBORA BERTI¹, E. ANN ELLIS², ANDREAS HOLZENBURG², ¹Department of Oceanography and ²Microscopy and Imaging Center, Texas A&M University, College Station, Texas 77843

Marine sediments consisting of chalks with various degrees of cementation from the northwestern margin of the Demarara Rise (offshore French Guyana) and clays from the northwestern Gulf of Mexico continental slope were examined by TEM and SEM to determine mineralogy, microfabric, and pore geometry. This study focused on samples in their natural condition and developed improved methods for specimen preparation. Sample preparation used cold microwave technology (Pelco Biowave) with dehydration in 5% steps of methanol starting at 5% methanol (vol/vol) in 1 min steps at 250 watts in the microwave. After dehydration through 100% methanol to propylene oxide, samples were infiltrated with a low viscosity epoxy resin formulation with a high anhydride: epoxide ratio (1.2:1.0) using the microwave. Specimen blocks were then polished for SEM and thin sectioned for TEM. Good specimen preparation was achieved for both TEM and SEM, which allowed for good morphological and analytical studies. Chalk samples had various mineralogies with fossiliferous carbonates and abundant clay minerals. TEM examination was important in detecting clays, which were missed by preliminary observations. SEM showed oozes and chalks from the Demerara Rise composed of complex mixtures of whole and broken coccolith spheres, micrite crystals and foraminiferae. Large pores in the sediments were filled by opal lepispheres and clinoptilolite. Gulf of Mexico clays consisted of mostly smectite and illite with low permeability. The microwave assisted specimen preparation gave good dehydration and infiltration, in a timely manner, which was essential to TEM and SEM analysis.



What Is It?" *Answer in Next Edition*



Light micrograph provided by **Dr. Irina N. Gostin**, Al.I. Cuza University, Biology Department, Iasi, Romania.

EDITORIAL POLICY

LETTERS TO THE EDITOR

Letters to the editor are printed as they are received in the order of their arrival. These letters reflect the opinion of the individual TSM member and do not necessarily reflect the opinions of the Editor or the Society. The content of the letters should be concerned with the philosophical or operational aspects of the TSM, the Journal and its contents, academic or national policies as they apply to TSM and/or its members and microscopy in general. Editorial privilege may be evoked to insure that the LETTERS SECTION will neither be used as a political forum nor violate the memberships' trust.

MICROGRAPHS AND COVER PHOTOS

Micrographs submitted for cover photos should be marked as such. The choice of photographs will be made by the Editor. Photograph receipt and/or dispensation will not be acknowledged. Photographs will not be returned. Electron micrographs to be used for cover photos and text fillers are welcome and should be selected with some attention to aesthetic appeal as well as excellence both in technique and in scientific information content.

EMPLOYMENT OPPORTUNITIES

The JOB OPPORTUNITIES section will be comprised of a "Jobs Available" and a "Jobs Wanted" sub-section. Anonymity of individuals listing in the Jobs Wanted or Jobs Available sub-sections may be maintained by correspondence routed through the Editor's office.

TECHNICAL SECTION

The Technical Section will publish TECHNIQUES PAPERS, and HELPFUL HINTS. The TECHNIQUE PAPERS will describe new or improved methods for existing techniques and give examples of the results obtained with methods. The format of the Technique Papers will be the same as that used for regular research reports. HELPFUL HINTS will be in the form of a brief report with an accompanying illustration, if required for clarity. Helpful Hints should embody techniques which will improve or expedite processes and/or procedures used in EM.

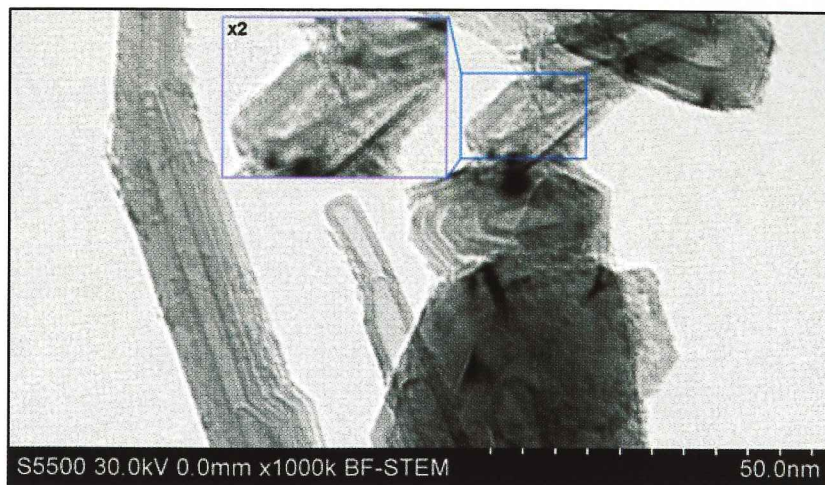
PUBLICATION PRIVILEGES

The right to publish Abstracts in the TEXAS JOURNAL OF MICROSCOPY is restricted to TSM members or to those whose membership is pending. A membership application form can usually be found in each issue of the TEXAS JOURNAL OF MICROSCOPY. Membership dues are as follows: student \$10.00; regular members \$30.00; corporate members \$300.00 (corporate dues include all meeting registrations for the year, a link on the corporate sponsors' page, and other benefits. Contact secretary for more information). Research articles are accepted from both members and non-members. Individuals who belong to TSM by virtue of a corporate membership are invited to participate in journal submissions as are our regular or student members. However, papers of a commercial nature, either stated or implied, will not be accepted for publication as a Research Report or Techniques Paper. Such papers may be acceptable as advertising copy.

The Ultimate in Resolution.

Hitachi S-5500

In-lens Field Emission Scanning Electron Microscope



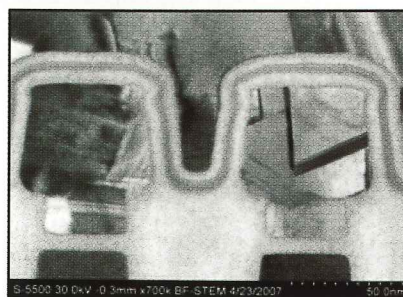
Fringes of MWCNT in STEM

The Hitachi S-5500 is a dedicated ultra-high resolution In-lens FE-SEM for leading edge research and development of nanotechnologies. The patented in-lens technology provides the ultimate performance of 0.4nm guaranteed imaging resolution.

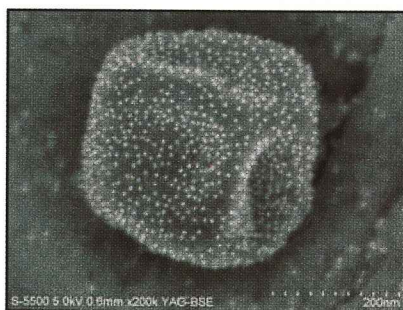
The S-5500 is equipped with a shielding system for reduced EMI and acoustic interferences. These improvements with a completely dry vacuum system ensures Hitachi's high-resolution guarantee for the life of the instrument.

A newly designed BF/DF Duo-STEM detector (patent pending) contains an adjustable dark field detector for tunable collection angles.

Sometimes a single image can change the way we look at life. The new S-5500 with its advances in information collection will lead you to those opportunities.



NAND double-gate cross-section in STEM



Immuno Labeling



Hitachi High Technologies America, Inc.

5100 Franklin Drive

Pleasanton, CA 94588

800.227.8877 (T) / 925.218.3230 (F)

www.hitachi-hta.com

HITACHI
Inspire the Next

APPLICATION FOR MEMBERSHIP OR CHANGE OF ADDRESS **TEXAS SOCIETY FOR MICROSCOPY, INC.**

Date _____

Please type or print legibly. Fill out completely. The numbers in parenthesis are the maximum number of characters and spaces the computer can accommodate for that blank. Though we will mail to your home address, we prefer to have your work address. Please note that membership is for Jan. - Dec. for each year.

- Check one: ☐ I am applying for new membership in T.S.M.
 ☐ I am a member and wish to change my address.
 ☐ I am a STUDENT and wish to upgrade to REGULAR membership.

Are you a member of MSA? ☐ Yes ☐ No

Name (last name first) _____ (35)

Institution _____ (35)

(Please write out completely. We'll abbreviate it.)

Department _____ (35)

(Please write out completely. We'll abbreviate it.)

Street & Number/P.O. Box _____ (35)

City _____ (20) State _____ (2) Zip _____ (10)

Work Phone (____) _____ (13) Extension _____ (4)

Electronic Mail _____ (40)

Home Phone (____) _____ (13) Fax No. (____) _____ (13)

Category of Membership (circle only one): **Regular** **Corporate** **Honorary** **Library**

Student: _____ Degree program _____ Signature of faculty sponsor _____

Broad field of interest in which you utilize Electron Microscopy: (circle only one):

Zoology	Botany	Microbiology	Cell Biology	Biochemistry
Medicine	Vet. Medicine	Chemistry	Sales	Service/Repair
Materials	Petroleum	Semiconductor	Environment	Minerals

If you are a member changing your address, please attach an old mailing label to help us identify your previous record in the computer. Applicants for membership should include a check or money order for one year's dues with application (Regular: \$30.00; Student: \$10.00; Corporate: \$300.00).

Applications for new membership, or for upgrading of membership category from STUDENT to REGULAR, will be presented to the Executive Council at their next meeting for their approval (majority vote). The applicants will then be presented by the council to the membership at the next general business meeting for their approval (majority vote). Applicants will be added to the membership rolls at that time.

Please return to: Tina Halupnik
5917 Inks Lake Dr.
Arlington, TX 76018

Nano-Technology Solutions



ORION™



ULTRA plus



EVO®



SUPRA™



NVision 40

SUPRA™



LIBRA® EFTEM

Carl Zeiss SMT offers a complete range of ultra high resolution GEMINI® FESEMs, multipurpose and extended pressure SEMs, energy filtering TEMs, helium ion microscopes and FIB systems for all your nanotechnology applications.

ORION™

The world's first commercial helium ion microscope, ORION™ provides topographic, material, electrical and crystallographic contrast

EVO®

Multipurpose SEM with a choice of HV, extended variable pressure and extended pressure systems

SUPRA™

The most versatile FESEM on the market

ULTRA plus FESEM

Provides ultra high resolution imaging and unmatched compositional data

NVision 40 FIB

The ultimate 3D research tool for analyzing samples at nano-scale

LIBRA® EFTEM

For unrivaled flexibility in imaging and analysis

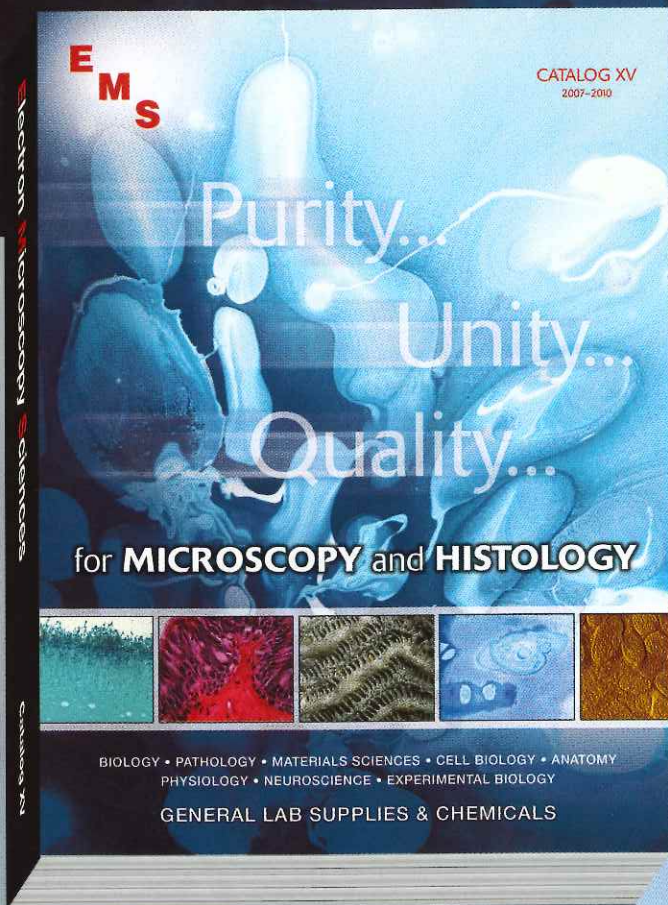
Enabling the Nano-Age World®

Carl Zeiss SMT Inc
One Corporation Way
Peabody, MA 01960
USA

Tel. +1 978/826 1500
Fax +1 978/532 2503
info-usa@smt.zeiss.com
www.smt.zeiss.com/nts



The new **2007-2010 EMS CATALOG** is now available!



Your one-stop shop for the latest products and solutions for Microscopy and Histology!

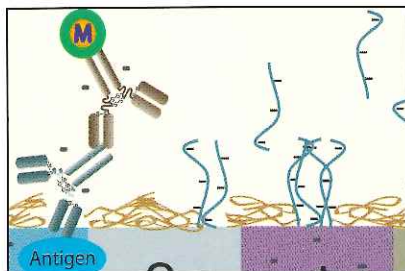
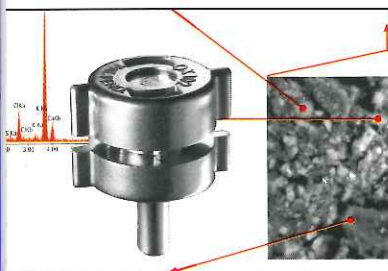
Exacting Research demands only the Highest Quality Products.

Introducing the 2007-2010 EMS Catalog, your comprehensive source for chemicals, supplies, accessories, and equipment for Microscopy, Histology and all fields of biological and materials research.

Featuring new and revolutionary products, including:

- C-flat™ Holey Carbon Grids for cryo-TEM
- Ilford Photography Papers and Photochemicals
- WETSEM™ Capsules for Hydrated SEM Samples
- DuraSIN™ Substrates for TEM & X-ray
- Diatome Oscillating Diamond Knife
- PathScan Enabler III
- Ultra-Thin Carbon Tabs
- Plunge Freezer
- EMS 9000 Precision Pulsed Laboratory Microwave Oven
- State-of-the-Art Oscillating Tissue Slicers
- NioProbe and TipCheck for AFM
- Aurion ImmunoGold Reagents and Accessories
- EMS LYNX Tissue Processor
- MAG*²CAL®
- EMS Carbon Coaters and Sputter Coaters

Application Notes • More Technical Support • Enhanced Product Lines • Revolutionary Products



QuantomiX WETSEM™ • AURION Newsletters • Diatome Diamond Knives • C-flat™ Holey Carbon Grids

To request our new catalog, please call or write us today, or visit us online at **www.emsdiasum.com**

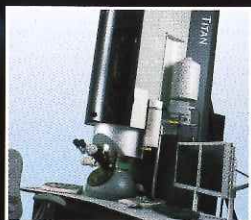
**Electron
Microscopy
Sciences**

P.O. Box 550 • 1560 Industry Rd. • Hatfield, Pa 19440
(215) 412-8400 • Toll Free: 1-(800) 523-5874
Fax: (215) 412-8450 or 8452
email: sgkcck@aol.com • stacie@ems-secure.com
www.emsdiasum.com

Explore, discover, build

with unparalleled access to the nanoscale

Today's advanced discovery and product development requires unimpeded 3D access to the nanoscale with the best resolution possible. FEI's Tools for Nanotech™ support the success of your most demanding projects by giving you the power you need to reach far into the nanoscale.



Titan™ 80-300 (S)TEM

The Titan™ breaks the Ångström barrier with atomicscale resolution. This dedicated platform for aberration corrected (scanning) electron microscopy delivers the highest resolution available on a commercially available (S)TEM system.



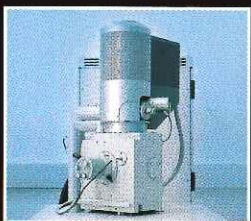
Tecnai™ G² Series

Any of the G² series offers a truly universal imaging and analysis solution that seamlessly embeds all peripherals and software in one powerful instrument. It offers total digital control of your advanced (S)TEM environment, and takes the proven Tecnai™ 'all-in-one' concept to a new level.



Helios™ NanoLab

The DualBeam™ for pushing the limits at the nanoscale, providing the best resolution and image quality down to the sub-nanometer level; producing the thinnest samples of the highest quality, enabling advanced 2D and 3D nanocharacterization, and delivering the most integrated solutions for nanoprototyping.



Nova™ NanoSEM

Experience the world's only true high resolution, low vacuum FEG-SEM for characterization of charging and/or contaminating nanomaterials or nanodevices.



Quanta™ 3D FEG

The Quanta™ 3D FEG is the most versatile high resolution, low vacuum FE-SEM/FIB for 2D and 3D material characterization and analysis. It can accommodate the widest range of samples of any SEM system and enables in situ study of the dynamic behavior of materials at different humidity levels (up to 100% RH) and temperatures (up to 1500 °C).

... Leading Edge Critical Point Dryers ...



- 35 Years of CPD Innovations
- Advanced Manual and Automatic Models
- Up to 8in Chamber Sizes
- Minimal Facility Requirements
- Small Foot Print Designs
- 2 Year Warranty
- Free Lifetime Tech Support
- Made in U.S.A.



Large Capacity Fully Automatic Critical Point Dryer